TECHNISCHE UNIVERSITÄT MÜNCHEN

Lehrstuhl für Bodenökologie

Modeling the impact of soil heterogeneity on the variability of crop growth at field scale

Xiaohong Duan

Vollständiger Abdruck der von der Fakultät Wissenschaftszentrum Weihenstephan für Ernährung, Landnutzung und Umwelt der Technischen Universität München zur Erlangung des akademischen Grades eines

Doktors der Naturwissenschaften

genehmigten Dissertation.

Vorsitzender : Univ.-Prof. Dr. Dr. h.c. A. Heissenhuber

Prüfer der Dissertation :

1. Univ.-Prof. Dr. J. C. Munch
2. Priv.-Doz. Dr. E. Priesack (Georg-August-Universität Göttingen)

Die Dissertation wurde am 28.04.2010 bei der Technischen Universität München eingereicht und durch die Fakultät Wissenschaftszentrum Weihenstephan für Ernährung, Landnutzung und Umwelt am 26.02.2011 angenommen.

For my husband *Dong*,
our son *Kuan* and our daughter *Li*.

Acknowledgements

This thesis would not be possible without the help and support I got from many sides.

At first I thank Prof. Dr. Jean Charles Munch, Institute of Soil Ecology, GSF-National Research Centre for Environment and Health, Neuherberg, for providing me the opportunity to work on my PhD study in his institute, for the excellent research facilities. I am deeply grateful that Professor Munch always gives me a hand, whenever I met a problem, or I felt confused or dispirited during the work. His steady support and encouragement have inspired me in completing my PhD study.

The next I want to express my deep gratitude to my supervisor, PD Dr. Eckart Priesack, Institute of Soil Ecology, GSF. Being a great supervisor, he has provided constant advice and valuable guidance on all aspects of my work. At the same time, he has encouraged independent work and grants sufficient freedom for trying my own idea. I thank him very much indeed for his continuous support, for his valuable suggestions and critical comments in completing this thesis.

My special thanks go to Dr. Sebastian Gayler, for his excellent support with Expert-N and application of other soft ware, his constructive criticism and creative suggestions. I also thank Dr. Hans Peter Hartmann for introducing me to the subject of the research work. Furthermore, I thank Rolf Schilling and Georg Gerl for their technical and experimental support at the field, thank Svetlana Schlund for her help on root washing, and thank Franz Buegger for the measurement of carbon and nitrogen content. I thank other collaborators in the soil ecology institute for their friendship, cooperation and help.

For support out of our institute, I thank Dr. Thomas Selige from Lehrstuhl für Pflanzenernährung, TUM for his guidance on performing the investigation of soil-root-profile, thank Dr. Helmut Blaschke

from Lehrstuhl für Ökophysiologie der Pflanzen, TUM for introducing me to the use of the root image analysis program WinRHIZO, thank Harald Schmidt from Lehrstuhl für Ökologischen Landbau und Pflanzenbausysteme, TUM for his suggestion and technical support on the root sampling by auger, thank Dr. Ludwig Nätscher from Bioanalytik Weihenstephan, Zentralinstitut für Ernährungs- und Lebensmittelforschung, TUM for measuring the soil texture and C/N content, thank Markus Demmel from Lehrstuhl für Landtechnik, TUM for providing the high-resolution crop yield data of 1994, 1997 and 2000.

I sincerely acknowledge the financial support of the GSF-National Research Centre for Environment and Health for this PhD work and the scholarship from the women's representative, TUM for completing this thesis.

I want to express my sincerely thanks to Dr. Christina Klier, Dr. Walkiria Levy, Dr. Jürgend Esperschütz, Dr. Isabelle Pattis, Dr. Heidrun Albrecht, and Dr. Maren Olbrich, for being both my excellent colleagues and friends, for sharing the research experiences, for their valuable suggestions on the editing of my thesis, and also for their steady encouragement.

Many thanks to my friends Dr. Xia Dong, Zhiwei He, Zheng Yu, Baodian Shi, Dr. Li Lin and Ruohe Yin for sharing the laughs and tears in our lives.

At last but most important, I want to thank my family, my husband Dr. Dong Chen, our son Kuan, our daughter Li, my parents and parents-in-law, for the unconditional support I have received.

Contents

List of abbreviations and symbols

A. The abbreviations:

Abbreviation	Definition
BD	soil bulk density [g soil $/cm^3$ soil]
Brooks & Corey	soil water retention function by Brooks & Corey (1966)
Brutsaert	soil water retention function by Brutsaert (1966)
Burdine	unsaturated hydraulic conductivity function by Burdine (1953)
Campbell	peto transfer functions by Campbell (1985)
CERES	crop models CERES-Maize by Jones & Kiniry (1986) and CERES-Wheat by Ritchie & Godwin (1989)
CERES+	modified CERES models by linking the new root model in this study
CHCB	approach using peto transfer functions by Campbell (1985) to parameterize hydraulic functions by Hutson & Cass (1987) and Burdine (1953)
Gardner	unsaturated hydraulic conductivity function by Gardner (1958)
HF(s)	hydraulic function(s)
Hutson & Cass	soil water retention function by Hutson & Cass (1987)
LAI	leaf area index [m^2 leaf surface / m^2 land surface]
PTF(s)	pedo transfer function(s)
Rawls & Brakensiek	peto transfer functions by Rawls & Brakensiek (1985)
RBMD	root biomass density [g root biomass $/cm^3$ soil]

continued on next page

Abbreviation	Definition
RBBCB	approach using peto transfer functions by Rawls & Brakensiek (1985) to parameterize hydraulic functions by Brooks & Corey (1966) and Burdine (1953)
RLD	root length density [cm root length $/cm^3$ soil]
RSAD	root surface area density [cm^2 root surface area $/cm^3$ soil]
SD	standard deviation
SRL	specific root length [cm root length $/g$ root biomass]
SRSA	specific root surface area [cm^2 root surface area $/g$ root biomass]
SWC	soil water content [cm^3 water$/cm^3$ soil]
VBG	approach using peto transfer functions by Vereecken et al. (1989) and Vereecken et al. (1990) to parameterize hydraulic functions by Brutsaert (1966) and Gardner (1958)
Vereecken	peto transfer functions by Vereecken et al. (1989) and Vereecken et al. (1990)
vGM	soil water retention function by van Genuchten (1980) and unsaturated hydraulic conductivity function by Mualem (1976)
V+CHCB	approach using peto transfer functions by Vereecken et al. (1989), Vereecken et al. (1990) and Campbell(1985) to parameterize hydraulic functions by Hutson & Cass (1987) and Burdine (1953)
WRC	soil water retention curve

B. The symbols:

Symbol	Definition [common unit]
α	empirical parameter of van Genuchten model and Brutsaert model $[1/cm]$
α_{BD}	stress factor due to high soil bulk density [-], $\in$[0.0, 1.0]
α_{coarse}	stress factor due to high coarse fraction in soil [-], $\in$[0.0, 1.0]
α_N	stress factor due to deficit of soil mineral nitrogen content [-], $\in$[0.0, 1.0]
α_{O_2}	stress factor due to poor aeration, [-], $\in$[0.0, 1.0]
$\alpha_{strength}$	stress factor due to high soil hardness, [-], $\in$[0.0, 1.0]
$\alpha_{sub,sum}$	the sum of $\overline{\alpha(i)}$ of a user-defined rooting depth in sub soils [-], $\in$[0.0, 1.0)
α_{sum}	the sum of $\overline{\alpha(i)}$ over the rooting depth [-], $\in$[0.0, 1.0]
α_{Temp}	stress factor due to inadequate soil temperature [-], $\in$[0.0, 1.0]
α_θ	stress factor due to deficit of soil water content [-], $\in$[0.0, 1.0]
$\alpha_{\theta_{PAW}}$	the fractional plant available water content [-]
$\alpha(i)$	the most limiting stress factor in the i -simulation layer of soil [-], $\in$[0.0, 1.0]
$\overline{\alpha(i)}$	a weighted stress index to assess the relative adequateness of the i-simulation layer of soil for root growth [-]
γ_{cri}	a user defined critical value to evaluate if the root growth ceases due to inadequate soil condition in sub soil [-], $\in$(0.0, 1.0)
λ	Brooks & Corey exponent $[-]$
$\lambda(i)$	the layer-weighting root growth partitioning index [-]
ϕ	the soil porosity $[cm^3/cm^3]$

continued on next page

Symbol	Definition [common unit]
ρ_s	soil bulk density $[g/cm^3]$
τ	shoot:root ratio [-]
θ	volumetric soil water content $[cm^3/cm^3]$
$\theta_{cri,poro}$	critical water-filled porosity [-]
θ_{fc}	volumetric soil water content at field capacity $[cm^3/cm^3]$
θ_i	initial water content $[cm^3/cm^3]$
θ_{pwp}	volumetric soil water content when crop at permanent wilting point $[cm^3/cm^3]$
θ_{res}	residual volumetric soil water content $[cm^3/cm^3]$
θ_{sat}	saturated volumetric soil water content $[cm^3/cm^3]$
$\theta(h)$	soil water retention function $[cm^3/cm^3]$
$\omega(i)$	the root distribution factor in the i-simulation layer of soil [-], $\in(0.0, 1.0)$
ξ	a crop-specific parameter
A or Gardner A	an empirical parameter of Gardner model $[cm^{-1}]$
a	an empirical parameter in Brooks & Corey hydraulic function which presents the pressure head at the air entry value $[cm]$
a or Campbell A	an empirical parameter of Hutson & Cass model which presents the pressure head at the air entry value $[cm]$
b or Campbell B	an empirical parameter of Hutson & Cass model [-]
B or Gardner B	an empirical parameter of Gardner model [−]
BD	soil bulk density $[g/cm^3]$
BD_O	the moist bulk density at which the maximal root growth occurs $[g/cm^3]$

continued on next page

Symbol	Definition [common unit]
BD_X	the moist bulk density at which no root growth occurs $[g/cm^3]$
$C(h)$	differential moisture capacity $\partial\theta/\partial h$ $[cm^{-1}]$
C_{org}	soil organic carbon content [-]
EF	modeling efficiency
f_{clay}	clay content in soil [-]
$f_{C_{org}}$	organic matter content in soil [-]
f_{sand}	sand content in soil [-]
f_{silt}	silt content in soil [-]
GS	growth stage [-], $\in$[0.0, 1.0]
GSD	growth stage at which the root senescence begins [-]
h	soil pressure head [cm]
h_0	supply pressure head imposed by the tension-disc infiltrometer $[cm]$
m	empirical parameter of van Genuchten model [-]
M_i	the measured values for calculation the modeling efficiency
n	empirical parameter of van Genuchten model and Brutsaert model [-]
K_{sat}	saturated hydraulic conductivity $[cm/s]$
$K(h)$	unsaturated hydraulic conductivity function $[cm/s]$
$LWA(i)$	the actual root length/weight ratio $[km/kg]$
$LWM(i)$	the root length/weight ratio of mature root system $[km/kg]$
$LWN(i)$	the normal root length/weight ratio without stress effect [km/kg]

continued on next page

Symbol	Definition [common unit]
$LWS(i)$	the root length/weight ratio of seeding roots $[km/kg]$
P_i	the predicted values for calculation the modeling efficiency
r	radial coordinate $[cm]$
r_0	the disc radius $[cm]$
$RB(i)$	actual root biomass in the i-simulation layer of soil $[kg]$
$RBDEATH(i)$	daily actual root biomass death $[kg]$
$RBGROW_{act}$	daily actual root biomass growth $[kg]$
$RBGROW_{pot}$	daily potential root biomass growth $[kg]$
$RBGROW(i)$	daily actual root biomass increase in each simulation layer of soil $[kg]$
RD_{max}	the maximum rooting depth $[cm]$
$RLGROW(i)$	daily actual root length increase in i -simulation layer of soil $[km]$
R^2	the statistical parameter coefficient of determination
S_e	the effective water content ratio $[-]$
S_w	sink term for root water extraction$[cm^3/cm^3/s]$
t	time $[s]$
$Z_{mid}(i)$	the depth from soil surface to the middle of the i -simulation layer of soil $[cm]$
z	vertical distance $[cm]$

List of Figures

LIST OF FIGURES

List of Tables

Chapter 1

Introduction

1.1 Application of computer models for precision agriculture

To understand the processes and factors that govern the within-field variability in crop yield, the major importance of the effective precision agriculture application has to be appreciated (Duffera *et al.*, 2007; Green & Erskine, 2004; Kravchenko *et al.*, 2005; Perez-Quezada *et al.*, 2003; Plant, 2001; Wong & Asseng, 2006). Crop growth is a dynamic process involving the interactions of numerous biotic and abiotic factors, including field and soil characteristics (e.g. topography and soil holding capacity), weather conditions (e.g. temperature and precipitation), and management practices (e.g. irrigation, fertilization and tillage). Depending on the observation scale used, the soil and weather factors can vary significantly with space and time. The numerous inherent properties combined with temporal variations make it very difficult to identify and manage the variability pattern.

This variability at field scale is often ignored by conventional mechanized land use management which is aimed at maximizing the crop yield by increasing inputs. Simple uniform agricultural management based on the average information often leads to the unnecessary expense of excessive input, contamination of ground water by leached fertilizers, and a decrease in soil fertility. Precision agriculture, also known as site-specific management, has emerged as a solution to this situation. The principle of precision agriculture is to reduce overloading of the environment by considering the variability on a spatial scale that is smaller than that of the whole field. Plant (2001) pointed out that the application of site-specific management is only justified, where (1) significant within-field spa-

tial variability exists for factors that influence crop yield, (2) the causes of this variability can be identified and measured, and (3) the information from these measurements can be used to modify crop management practices.

For the purpose of identifying the prominent yield-affecting factors in individual cases, process-oriented simulation models that describe the dynamics and interactions of physical, chemical and biological processes in agriculture systems are very useful tools (Ahuja *et al.*, 2002; Ascough *et al.*, 2008; Priesack *et al.*, 2008). Models enhance the understanding of data taken under certain conditions and help to extrapolate applications to other conditions and locations. Valid models can be used in scenario studies to develop and evaluate alternative methods for sustainable agricultural management (Priesack *et al.*, 2008). However, the contribution of computer models depends on how quantitatively is our knowledge of the influence of environmental factors on crop growth, and how accurately this knowledge can be integrated into the models.

1.1.1 Development of agricultural system models

The major components of agro-ecosystem include plant, soil, atmosphere and human activity. The aim of agricultural system integration and modeling is to simulate not only plant growth processes but also energy and matter flux between the atmosphere and the soil as well as influencing agricultural management (Priesack, 2006). The relevant processes that are commonly considered in agricultural system models are summarized in the three frameworks of *Crop*, *Environment* and *Management* in Fig.1.1. The system models focus on the modeling of crop growth describing the input of C into the agro-ecosystem through the process of photosynthesis and the internal partitioning and cycling process of organic matter in the system (e.g. biomass growth, root growth, crop senescence, soil organic matter turnover). Owing to the high water and nitrogen demand of the growing crop on the soils via root uptake, the crop growth process is closely related to the soil water balance and soil nitrogen balance processes. The coupling of the simulation of soil water flow and soil nitrogen transport with the crop growth model is realized by the calculation of the sink term as a consequence of the root uptake of the available water and nitrogen. The availability of water and nitrogen in the soil is determined by a series of physio-chemical processes such as evapotranspiration, drainage of water, mineralization of organic matter, etc., which are strongly influenced by the soil properties and climate conditions. In addition, the

water and nitrogen balance can also be influenced by agricultural management of irrigation, fertilization and tillage, which change the input of water, and nitrogen as well as the soil structure and permeability (Benbi & Nieder, 2003; Priesack, 2006).

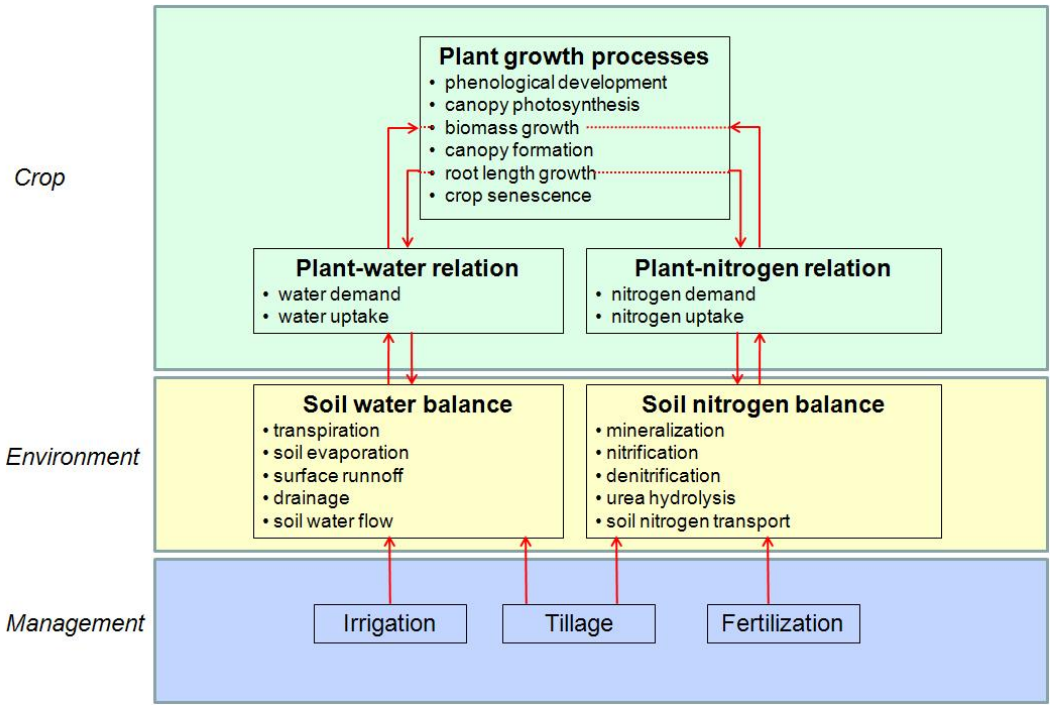

Figure 1.1: Relevant processes to be integrated in agricultural system model.

As Ahuja *et al.* (2002) registered, before the explicit development and use of agricultural system models in the 1980s, modeling work was only conducted on individual processes in agricultural systems such as infiltration, photosynthesis and soil nutrients dynamics. Nevertheless, these works built the foundation for system modeling. In the 1980s several system models that included the multiple components of an agricultural system were developed. Some of these are well-known worldwide and are still engaged in current applications, such as EPIC (Williams & Renard, 1985) and CERES (Ritchie *et al.*, 1986). Since the 1990s, agricultural system models have become more mechanistic, with more agricultural components. Examples of well-known and comprehensive system models are the American framework RZWQM (Ahuja *et al.*, 2000) and the Australian framework APSIM (McCown *et al.*, 1996). Some models are linked to a decision support system, such as DSSAT (the Decision Support System for Agrotechnology Transfer), which incorporates CERES and CROPGRO (Hoogenboom *et al.*,

1999; Tsuji *et al.*, 1994) and GPFARM (Shaffer *et al.*, 2000). In addtion, Priesack & Gayler (2009) pointed out, in order to address the increased demand for adequate fertilization management, several models have emerged with a focus on soil N-transport and N-turnover, e.g. DAISY (Hansen *et al.*, 1990) and Expert-N (Engel & Priesack, 1993). The recent state-of-the-science of applications of agricultural system models have been presented by Ahuja *et al.* (2002) and Priesack & Gayler (2009).

Because of the increased integration of complex processes, high modularity becomes desirable in the development of agricultural system models. Thus the open and modular model concept has been implemented in more and more models, such as RZWQM, APSIM and Expert-N. A modular modeling computer framework consists of a library of alternative modules (or subroutines) for different sub-processes. As mentioned above, most models in the early phase of the development were developed for a relatively simple purpose or for simulating a certain process of the Soil-Plant-Atmosphere System. They were usually simple and monolithic. Even the later more complex models, which consisted of separated subroutines, contained a specific part to simulate the growth processes of a specific plant species coupled with some soil and microclimate subroutines (Wang, 1997). If the subroutines are implemented in a modular structure, the validation and choice of certain single process for the individual application is possible. Furthermore, the modularity of a model enables quick updates of the sub model as new knowledge becomes available (Ahuja *et al.*, 2002; Priesack & Gayler, 2009).

The most difficult problem in the application of a model is how to determine model parameter values for the various parameters of the different components of the system and how they change with environmental stresses and management practices. In addition, most models are one-dimensional and do not take into account the changes in the model parameters with space and time (Ahuja & Ma, 2002). Hence, the model parameterization is further complicated by the spatial and temporal variability in the simulated field. The uncertainty in measured soil hydraulic parameters (Hupet *et al.*, 2004) and the simplified modeling of root growth (Wang & Smith, 2004) are the considerations that often lead to failure in simulating the crop growth variability under highly heterogeneous soil conditions.

1.1.2 Problems in parameterization of a water flow model

Application of Richards equation (Eq.3.1) to describe water flow and soil water storage in the soil matrix requires knowledge of two basic soil hydrologic relationships: (1) the **Soil Water Retention Curve (SWRC)**, which describes volumetric soil water content (denoted as θ) as a function of soil pressure head (denoted as h); (2) the **Unsaturated Hydraulic Conductivity Function**, which describes soil hydraulic conductivity (denoted as K) as a function of θ or h. These two functions define the soil hydraulic properties and their relationships are highly dependent on soil texture and soil structure (Scheffer & Schachtschabel, 1998). The effects of soil hydraulic properties on plant growth have been widely documented in the literature. Experimentally, Kribaa *et al.* (2001), for example, observed a significant variation in wheat yield due to altered hydraulic properties as a result of various cultivation methods in a semiarid climate. By combining measurements and agro-hydrological simulations, Hupet *et al.* (2004) also demonstrated the remarkable impact of within-field variability in the soil hydraulic properties on actual transpiration and crop yields for three contrasting climatic scenarios.

For use in models, the hydraulic relationships are fitted with a suitable mathematical equation or function, which is known as parameterizing the soil -water system. The parameterization problem is therefore to determine or estimate the independent parameters of a set of water retention and hydraulic conductivity functions. One of the best ways to determine these parameters is to fit the equations to the measured data on the hydraulic properties. Standard methods for measuring the relationships of $\theta(h)$ and $K(\theta)$ or $K(h)$ in the laboratory and field are detailed in (Dane & Topp, 2002). In general, these methods are time-consuming, tedious and expensive, especially when a large number of measurements are required to characterize the combined effects of inherent and management-induced spatial variability of these properties in a field (Ahuja & Ma, 2002). In the absence of measured data, hydraulic properties may be estimated conveniently using indirect methods from surrogate data that can be more easily measured or that are already available, such as soil texture, organic matter and bulk density. Such functions are usually referred to as pedo transfer functions (PTFs). However, owing to the empirical nature, predictions will be less reliable for conditions that are different to those for which the PTF was developed. The reliability or uncertainty of the PTFs is an important issue, as most PTFs are based on data sets containing sparse values, noise, and sometimes ambiguous data

that may yield parameter estimates covering a large confidence interval (Dane & Topp, 2002). Hence, the applicability of PTFs should be carefully considered and proved for individual cases.

1.1.3 Problems in modeling soil-root interactions

Another important soil-plant process that can be affected by heterogeneous soil conditions is the root growth. Although modeling growth and development of the aboveground crop biomass has been the main focus for decades, modeling of root growth and function has been simplified in most crop models (Wang & Smith, 2004). This historical neglect of a root growth model is mainly due to **(1)** the difficulty in investigating roots as they cannot be readily observed in soils (Skaggs & Shouse, 2008), and **(2)** the simplified assumptions of root behavior can mostly meet the requirements for crop growth simulation under homogeneous and unlimited conditions (Gregory, 2006; Wang & Smith, 2004). In the last decade, the importance of understanding the roots and their functioning in vadose zones has attracted more and more attention (Gregory, 2006; Pages *et al.*, 2000; Skaggs & Shouse, 2008; van Noordwijk & van de Geijn, 1996; Wang & Smith, 2004). In particular, when the spatial heterogeneity in agricultural fields needs to be taken into account in the crop growth modeling, a better understanding and a more adequate description of the root system and its interactions with different soil conditions are urgently required in order to quantify the differences in resource acquisition due to the site specific heterogeneity (Darrah *et al.*, 2006; Hopmans & Bristow, 2002).

Other than the constant and uniform behavior of root growth assumed in most models, in reality the root system is the response of the plant to the heterogeneous distribution of resources and soil constraints. A number of studies have documented the effects of environmental heterogeneity on root growth and root distribution, e.g. Doussan *et al.* (2003); Fitter & Stickland (1991); Fitter *et al.* (1991); Hutchings & John (2004); Pierret *et al.* (2007); Wang & Smith (2004). The most discussed environmental factors are soil temperature, soil water, soil aeration, high soil strength (hardness), soil structure, soil nutrient conditions (such as nitrogen and phosphorus), and soil microbiological conditions. However, besides the effect of soil temperature, soil water and soil nitrogen, little study has been carried out to quantify the stress effect of other factors on root growth. As a result, most root models are not responsive to the environmental factors, or

take into account only the stress effects of soil temperature, soil water and soil nitrogen, such as the subroutine of root growth in CERES. In addition, Aiken & Smucker (1996) and Hodge (2004) addressed the issue that the heterogeneous soil conditions not only restrict root growth, but also stimulate the plastic response of the root system to adapt to the environment. This adaptivity of root growth is rarely considered in the current root models. Thus if high soil heterogeneity is present within a field, neglecting the impact of heterogeneous soil conditions on root growth may lead to incorrect simulation of root distribution, which affects the simulation of root uptake and hence crop yield. In this case, the objective of applying a simulation model to identify the cause of the crop yield variability cannot be met. Therefore, extending our knowledge of the soil-root interactions for the application of crop models to precision agriculture management in an urgent issue.

1.2 Aim of this work

1.2.1 Current problems, hypothesis and objective

In this thesis, the variability of crop growth on an experimental area of field scale was studied by means of modeling the interactions of soil-root-crop. In the field experiments at the research farm Scheyern in Bavaria, Germany ($Long.11°27'E, Lat.48°30'N$), crop growth variability as well as high soil heterogeneity were observed within a field (Sinowski & Auerswald, 1999; Sommer *et al.*, 2003). Previous research by Sommer *et al.* (2003) indicated that the observed spatial crop growth variability was probably caused by an inadequate supply of water, which resulted in water stress in some places, and a deficit of O_2 in other places. The water uptake by crop roots is determined by the interactions between the soil water flow and root distributions, both of which are strongly influenced by the soil heterogeneity and climate conditions. As nitrogen fertilization has been applied at the site and no marked disease of the crop was observed, we hypothesize that the following relationships (Fig.1.2) between environmental factors and crop growth govern the crop growth variability in the study field.

The objective of this work is to explain the within-field crop yield variability by improving the quality of the soil water balance simulation as well as by improving modeling of the soil-root interactions. To understand the influence of soil and

climate on crop growth, the following relationships were analyzed by both field observation and model simulation:

1. Impact of soil and climate on resource (water, nitrogen) availability.

2. Impact of soil, resource availability and crop species on root distribution.

3. Impact of resource availability and root distribution on crop growth.

Firstly, the heterogeneity of the soil properties and soil water content as well as the variability in root distribution and crop yield in the field were characterized by field observation. Secondly, the hypothesized relationships between soil, soil water, root growth and crop growth were analyzed by simulation experiments using the model package Expert-N (Priesack, 2006). By comparing an estimation of the hydraulic parameters from infiltration data in the field and the estimation by different PTFs, the most appropriate approach to the hydraulic parameterization was chosen for the study field. Based on the observed root length density (RLD) distribution in the field, a new root model was developed and linked to the existing crop models –CERES Maize proposed by Jones & Kiniry (1986) and CERES Wheat by Ritchie & Godwin (1989). Finally, the capabilities of the simulation of crop growth variability for the original CERES and the modified CERES+ by adding the new root growth model were compared.

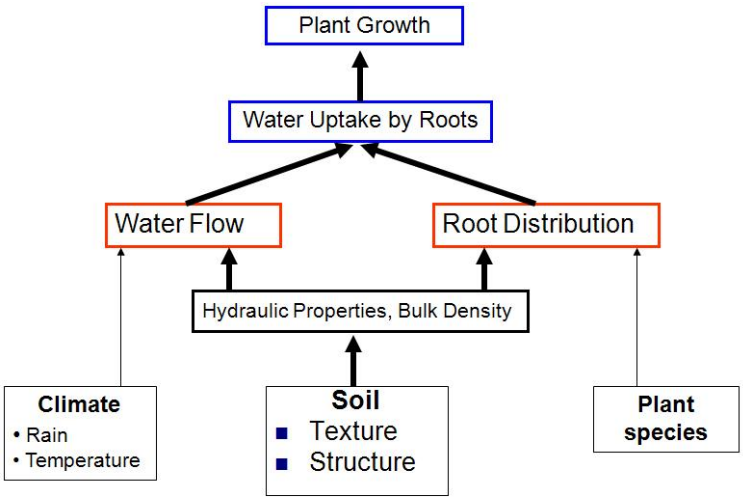

Figure 1.2: Hypothesized relationships between environmental factors and crop growth in the study field.

1.2.2 Outline

This thesis is divided into seven chapters as follows: In **Chapter 1**, the background, the problem and the objective of the study are introduced, followed by a brief outline of the thesis. In a review of the problem, a general introduction to the application of crop models for precision agriculture, the current challenges in the parameterization of the water flow model and the oversimplification of root modeling are presented.

The major discussion begins in **Chapter 2**, on field observation. Here the background of the research field, the methods and the materials used to measure the soil properties, soil water content, crop root distribution and crop growth are described, with special focus on the root distribution investigation. After this, the results are presented and the relationships between soil, climate and crop/root growth are discussed based on the observations.

Chapter 3 switches to the first part of the simulation work with a focus on the parameterization of the water flow model. Here the background of the water flow model, the methods for the estimation of hydraulic parameters, and the simulation environment Expert-N are initially introduced. In the "materials and methods", details of the method for the infiltration experiment, the mathematical formulations of the hydraulic functions and the pedo transfer functions used are presented. Next, the results for the estimation of the hydraulic parameters, the simulation of soil water content and crop yield using different hydraulic parameter sets are presented and compared.

Chapter 4 contains the second part of the simulation work with the focus on the development and validation of a new root model. The mathematical formulations of the new root model are described. Simulation results of the impact of two root models on the crop growth simulation are then demonstrated.

Chapter 5 is the last part of the simulation work, focusing on the application of the calibrated crop model to simulate the crop variability in the field. By comparing the observed and simulated crop yield at 13 grid points of the study field over three years, the improvement to the modified CERES model to simulate the crop yield variability is demonstrated.

A general discussion and a brief conclusion can be found in **Chapter 6**. Here the interactions between soil, climate, root and crop are discussed based on the field observation and computer simulation. The relevance of the use of the crop model for precision agriculture is indicated.

Chapter 7 is the closing chapter, which contains a summary of the study.

In **Appendix A**, some of the raw data of the field experiments are given.

Chapter 2

Field observation of soil properties, soil water content, root distribution and crop growth

2.1 Introduction to the study site

The field work was conducted in a tertiary hilly landscape located 40 km north of Munich, Germany ($Long.11°27'E, Lat.48°30'N$). Climate is characterized by a 30-year mean annual precipitation of 803 mm and a 30-year mean annual temperature of $7.4°C$ (Sommer *et al.*, 2003). The study field named A15 (4.5 ha) has been cultivated under integrated management with moderate tillage and fertilization. Since 1993, crop rotation consisting of **winter wheat** followed by **maize**, **winter wheat** and finally **potato** has been applied in this field.

The field A15 is characterized by highly heterogeneous underground materials derived from the tertiary and quaternary periods. The tertiary sediments, as the parent material in the underground, consist primarily of sand with a varying content of gravel. Clay lenses are occasionally embedded. Up to 3 m loess cover developed in the Quaternary can be found on gentle east-facing slopes, while loess is missing on the steeper west-facing slopes probably due to erosion. A large variation within the soil properties resulted from the wide range of parent materials, the hilly relief and the diverse land use (Sinowski & Auerswald, 1999; Sommer *et al.*, 2003). After intensive analysis, Sommer *et al.* (2003) divided the field into eight soil patterns (Fig. 2.1).

In addition, high spatial variability in crop growth was also observed in this field. Fig. 2.2 shows the high-resolution wheat yield maps observed in 1994 and

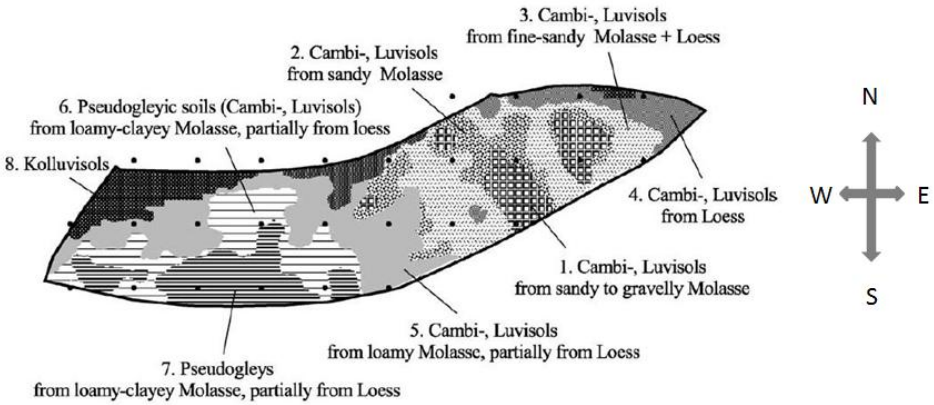

Figure 2.1: Soil map units of the field A15. Cited from Fig. 11 of Sommer *et al.* (2003).

2000, the maize yield map from 1997, and also the total rainfall in the vegetation period of the respective year. On these yield maps, the green color class indicates yield value ≤ 4.0 [t/ha], the yellow color class indicates yield value between 4.0 and 7.0 [t/ha], and the red color class indicates yield value ≥ 7.0 [t/ha]. The two wheat yield maps are from contrasting climatic conditions that 1994 had much lower rainfall than 2000. But the maps show similar crop yield patterns at the field in spite of the significant different climate condition in the two years. The low-yield pattern in green are found at the east side and the south-west side of the field in both years. Similarly, the reappearance of high-yield-patterns represented by the red color were observed at the north side of the field. If we compare the wheat yield maps with the soil map (Fig. 2.1), we can find that the distribution of the yield patterns are related to the soil patterns. The low-yield-patterns at the east side of the field are related to soil type 1 defined by Sommer *et al.* (2003) (Cambi-, Luvisols consisting of materials from sandy to gravelly Molasse). Another low-yield pattern at the south-west side are related to soil type 7 (Pseudogleys consisting of materials from loamy-clayey Molasse, partially from Loess). The high-yield patterns are related to soil types 8 and 4 (Kolluvisols and Cambi-, Luvisols from Loess).

Beside these stable patterns it is interesting to see two patterns that change according to the weather conditions. One is located next to soil type 1 – soil type 3 (Cambi-, Luvisols from fine-sandy Molasse + Loess). The wheat yields at these locations belong to the medium class in the dry year 1994, but were

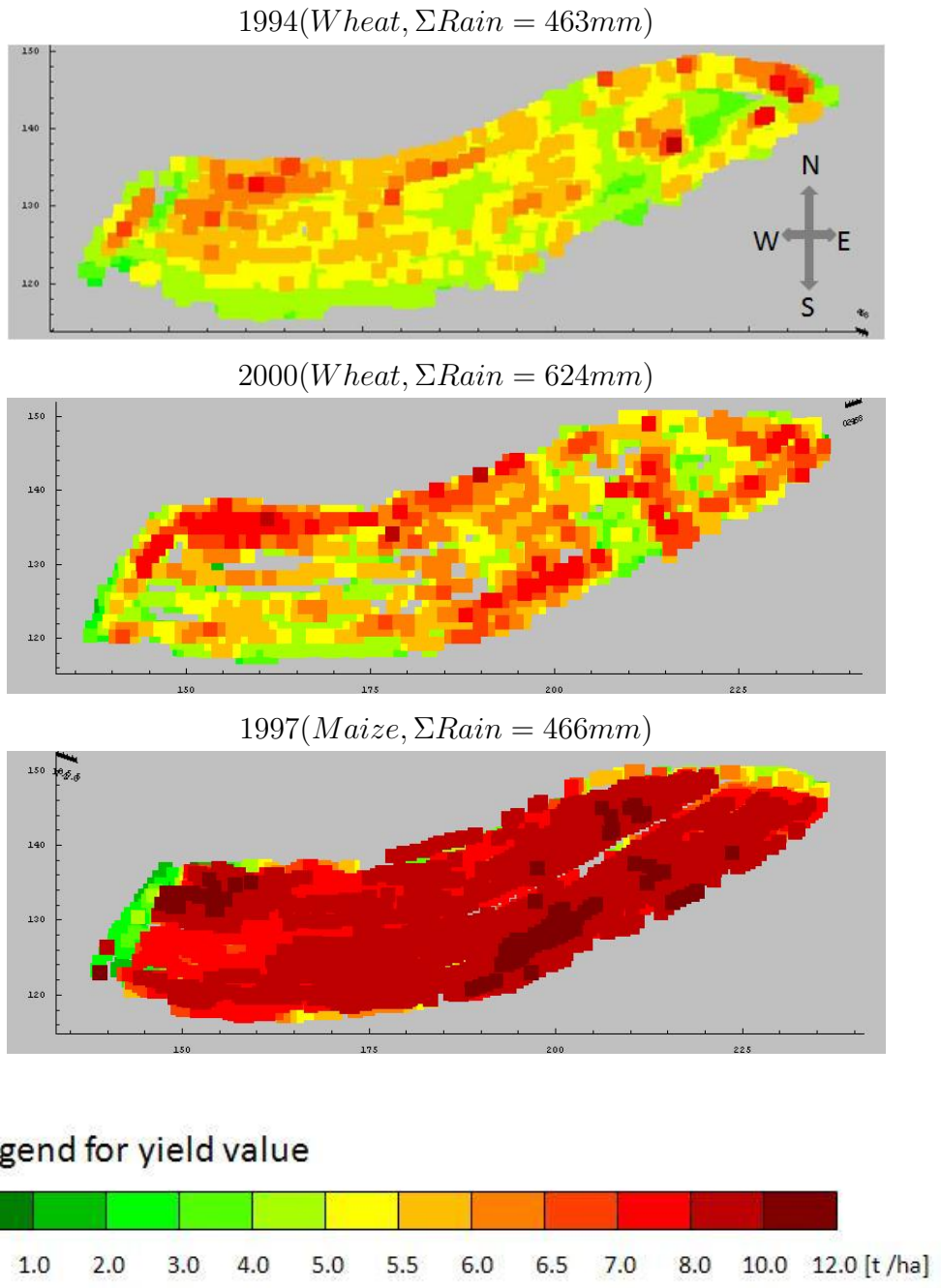

Figure 2.2: Yield maps of wheat in 1994 (top) and 2000 (middle) and of maize in 1997 (bottom).

significantly improved by the plentiful rainfall in 2000 to jump into the high yield class. The other pattern is located around soil type 7 – the soil type 6 (Pseudogleyic soils consisting of materials from loamy-clayey Molasse, partially from Loess). In contrast to the last pattern, the crop yields at these locations

were better in the dry year than in the wet year.

Compared with the wheat yield maps, the maize yield map shows a less noticeable yield variability pattern. High yield patterns are still found at the location of soil types 8 and 3. Other than the wheat yield, a pattern of yield decrease, which can be related to the soil patterns, was only shown at the locations of soil type 6. The sharp yield decrease at the west side boundary could be due to the edge effect.

In order to explain the observed crop yield variability in relation to soil, weather and species, four representative soil patterns were defined for the proposed study. The sampling locations are marked in Fig. 2.3, named S1, S2, S3 and S4. Plot S1 is located at soil tpye 3 according the definition by Sommer *et al.* (2003), plot S2 at soil type 1, plot S3 at soil tpye 6 and plot S4 at soil type 8. With respect to relief, plots S1 and S4 are located at a flat summit and depression, respectively. Plot S2 is located at a hillside facing north-east and S3 is located on another hillside facing south, both have steep slopes of over 12% (Tab. 2.1). The maize growth in 2005 and wheat growth in 2006 at these four plots were studied in detail. The field work is presented in this chapter.

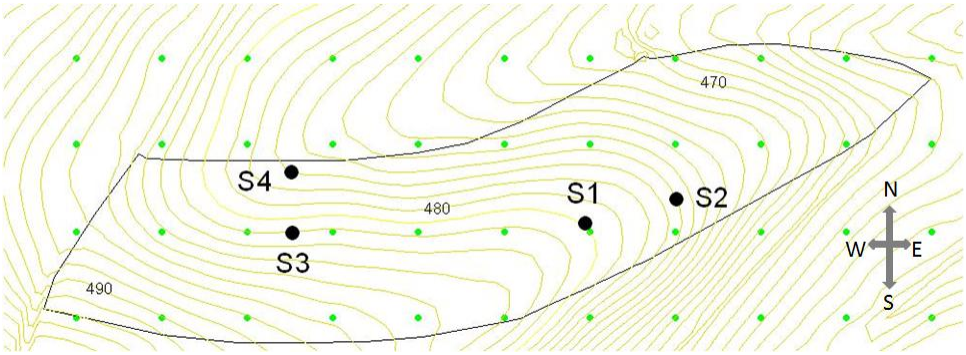

Figure 2.3: Elevation map of the field A15.

Table 2.1: General geographic information of plots S1, S2, S3 and S4 at field A15 of research farm Scheyern.

Plot	Landform	Slope	Altitude m	Exposition
S1	summit	5˜9%	481	NE
S2	side slope	12˜18%	477	NE
S3	side slope	9˜12%	482	N
S4	depression	2˜3%	477	NE

2.2 Materials and methods

In 2005, maize was sown on 12^{th} May and received 153 kg N/ha fertilizer on the next day. After harvesting the maize on 14^{th} November, winter wheat was seeded for the next growing season. In April 2006, most of the offshoots of the winter wheat were dead, which was assumed to be caused by the unusually late frost at that time. Therefore, the winter wheat was killed by Glyphosat and spring wheat was then immediately seeded on 21st April 2006. Up until the harvesting on 21^{st} August, the spring wheat was fertilized three times and received 150 kg N/ha in total. During the period of observation, the crops showed little evidence of weed infestation or diseases. The cultivation actions in 2005 and 2006 are listed in Tab. A.1 in the appendix.

2.2.1 Soil sampling and analysis

To characterize the four soil plots, soil samples were taken from soil profiles to a depth of 140 cm. The basic soil properties of soil texture, soil bulk density, organic matter content and the pH value of the soil were then determined in the laboratory according to the methods described in VDLUFA-Methodenbuch (2004).

Additionally, soil samples up to a depth of 90 cm were taken by an auger-set during the growing seasons 2005 and 2006 for the measurement of the soil water content. At each sampling place, the biggest auger of 14-mm diameter was used initially to take a sample from the top 30 cm of soil, another auger of 12-mm diameter was used for the 30-60 cm soil depth, and then the last auger of 10-mm for the soil from 60-90 cm was used. Considering of the local spatial heterogeneity in the field, three samples were taken per depth in each plot (i.e., nine samples per plot). All samples were stored in cooled camping boxes immediately after collection. The water content was determined by oven drying in the laboratory (Dane & Topp, 2002).

2.2.2 Investigation of root distribution in the rooting zone

Two methods were respectively used for the investigation of vertical root distribution in 2005 and 2006. The sampling of maize roots by harvest was carried out by hand auger up to 45 cm soil depth according to the method described by Böhm

(1979). This method is sufficient in the case of maize because of its flat rooting. Considering that the maize grew in rows, for each sampling location samples were taken from "at row", "mid-row" and "1/4 from the row", respectively (Fig. 2.4). Roots were then washed out from the bulk soil in the laboratory (Böhm, 1979). Clean roots were scanned with an Epson scanner (Seiko Epson corporation, Japan) and the root images were analyzed by the specific root image analysis program WinRHIZO pro 2003 (Regent Instrument Inc. Quebec, Canada). An example of the analysis of a root image by WinRhizo is shown in Fig. 2.5. In

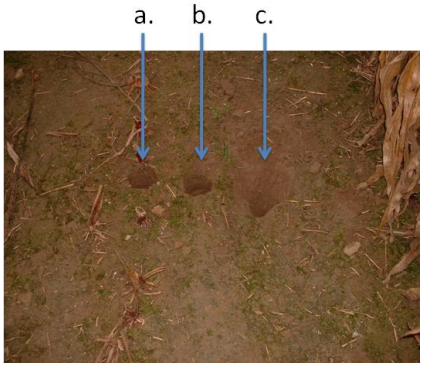

Figure 2.4: Sampling position for measuring the maize root distribution: a. at row; b. mid-row; c. 1/4 from row.

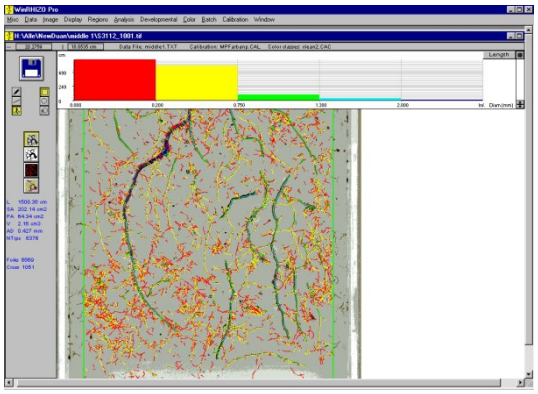

Figure 2.5: Interface of WinRhizo. In the middle displayed the root image. The grey background displayed the transparent Plexiglas tray filled with water which was used to spread the roots. Detected roots were marked by different colors according to the diameter. The root distribution graphic above the image displayed the root length as a function of root diameter.

principle, measurements are taken by detecting the number of pixels according to the color or grey level which are distinguishable from the background (Smit *et al.*, 2000). WinRhizo displayed the analysis over the image. The color used to draw the root skeleton indicates into which diameter class the part of the root had been classified. The same color was used for drawing the root distribution graphic above the image. The root distribution graphic displayed the root length, area, volume or number of tips as a function of root diameter or color). The number and the width of the classes were user-definable and can be changed at any time. The analysis of maize roots in this study, root diameter class of $0.0 \leq 0.2$ mm, $0.2 \leq 0.75$ mm, $0.75 \leq 1.3$ mm $1.3 \leq 2$ mm and ≥ 2 mm were chosen. In Fig. 2.5, maize roots were swimming in a transparent Plexiglas tray filled with water which displayed the grey background. The finest roots were marked by red color, and the biggest roots by blue color. Measurement data of the sample under analysis were summarized on the left side of screen and were available in detail in data files. By this means, root length, root surface area, root volume and average diameter were estimated.

For the root measurement of spring wheat at maturity, the Soil-Root Profile method (Böhm, 1979) was used in order to obtain an overview of the wheat root system in the deeper soil up to 1.5 m (Fig. 2.6). In the field, four soil pits were

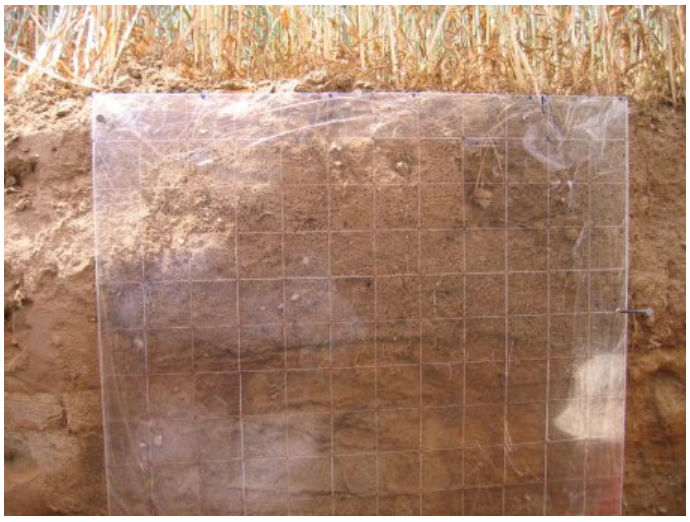

Figure 2.6: Mapping the roots in the field.

dug in the four study plots S1 to S4, respectively. Roots of a soil wall in cross-section to the crop row were exposed by washing using a hand sprayer (High pressure sprayer, Gloria 142 T Spezial, Rasenmäher Wendik Gmbh, Germany).

The thickness of the washed soil was controlled to be 5 mm, so that the soil volume of a given surface area at the profile wall could be traced back. The roots were then mapped on a foil with the help of a Plexiglas frame, which was scribed with square grids of 5 x 5 mm (Fig. 2.6). The roots were mapped by dots, each dot on the map corresponding to one root of 5 mm length at the profile wall. Roots within each grid were counted in the laboratory and the root length density was calculated.

2.2.3 Crop sampling and analysis

Sampling In 2005, maize samples were taken by harvest. In 2006, spring wheat samples were taken four times during the growing season. These were at 47, 67, 86 and 119 days after sowing, respectively. The last sampling was carried out during the harvest. In order to obtain representative measurements, four samples were taken from each plot. For maize, "each sample" refers to a bond of maize plants that were cut from a 2-meter long maize row. For spring wheat, the samples were cut from a 1-meter long crop row. The land surface for each sample can then be calculated using the length of the cut crop row and the row distance.

Measurement Dry weight biomass and yield were determined by oven drying. For measurement of the carbon and nitrogen content, the dry green plant and corn samples were milled into powder. About 1.5 mg of the crop sample was weighed in a tin (Sn) capsule, and the carbon and nitrogen contents were then estimated by Elementary Analysis Measurement. The samples were burned in an Elemental Analyzer EURO EA (Eurovector, Milan, Italy). The sample stored in the auto sampler was dropped into a tube filled with catalyst and heated at 1000°C, and then combusted completely at temperatures of up to 1700°C. The process was carried out under an excess of oxygen to achieve complete combustion using helium as the gas carrier. After combustion, CO_2, NO_x, and H_2O were produced. The gas stream was then passed through a tube filled with Cu at a lower temperature of 600°C. The Cu and the remaining O_2 favour a redox reaction where NO_x is reduced to N_2. The Elemental Analyser was coupled to a gas chromatography (GC) isotope ratio mass spectrometry (MS) (Finnigan MAT DeltaPlus) where C is measured as CO_2 and N as N_2.

Beside the biomass, the LAI of spring wheat was determined for two of the samplings. For the determination of LAI, 25 wheat plants were randomly chosen

and their leaves cut off from each sample (1-meter-long wheat bond). Then the leaves were then scanned by an EPSON scanner at a resolution of 300dpi (Fig. 2.7 shows some examples). The area of the leaves was estimated by an Image Analyze Program SigmaScan (Systat Software Inc.). The mean leaf area and standard deviation of one plant were calculated based on four replications. The mean land surface for one plant was derived from the seeding density.

$S1$ $S2$ $S3$ $S4$

Figure 2.7: Scanned images of wheat samples for LAI-Estimation.

2.2.4 Weather data

Daily weather data, such as precipitation, global radiation, maximum and minimum air temperature, wind speed and relative air humidity, were taken from one of the national weather station network of Bavaria, the weather station at Voglried. The station is located in north-east direction about 3 km away from the study field A15 (Fig. 2.8).

Figure 2.8: Location of the weather station Voglried and the field A15.

2.3 Results

2.3.1 Physical and chemical properties of the soil

Large differences between the four plots are indicated by the determination of the basic physical and chemical properties of the soil. Fig. 2.9 shows the soil profile overview of the four plots and Fig.2.10 shows the measured soil texture, bulk density (BD), and organic carbon content (C_{org}).

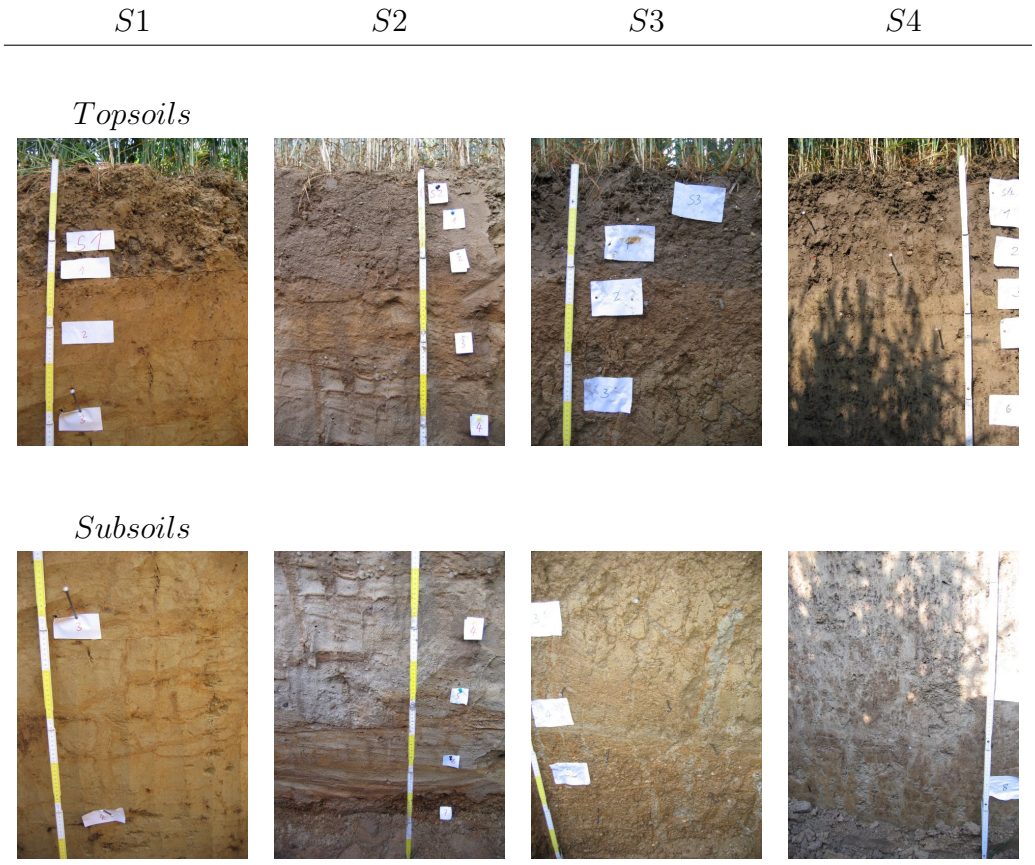

Figure 2.9: Photographs of soil profiles of plots S1, S2, S3 and S4. The four photographs at the top show the top soils, those at the bottom show the sub-soils.

In general, much larger differences are found in the sub-soils below a depth of 30 cm than in the surface soils.The most obvious difference is found in the **soil textures** (Fig. 2.10, left charts). Plot S2 is dominated significantly by sand particles. The sand fraction ranges from 65 to 85% in the top 30 cm depths and

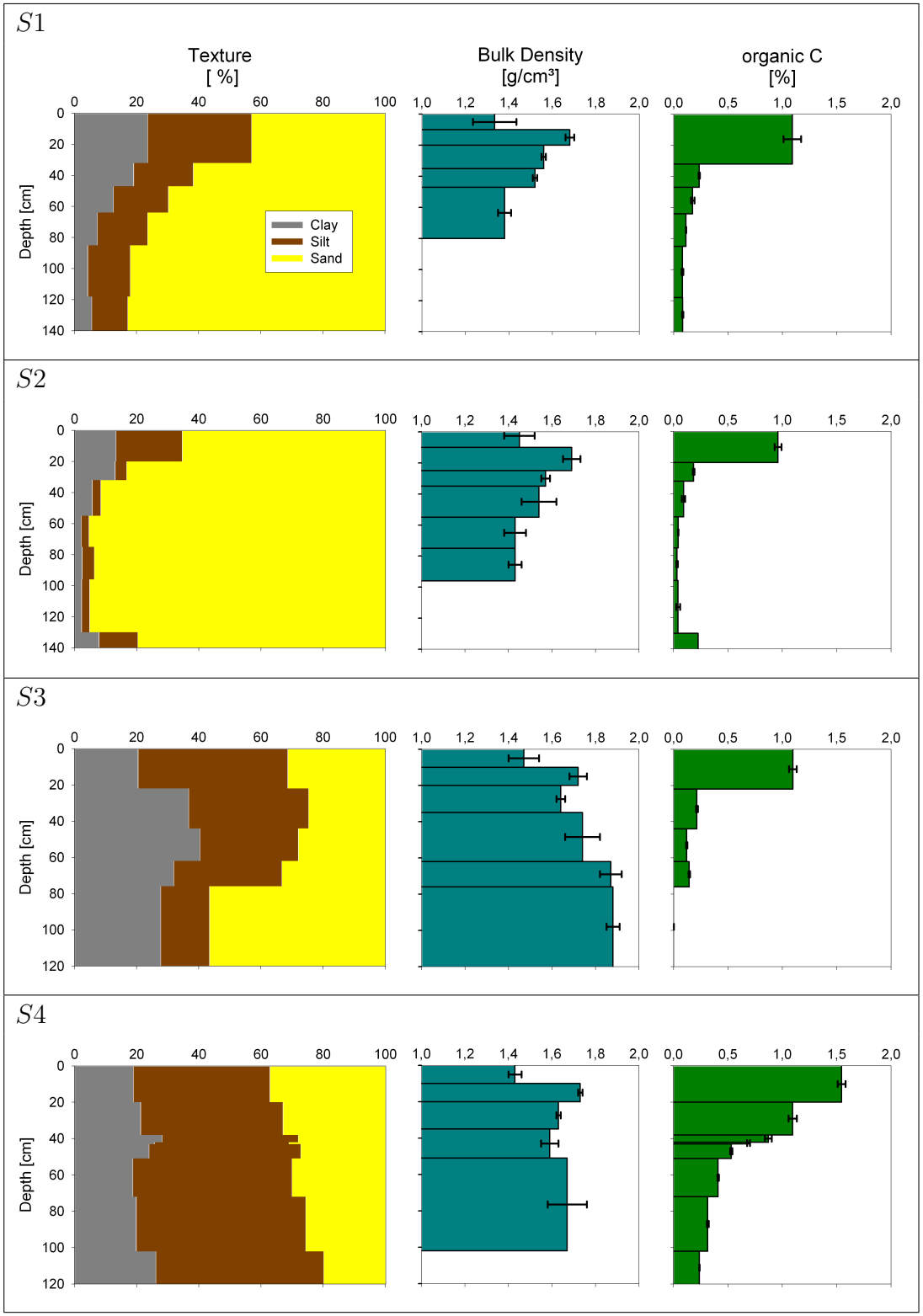

Figure 2.10: Soil texture, soil bulk density and soil organic carbon content in the soil depths of plots S1, S2, S3 and S4.

it increases to over 90% in the depths at 30 -130 cm. High sand content is also observed in plot S1, but the amount is not as high as in plot S2. Its sand fraction is ca. 60% in the top 30 cm soil depth and increases gradually to 80% beneath the 90 cm depth. In comparison with the two sandy plots, plot S3 and plot S4 are more similar in texture with respect to their higher clay content. A high clay fraction is especially noticeable in plot S3. The average clay fraction at a depth of 20 -120 cm in this plot is 35%. The highest clay content of 40% is observed at the 45 -65 cm depths. Plot S4 features a high silt fraction of 50%, on average for the whole 120 cm depth, while the remaining 23% consists of clay and 27% sand. Besides the fine fractions, a **coarse fraction** with particle sizes larger than 2 mm is also determined for the same soil horizons. Noticeable gravelly zones are observed beneath a depth of 75 cm in plot S3 for a 52% weight fraction, beneath a depth of 130 cm in plot S2 of 5% and at the 42 -43 cm depth in plot S4 for 9% fraction. In other soil horizons, there are generally more coarse particles observed in plot S4, with fractions ranging from 3 to 5%. This is about 3% in the top 75 cm depth of plot S3 and about 2% in the top 130 cm depth of plot S2. No more coarse fractions are found in the remaining horizons of plot S1 except for a 2% rock content in the top 30 cm depth.

In addition to the difference in the composition of the soil particles, specific characteristics are also observed with respect to **soil bulk density** (BD), **soil organic matter content** and **soil pH**. The soil BD is generally lower in the sandy soils than in the clayey soils (Fig.2.10, middle charts). The value of 1.88 [g/cm^3] at the 70 cm depth of plot S3 is unusually high for agriculture soils. It is also remarkable that a dense horizon at 10 -20 cm depth is found in all soil plots having a BD of about 1.65 [g/cm^3]. The soil organic carbon content is overall highest in the surface soils to a 20 cm depth (Fig.2.10, right charts). Among the four plots, plot S4 has noticeably higher C_{org} than the other plots and the C_{org} in plot S2 is slightly lower than plots S1 and S3. The pH value of the surface soils down to a 20 cm depth ranges from 5.5 to 5.8 in all plots. The pH value in plots S2 and S4 remains at 5.8 in the sub soils, whereas the pH in the sub soils of plot S1 drops to 4.7 and 4.3, and in plot S3 to 4.4 and 4.1.

2.3.2 Soil water content

2.3.2.1 Climate conditions

Daily temperatures and precipitation for the growing seasons of 2005 and 2006 are presented in Fig.2.11. Compared with 2006, 2005 was a precipitation-rich year.

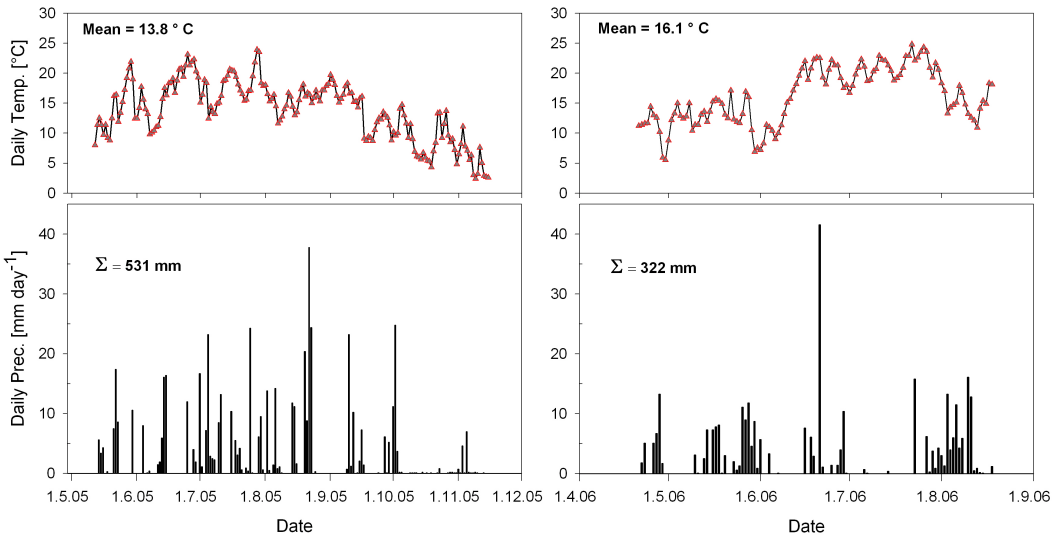

Figure 2.11: Daily temperatures and precipitation in the growing seasons of 2005 (left) and 2006 (right).

Its annual precipitation was 897 mm, which was 12% higher than the 30-year mean of 803 mm. The annual precipitation of 2006 was 759 mm. The vegetation period of 2005 (from 12^{th} May to 12^{th} Nov.) received 59% of the annual rainfall (i.e., 531 mm). These rainfall events were uniformly distributed over the whole period, except for a dry period from 25^{th} Aug. to 8^{th} Sep. (Fig. 2.11, left). The total rainfall over the vegetation period for 2006 (21^{st} Apr. to 15^{th} Aug.) was 322 mm, 42 mm of which were contributed by the heavy rainfall on 21^{st} June. There was a long dry period from 30^{th} June to 22^{nd} July in that year (Fig. 2.11, right). The mean air temperature in the growing season of 2005 was $13.8°C$, while 2006 had a $2°C$ higher mean air temperature of $16.1°C$ during the vegetation period.

2.3.2.2 Soil water content

The measured SWCs for each sampling in 2005 and 2006 are presented in Fig.2.12 and the mean SWC for each year are presented in Fig. 2.13. In general, the

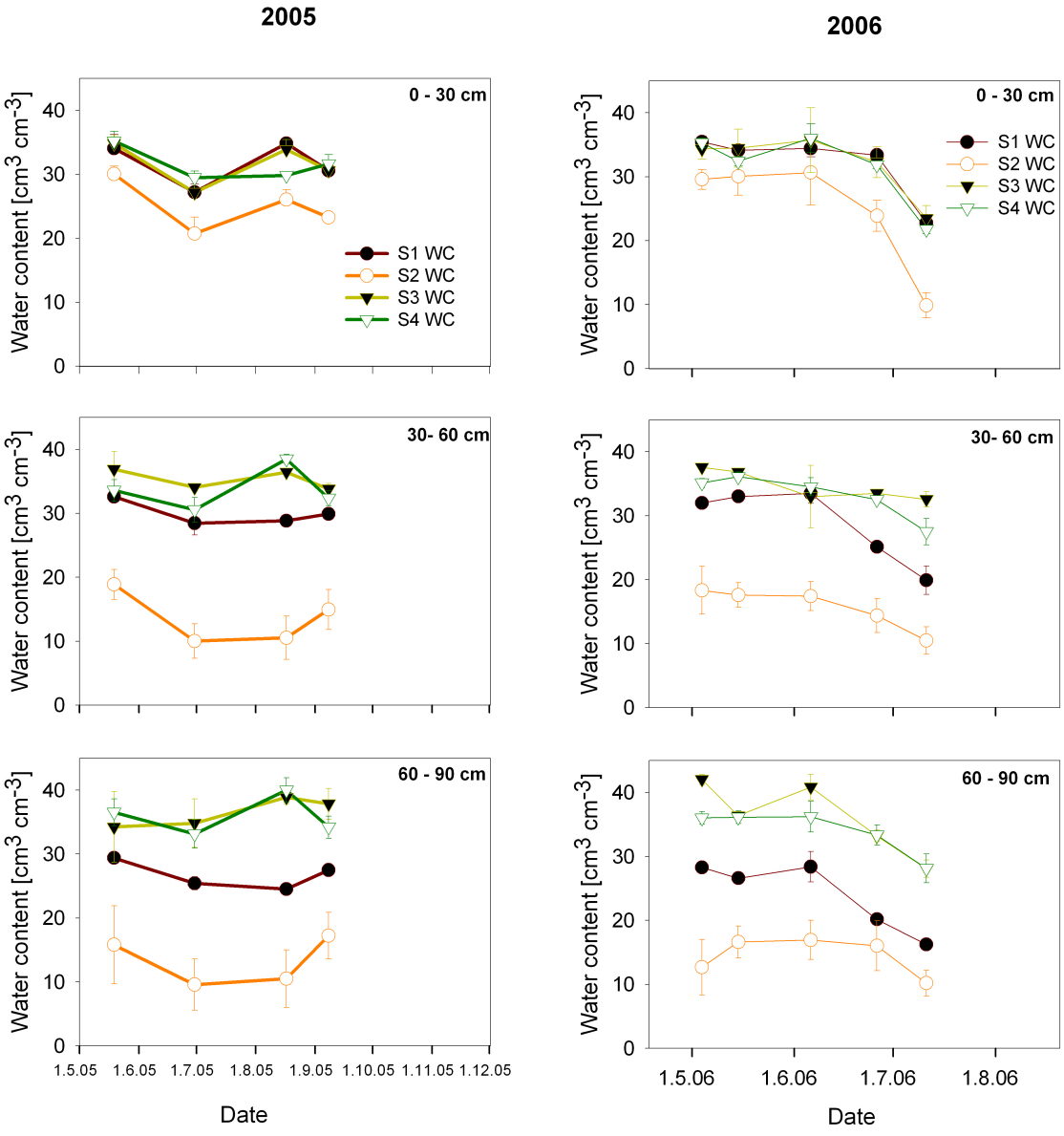

Figure 2.12: Soil water content observed at 0 -30, 30 -60 and 60 -90 cm soil depths in growing seasons 2005 (left) and 2006 (right).

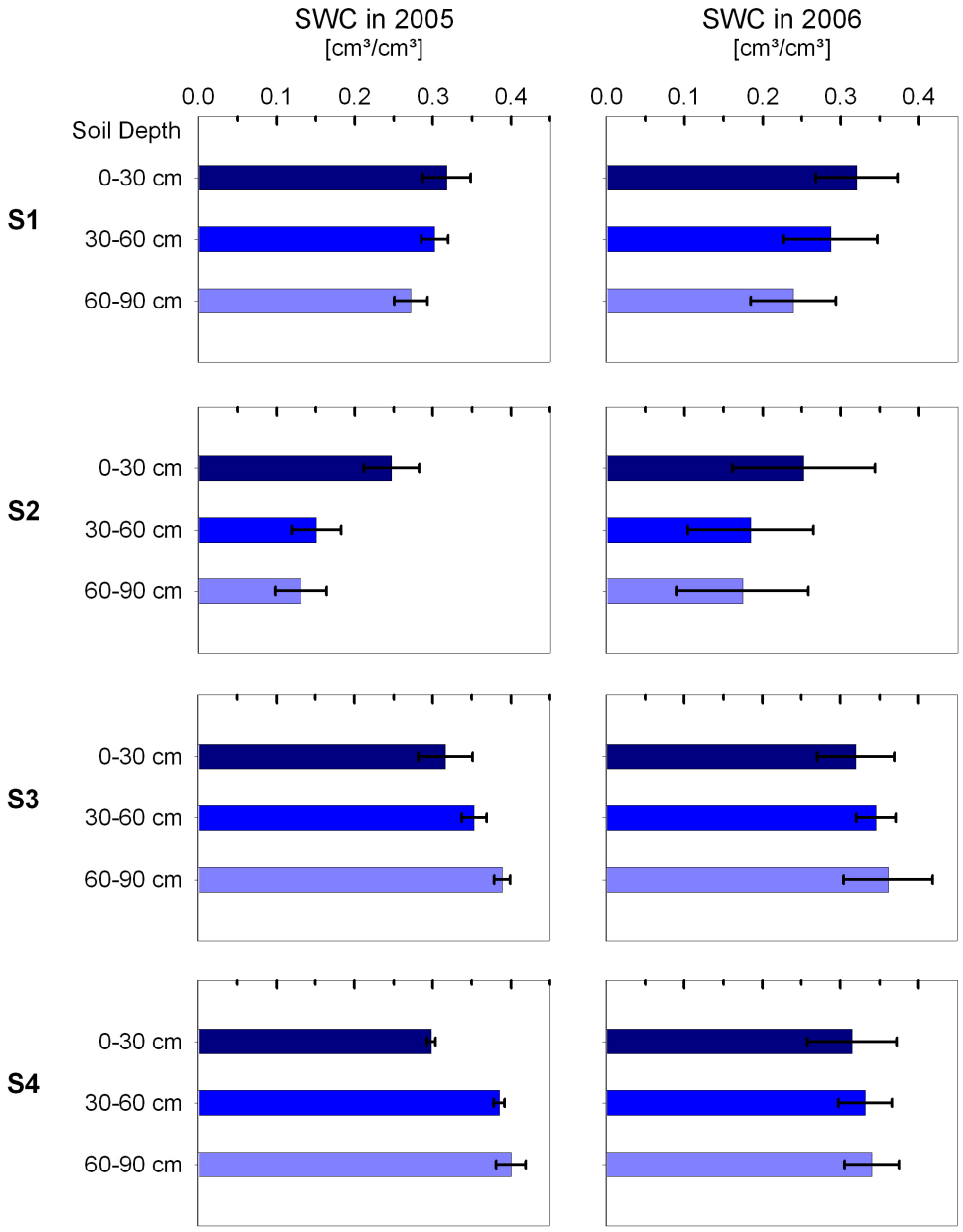

Figure 2.13: Average soil water content at 0 -30, 30 -60 and 60 -90 cm soil depths in growing seasons 2005 (left) and 2006 (right). Charts and error bars represent the means and the standard deviations, sample numbers n=15.

difference between the plots is more significant than that between the years. The mean SWCs at a particular depth for a particular plot are fairly close in both years, except that the standard deviations (SD) in 2006 are higher than those in 2005. The difference in the weather conditions seems to affect only the fluctuation in the SWC. A comparison between the plots shows that there is generally more water stored in the clayey plots S3 and S4 than in the sandy plots S1 and S2. Additionally, the SWCs in plots S1 and S2 decrease with the soil depth, whereas the SWCs in plots S3 and S4 are higher in the two sub soil depths than in the surface soil depth. Plot S2 is obviously the driest one and plot S3 the wettest one. For each sampling, the SWCs in the 0 -30 cm of S2 are about 20% lower than those of S3 and in the two sub soil depths are even lower by 50-70%.

2.3.3 Root distribution in rooting zone

2.3.3.1 Maize root distribution in 2005

Root Length Density (RLD) The absolute maize RLD observed at harvest for three soil depths of the four plots as well as their relative distribution in those depths are compared in Fig. 2.14. In general, the RLD decreases with the soil depth. The highest absolute RLD is found at the 0 -15 cm depth of plot S2 (Fig.2.14, top). The mean value of 8.6 $[cm/cm^3]$ here is twice the mean RLDs at the same depth of plots S1, S3 and S4 of around 4.0 $[cm/cm^3]$. At a 15 -30 cm depth, the RLDs in the two sandy plots are about 2.0 $[cm/cm^3]$, which are double those of the clayey plots. At 30 -45 cm depths, the RLDs in plot S1 of 1.5 $[cm/cm^3]$ is higher than that in the other plots of around 0.6 $[cm/cm^3]$. The relative distribution of the RLDs in the three depths are similar in plots S2, S3 and S4, which is about 73%, 18% and 9% from the top to the bottom, respectively (Fig. 2.14, bottom). Following a different pattern, the RLD-distribution in plot S1 is 55%, 25% and 20% from the top to the bottom. This suggests that roots in plot S1 tend to grow more in the sub soil depths in comparison with the other plots.

Root Surface Area Density (RSAD) Compared to the RLD, the RSAD takes the effect of the root diameter more into account. The global trends between depths and plots showed by the RSAD are fairly similar to that shown by the RLD. The average RSADs of the four plots are 0.6, 0.15 and 0.08 $[cm^2/cm^3]$ for the three depths, respectively. The highest absolute RSAD is 1.0 $[cm^2/cm^3]$ at a

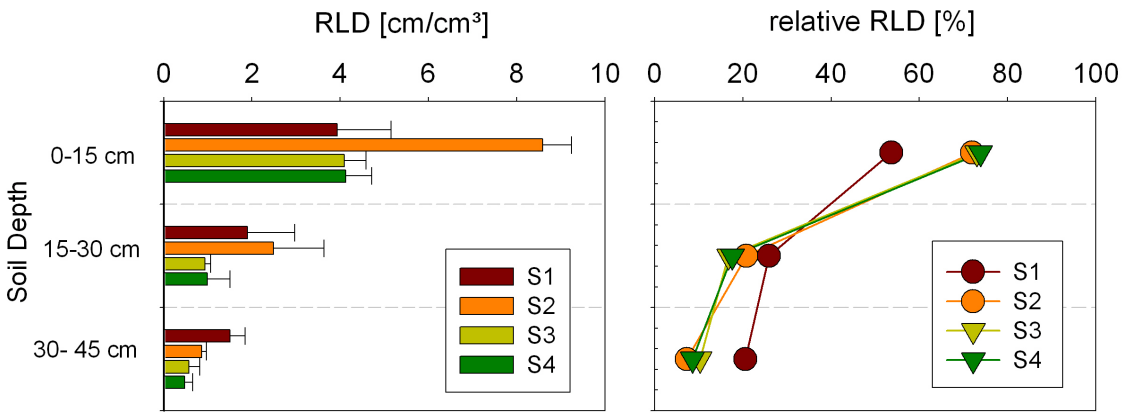

Figure 2.14: Root length density of maize observed at three depths for four plots at harvest in 2005 (left); relative distribution of root length density at three depths for four plots (right).

0 -15 cm depth in plot S2 (Fig. 2.15, left). By comparison of the four plots, it can be seen that the relative distribution in plot S1, which are of 53%, 27% and 20%, also differs from the other three plots, which are of 78%, 15% and 7%.

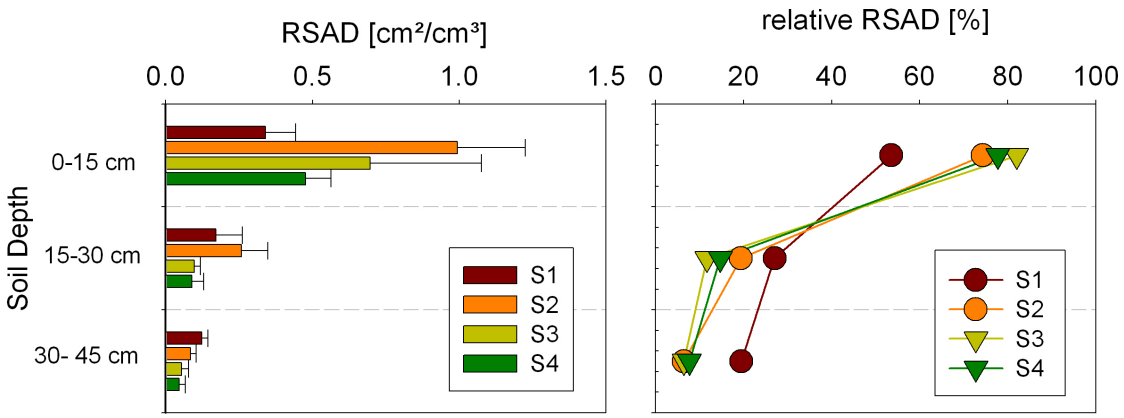

Figure 2.15: Root surface area density of maize observed at three depths for four plots at harvest in 2005 (left); relative distribution of root surface area density at three depths for four plots (right).

Root Biomass Density (RBMD) The average RBMDs of for four plots at three depths are 1.22, 0.22 and 0.09 $[g/cm^3]$, respectively. Just as is shown by

the RLD, the highest absolute RMBD is observed at a depth of 0 -15 cm in plot S2, the value of which is 1.9 $[g/cm^3]$ (Fig. 2.16, left). However, some differences from the RLD are found. The average fraction of the RBMD at the 0 -15 cm depth is 80%, which is 12% higher than for the RLD. This means that-, although nearly 80% of the root biomass is concentrated in the surface soil, this provides only 68% of the root length. This indicates that the roots in the surface soils have larger diameters than the roots in the lower soil depths. In respect to the relative root distribution, the difference between the plot S1 and the other plots is not so significant as is shown by the comparison for the absolute RLD (Fig. 2.16, right). This might indicate that the crop in plot S1 has increased the root length in sub soils by growing finer roots there.

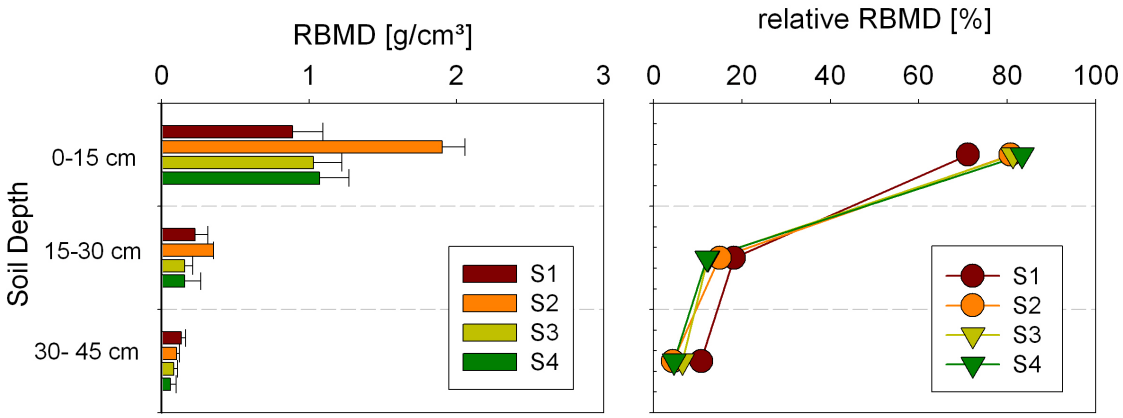

Figure 2.16: Root biomass density of maize observed at three depths for four plots at harvest in 2005 (left); relative distribution of root biomass density at three depths for four plots (right).

Specific Root Length (SRL) and Specific Root Surface Area (SRSA) Information on root diameter can be obtained by dividing the root length or root surface area by the root biomass, which results in the parameter SRL or SRSA. The larger the SRL or SRSA, the narrower the root diameter. In an opposite to the trend found for the RLD, RSAD and RBMD, the SRL and SRSA decrease with the depth (Fig. 2.17, Tab. 2.2). The difference between the surface soil horizons and the sub soil horizons is more significant than the difference between the subs soil horizons of the four plots. Between the four plots, there is little

difference at 0-15 cm, except that the SRSA in plot S3 is slightly higher. For the two sub soil depths, both the SRL and SRSA values are larger in plots S4 and S1 than in plots S2 and S3.

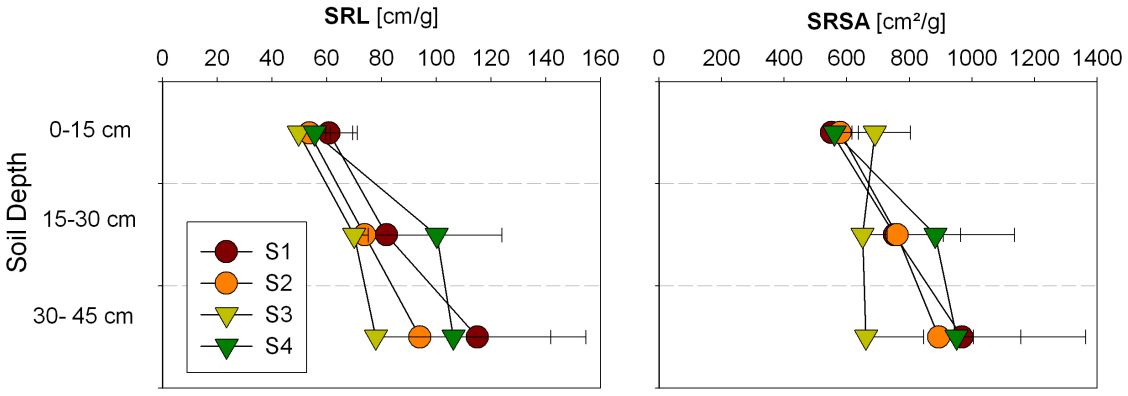

Figure 2.17: Specific root length of maize observed at three depths for plots S1, S2, S3 and S4 at harvest in 2005 (left); specific root surface area of maize (right).

Table 2.2: Mean specific root length and mean specific root surface area of maize root at different soil depths, n = sample numbers, SD = standard deviation.

		0-15 cm n=36	15-30 cm n=36	30-45 cm n=36	0-45 cm n=108
SRL	mean (SD)	55 (5)	81 (13)	98 (16)	78 (22)
SRSA	mean(SD)	595 (64)	761 (95)	868 (142)	741 (151)

2.3.3.2 Spring wheat root distribution in 2006

Root maps of spring wheat in the four plots can be found in appendix A (Fig. A.1, A.2, A.3 and A.4). Root length densities are summarized in the Fig.2.18. In general, the root density was highest in the top soil and decreased with the soil depth. The deepest maximal root depth is found to be 140 cm in plot S1 and S4. Among the four plots, plot S2 obviously has the shallowest root depth and roots are also the sparsest. The boundary of the main root system is at about a 30-cm soil depth. The average RLD within the 0 -30 cm soil depth is about

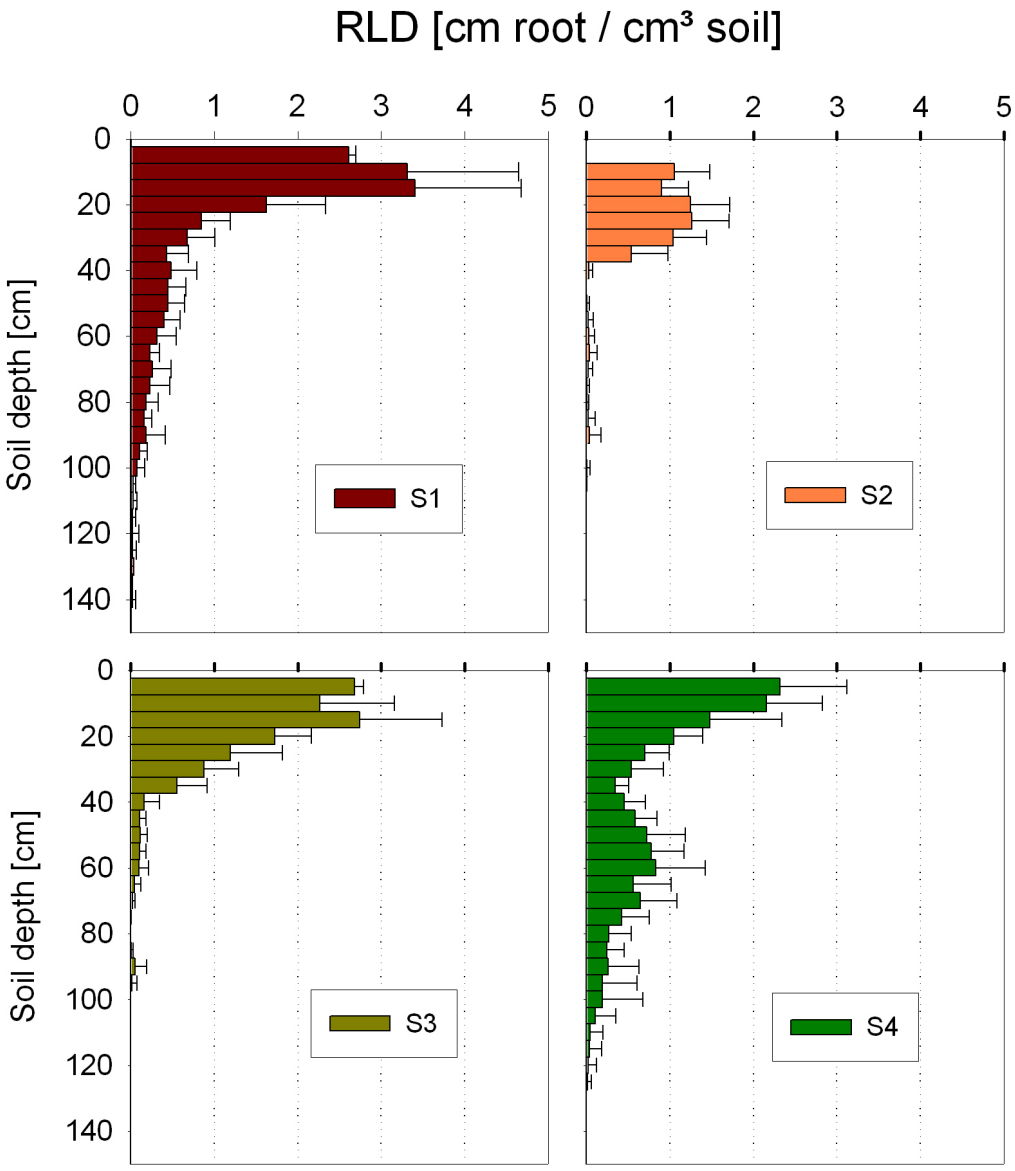

Figure 2.18: Root length density of spring wheat in plots S1, S2 ,S3 and S4 in 2006.

1.2 [cm/cm^3]. The second sparsest root system is found in the plot S3, although the RLD in the surface soil in this plot is actually slightly higher than that in the other plots. However, the RLD decreases dramatically from a depth of 40 cm downwards and the main root system ceases at about a 70 cm depth. Compared with other plots, roots distribute most homogeneously in the bulk soil of plot S1. The RLD in the first 20 cm depth is about 3.0 [cm/cm^3] and it decreases gradually down to the 140 cm soil depth. The roots in S4 are most plentiful. However, unlike the gradual gradient in S1, the RLD here decreases firstly from the top soil to the 40 cm soil depth, and then it increases again and reaches its second maximum at a 60 cm depth. The relative root length density in the 0 -140 cm soil depth is calculated in 30 cm intervals (Fig. 2.18 left and right). Most

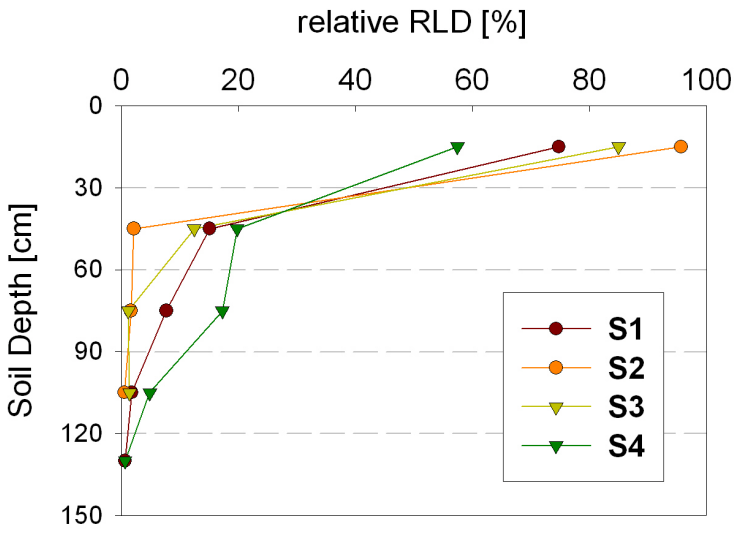

Figure 2.19: Relative distribution of root length density of spring wheat at three depths for four plots in 2006.

roots are located in the top 30 cm soil depth. For plot S2 and S3 in particular, the fraction in this zone is up to 95% in S2 and 85% in S3. In comparison, plots S4 and S1 have lower fraction here of 57% and 75%, respectively. The sequence is the converse in the sub soil depths. There are still 20% and 10% RLDs found for the 60 -90 cm depths of S4 and S1, while the value is only 1% in the plots S2 and S3.

2.3.4 Crop growth

2.3.4.1 Maize growth in 2005

First differentiation Maize was sown on May 12^{th}, 2005, and after 50 days, different growths of the maize in the four plots were observed (Fig. 2.20). The auger shown on the photographs is about 1 meter in height. Using this as a scale for a comparison of maize height, the maize plants in plot S4 are obviously the highest, followed by the maize in plot S1. The plants in plots S2 and S3 are only 2/3 the height of those in plot S4.

Figure 2.20: Photographs of maize plants at 50 days after sowing in 2005.

Dry total biomass and dry yield The measurement of the total biomass sampled by harvest shows that the lowest total biomass in plot S3 and the highest biomass in plot S4, which is only slightly higher than that in plots S1 and S2 (Fig.2.21, top). When considering the dry weight of the maize grain, the lowest value is also found in plot S3, while there is little difference between the other plots (Fig. 2.21, bottom). The last stack to the right side is the mean yield for A15, which is estimated from the total harvested grain. This agrees well with the mean value, which is estimated by the measured yield in the four plots (second to last second stack in the Fig. 2.21).

Water content of biomass Fig.2.22 shows the water content of the fresh biomass (left graphics) and the maize grain (right graphics). The level of dryness for the total biomass is similar for all plots. The water content of maize grain in plots S1 and S2 is lower than that in plots S3 and S4. The maize grain in plot S3 has the highest water content.

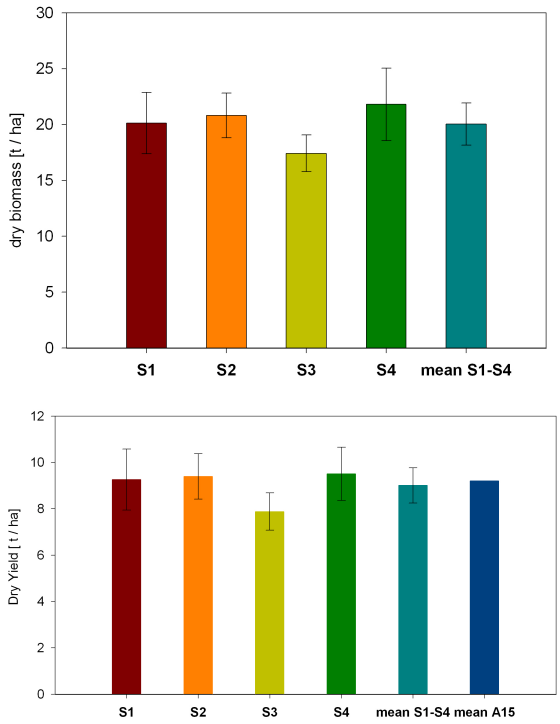

Figure 2.21: Total dry biomass and dry yield of maize by harvest in 2005.

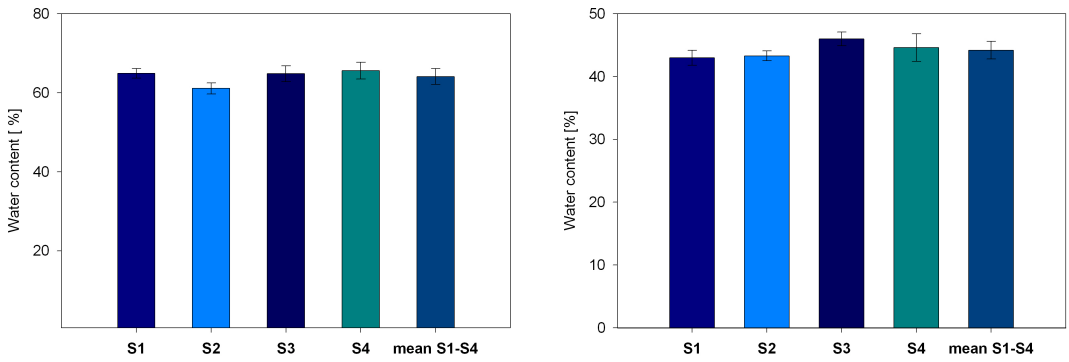

Figure 2.22: Water content of the fresh biomass (left) and the fresh maize grain (right) in 2005.

Carbon and nitrogen content of biomass The green parts of the maize and maize grain are measured separately for their carbon and nitrogen contents. The top graphics in Fig. 2.23 shows that the maize in plot S2 has a lower nitrogen content in the green part than the other plots. However, a similar nitrogen content

for the maize grain is observed for the four plots, except for the slightly higher content in plot S4. In contrast, the lowest carbon content in the green part is found for plot S4, while there is little difference between the other plots. There are also no significant differences for the carbon content of the maize grain. The lower nitrogen content in the green part of the maize in plot S2 leads to the higher C/N ratio (Fig.2.23, bottom).

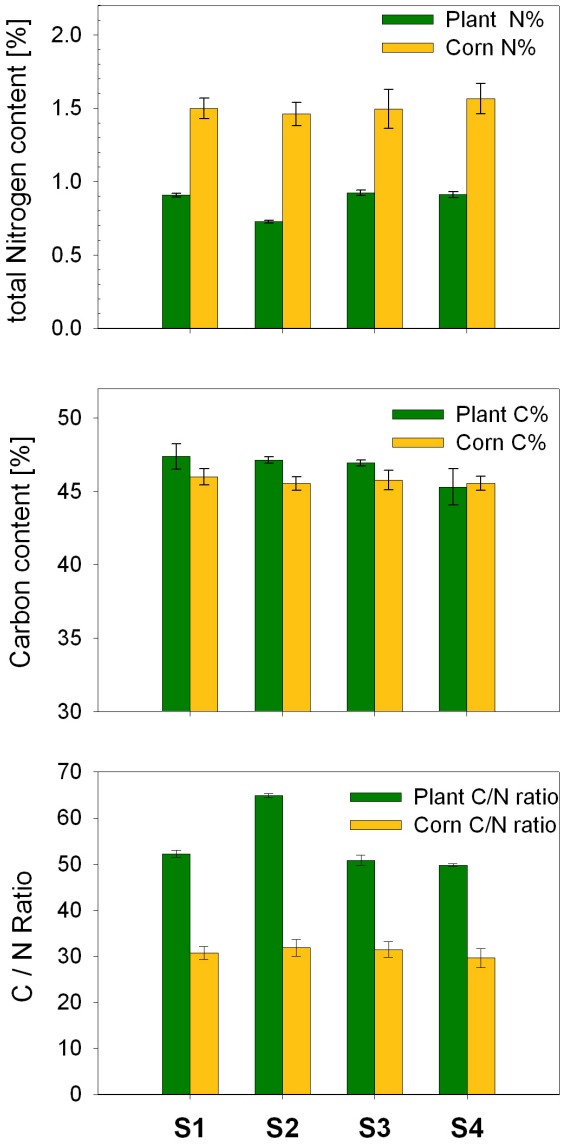

Figure 2.23: Nitrogen and carbon contents of maize at harvest in 2005.

2.3.4.2 Spring wheat growth in 2006

Compared with maize growth, a larger differentiation between the four plots for spring wheat growth is observed in 2006. The first differentiation in crop size is observed 31 days after sowing. On this day, the spring wheat in S4 is highest (by about 25 cm) and has broader leaves. Next is the wheat in S1, which shows a slightly sparser leaf-cover. The smallest wheat is found in S3, where the height is only about 16 cm. The crop in S2 does not show such noticeably reduced growth compared with that in S3, but it is of smaller size than that in S1.

Dry biomass and water content The trend S4>S1>S2>S3 is confirmed again by the measurement of biomass 47 days after sowing (Fig. 2.24, left-top). The water content of the biomass does not show any significant differences (Fig. 2.24, left-bottom). The samples of S2 are not drier than those of other plots. On

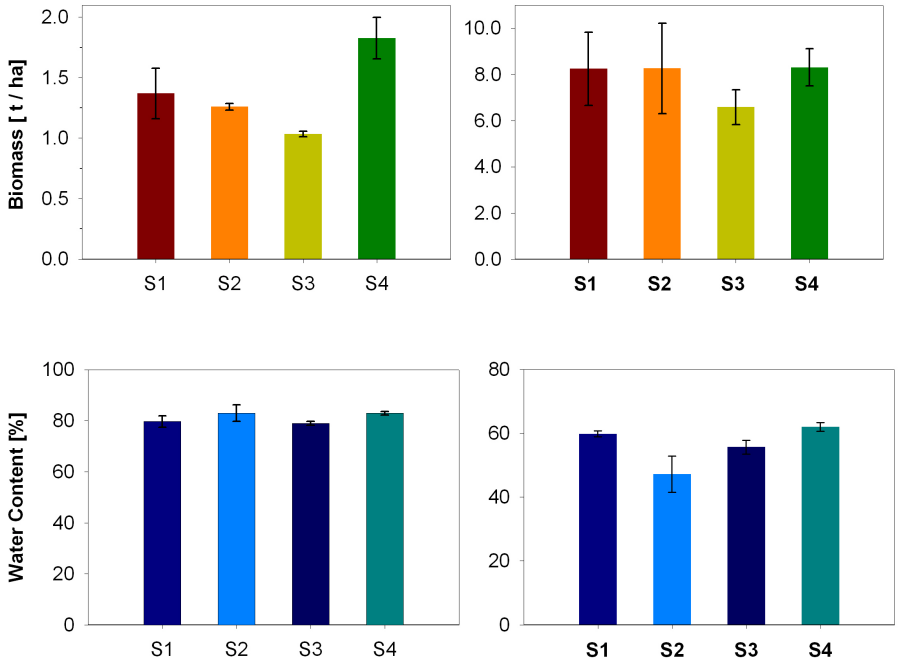

Figure 2.24: Total biomass (top) and water contents (bottom) of spring wheat in 2006 (left: 47 days after sowing; right: 86 days after sowing).

the contrary, they actually show a slightly higher mean water content. However, the second measurement of the biomass 86 days after sowing shows a different

trend (Fig.2.24, right-top). In this sampling, the wheat biomass in plot S3 continues to be the lowest one. The increase in biomass in plots S1 and S2 has caught up with that in plot S4. In comparison with the measurements in plots S3 and S4, the measurements in plots S1 and S2 show a larger standard deviation. In contrast to the similarity of the water content in the last sampling, it is noticeable that the water content in plot S2 has decreased (Fig.2.24, right-bottom).

Leaf area index (LAI) The difference in LAI 47 days after sowing agrees well with the observations for biomass on the same day, i.e. S4>S1>S2>S3 (Fig.2.25, left). Only the measurements in plot S2 show a high standard deviation. This trend has changed by the next observations taken 67 days after sowing (Fig. 2.25, right). This time, the LAI in S4 remains the highest and it is followed by that in S1. However, as opposed to the last time, S2 exhibits the lowest plant cover, instead of S3.

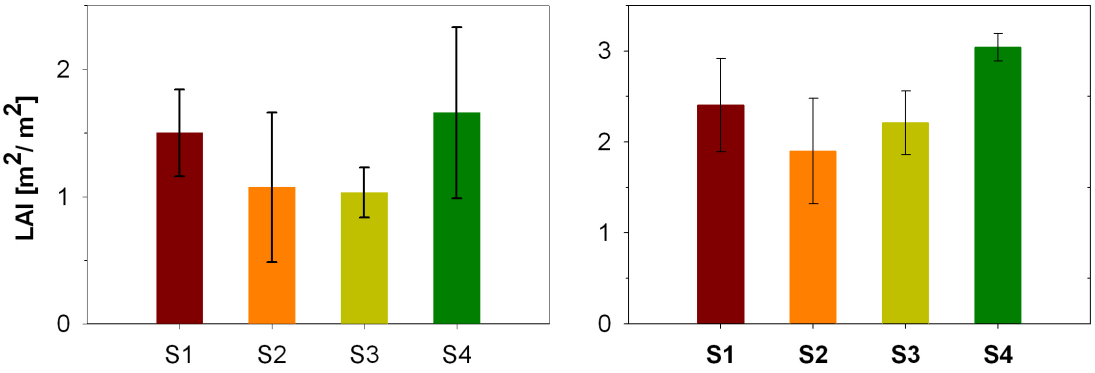

Figure 2.25: Leaf area index (LAI) of spring wheat in 2006. Left, 47 days, and right, 67 days after sowing.

Dry yield and C/N content of wheat grain Fig. 2.26 shows the measured dry yield sampled 119 days after sowing, at harvest. Unlike the trend shown in the previous samplings, the lowest yield is found in plot S2, which is followed by that in plot S3. The yield from plot S4 remains the best, followed by that in plot S1. The average yield for the four plots is 5.2 t/ha (SD 0.8 t/ha), which agrees well with the independently estimated average yield of 5.14 t/ha for the whole field A15. Qualitatively, with respect to the carbon and nitrogen contents, there

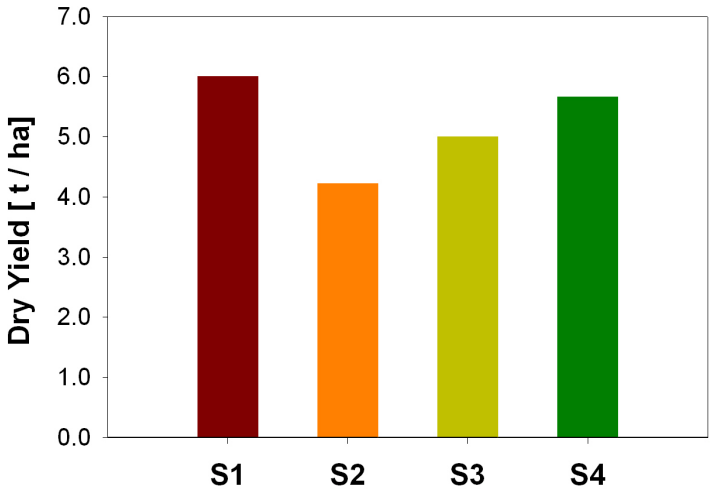

Figure 2.26: Yield of spring wheat by harvest in 2006 (119 days after sowing).

is little difference for the wheat grain between the plots (Fig. 2.27, B). However, for the leaves and stems a larger difference is found in the C/N contents. There is significantly more N in the leaves and stems in S4 than in the plants of the other plots (Fig.2.27, A).

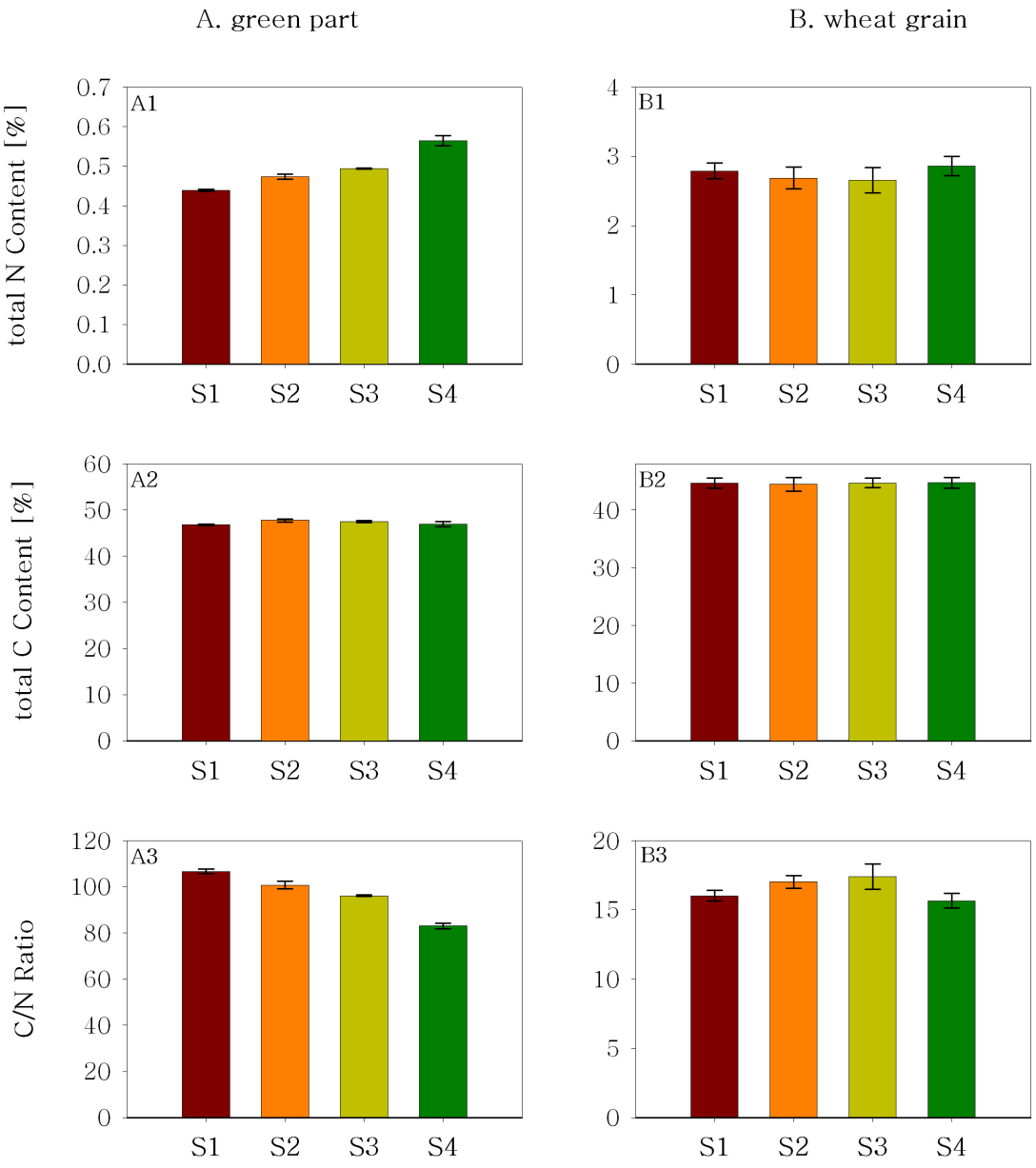

Figure 2.27: Carbon and nitrogen contents of wheat grain at harvest in 2006 (A: leaves and stems of the wheat; B: wheat grains).

2.4 Discussion of relationships between soil, climate and crop growth

2.4.1 Effect of soil and climate on availability of water

Measurements of the soil water content (SWC) at the four different plots showed that the field water balance was impacted mainly by the soil texture. However, climate conditions also influenced the fluctuation of the SWCs over the growing season. Owing to the high content of sand (over 90% below a depth of 30 cm), rapid leakage and poor water holding capacity are expected for plot S2. Thus water deficiency could be the main factor hindering crop growth in this instance.

Following the same reasoning, the water stress could also occur in plot S1, which has a sand content of 80% below a depth of 60 cm, but it is not as extreme as that for plot S2. In contrast, water transport in plot S3 could be inhibited by the high clay content (up to 40%). Additionally, the observed grey color of the bulk soil and the red -brown color due to an iron coating (Fig.2.9, S3-sub-soil) indicates that there is an impermeable clay horizon and that seasonal water saturation has occurred here. The grey and the red-brown colors in turn are typical appearance of a redox-oxidation process of the minerals due to the alternating anaerobic-aerobic conditions. Thus, a higher water holding capacity is expected for plot S3. In a wet year, however, this could lead to an O_2 deficiency for the root system.

Of the plots, plot S4 could provide the best soil -water relationship for favorable crop growth. The high fraction of silt in this plot guarantees a high water holding capacity. The presence of the grey bulk soil interspersed with iron and manganese oxide (Fig. 2.9, S4- sub-soil) indicates that the relatively higher fraction of clay also slows down the water flow, but does not lead to water saturation as it does in S3. Therefore, ther will not be a deficiency of water or of O_2 here.

2.4.2 Impact of soil, water availability and species on root distribution

Impact of soil properties

Field observations of the root-soil profile showed that the differences in root proliferation and distribution between the four plots might be influenced by the soil texture, soil structure and soil bulk density.

In S1, the loose but coherent structure and low bulk density allowed the roots to be distributed homogeneously throughout the soil profile (Fig.A.1). In contrast, although the soil in S2 has the same low bulk density, the root biomass is reduced dramatically (Fig.A.2), because below a soil depth of 30 cm, over 90% is sand, which is unstructured as single grains. The obvious impact of soil structure on root distribution was observed in plots S3 and S4. Unlike the homogeneous proliferation in the bulk soil, such as that in plot S1, most roots in plot S3 were found in the interspaces between aggregates in the angular blocky structure (Fig. 2.28, left). In S4, there were numerous holes in the top soil, and roots bands were observed in the macro pores with diameters of about 2 cm (Fig. 2.28, right). Compared to a homogeneous vertical root distribution in soil, this inhomogeneous distribution can reduce the area of the contact surface between the roots and bulk soils so that increased resources of water and nutrients are required to meet the crop demand.

Figure 2.28: Wheat roots observed in the structured soil of plot S3 (left) and plot S4 (right).

Moreover, a correlation between root diameter and soil bulk density was observed. Lower specific root length (SRL) corresponds to thicker roots. Thick roots grow in order to penetrate the dense soils of high resistance. The lower SRL in S3 and S2 suggest a higher soil resistance there. The high soil resistance in S3 might be due to the high content of clay and the high bulk soil density.

Although the bulk density in S2 was low, the roots there could have experienced high resistance when the coarse sand becomes very dry (Doussan *et al.*, 2003).

Impact of water availability

The higher RLD for S2 in the top 15 cm of the soil suggests an inhomogeneous supply of resources across the soil profile. There might be a deficit of water in the sub-soil of S2 so that crops had to rely on the resources in the top soil by enriching the roots there. This can be supported because much higher SWCs were found in the top 30 cm soil depth of S2 than in the sub soils.

Impact of crop species

The differences between the root distributions of maize and wheat show the various adaptabilities of the species under the same environmental conditions. In the dry, sandy plot S2, both maize and wheat have difficulty in growing roots in the sub-soils. However, for maize, which can adapt well to growing roots in the top soil, it seems that the demand for the necessary resource could be met by enhancing the root proliferation in the top soil. In contrast, wheat, which prefers deep rooting, cannot enlarge its root system in the top soil as well as the maize does, and hence cannot utilize the resources available there.

2.4.3 Impact of resources and root distribution on crop development

The crop measurements taken in 2005 and 2006 showed us that there were differences in crop development in the four plots. At harvest time for maize in 2005, plot S3 had the lowest yield and aboveground biomass. The yield in the other three plots were similar. Qualitatively, there was little difference for the nitrogen contents of the maize grains yielded from the four plots, the value being only slightly higher for plot S4. A larger differentiation was observed for spring wheat in 2006. At harvest, plot S2 had the lowest yield, with plot S3 being slightly higher. The yields from plots S1 and S4 were greater, and were similar to each other. S4 was qualitatively the best due to the highest nitrogen content of the wheat grain. Based on the differences in the soil properties and soil water content for the four plots, as discussed earlier, the variations in crop growth must be related to the different environmental conditions provided by the four plots. However, crops can regulate their root growth to adapt to poor conditions to

some extent. For example, although the sub-soil of plot S2 was unsuitable for root proliferation due to the high sand content and the dryness, maize could enhance its root system in the top soil so that its demand for water and nutrients could be met. Thus, the yield from S2 did not show any degradation compared with the other plots. However, the wheat roots could not grow well in the top soil in plot S2. As a result, between the four plots, the wheat yield was the lowest for plot S2.

In addition to the roots being able to orientate themselves according to the soil properties and the resources available, their diameter could also be affected. Among the four plots, the mean SRL/SRSA across the 0 -45 cm soil depth was the highest for plot S4, followed by plots S1, S2 and in S3, respectively. It is interesting to note that this ordering sequence coincides with the ordering sequence for maize growth also. Tab. 2.3 shows the correlations of mean SRL, mean SRSA, yield and above ground biomass for maize by harvest in the four plots. A high correlation between the SRSA and biomass suggests that the low SRSA could be an indication of crop growth restriction. Low value of SRSA indicates low root-soil contact surface per root biomass. This could suggest that: (1) the roots have to be thicker to grow through the difficult soil environment, and (2) the average water content in bulk soil is not related to the total amount of water available to roots because of the low root-soil contact surface area.

Table 2.3: Correlation between specific root length (SRL), specific root surface area (SRSA) of maize roots, yield and total aboveground biomass of maize at harvest in 2005.

	SRL	SRSA	Yield	abv. Biomass
SRL	-	0.92	0.80	0.79
SRSA	-	-	0.94	0.97
Yield	-	-	-	0.97

2.5 Conclusion

By comparing some of the important physical and chemical properties of the soil, strong heterogeneity was found especially in the sub-soils of the four plots studied. The differences in soil properties lead to variations in the resources that are available and in the root distributions across the soil profiles. The differences

in the crop growth can be seen as the result of interactions between the soil, water flow and root growth.

With respect to crop growth, plot S2 appeared to provide the worst conditions due to the dominance of the abundance of sand and the gravelly nature below a soil depth of 30 cm. Sandy soil is supposed to have a low water holding capacity and high water permeability (Scheffer & Schachtschabel, 1998). In dry periods, a deficiency of water might be a problem for crop growth here. The nutrient availability can also be decreased in dry soils due to the reduced uptake of nutrients carried by soil water and lower microbiological activity. A decrease in the water content in the soil can also lead to an increase of soil hardness (Doussan *et al.*, 2003). Because of the lower water and nutrient availability as well as the high mechanical resistance, roots were rarely found in the sub-soil of S2. However, maize plants can adapt their roots to grow in the top soils, which have more water and nutrients available to meet the uptake demands. Thus, because of the root adaptability, maize did not show any degradation in yield despite the difficult soil conditions in this plot, whereas the yield for the spring wheat was much more restricted, being the lowest of the four plots.

Compared with plot S2, plot S1 had a lower content of sand and a more coherent structure, which could thus hold more moisture and was more suitable for rooting. Unlike the radical reduction in the SWCs and RLDs below a depth of 20 cm in plot S2, both the SWCs and RLDs in plot S1 decreased gradually along the soil profile. Among the four plots, the vertical root distribution was most homogeneous in plot S1. The soil conditions here guaranteed relatively good growing conditions for the crops. In comparison with the other plots, the yields for both maize and wheat for plot S1 just followed the plot S4.

Compared with the two sandy plots, plots S3 and S4 were more characterized by their high clay contents. Clay soil is assumed to have a high water holding capacity and low water permeability (Scheffer & Schachtschabel, 1998). The low water permeability can lead to water saturation and therefore a lack of O_2 in the wet season. Hence, it is to be expected that O_2 deficiency might be the main reason for the poor crop growth in plot S3 in rainfall rich years. The high water content held in clay soils is not necessary related to the high water availability for crops, because the water can too tightly adhere in the fine soil pores to be uptaken by crop roots (Scheffer & Schachtschabel, 1998). However, the yield increase at plot S3 in dry year 1994 than in wet year 2000 (Fig. 2.2) suggested that the high water holding capacity of plot S3 could have guaranteed the water

supply in dry year. Besides its influences on soil water relationship, a high content of clay usually corresponds to a high soil bulk density. The high bulk density, blocky soil structure and the high content of gravel in the sub-soils might have prevented the root growth activity in S3. The roots had difficulty in growing through the hard bulky soil. They had to be thicker and could only proliferate on the surface of aggregates in the angular blocky structure, which thus reduced the root-soil contact surface area. As a result of the possible O_2 deficiency and restricted root growth, yield decrease of both maize and wheat were observed in plot S3. The maize yield in 2005 was actually the lowest among the four plots, which corresponds to the excess rainfall in this year.

Compared with plot S3, plot S4 had lower clay content and a higher content of silt. Because of its location in a depression, an additional availability of water and nutrients, relative to the other plots, was expected here. The coherent soil structure and macro pores seemed to compensate for the effect of the high bulk density on root growth. Hence plot S4 could provide the best conditions for water and nutrient availability relative to the other plots. Correspondingly, because of rich resources and plentiful roots in the sub-soils, the crop yield here was always the best.

Chapter 3

Impact of hydraulic parameterization of the water flow model on the simulation of the soil water balance and crop yield

3.1 Introduction

3.1.1 The model package Expert-N

The simulation study was conducted using Expert-N software environment, version 3.0. The Expert-N system is a model package that has a modular structure. It comprises a number of modules that provide different approaches to the simulation of vertical one-dimensional soil water flow including evapotranspiration, soil heat transfer, nitrogen transport, soil carbon and nitrogen turnover, crop growth, and soil management (Klier, 2006; Priesack *et al.*, 2008).

The modular structure allows an easy exchange of model units for comparison of various sub-models or model algorithms that describe the same process. For each model component and model unit, several distinct interchangeable sub-models are available and additional user defined sub-models can be easily included through the use of supporting dynamic link libraries (Klier, 2006; Priesack *et al.*, 2008). This makes it possible to analyze the impact of different or new modeling approaches on the simulation results component by component. The currently

available process models in Expert-N have either been taken from published models or have been developed by the Expert-N team (Engel & Priesack, 1993; Klier, 2006; Priesack, 2006; Stenger *et al.*, 1999; Wang, 1997).

For the simulations, Expert-N comprises a user friendly graphical interface for the model of choice and a graphical display of the simulation results (Fig. 3.1). In addition, there is a menu driven database for the variable input system to enter all necessary soil, weather, fertilizer and crop data for a particular field and growing season. The current model description can be found in Priesack (2006) and Priesack *et al.* (2008).

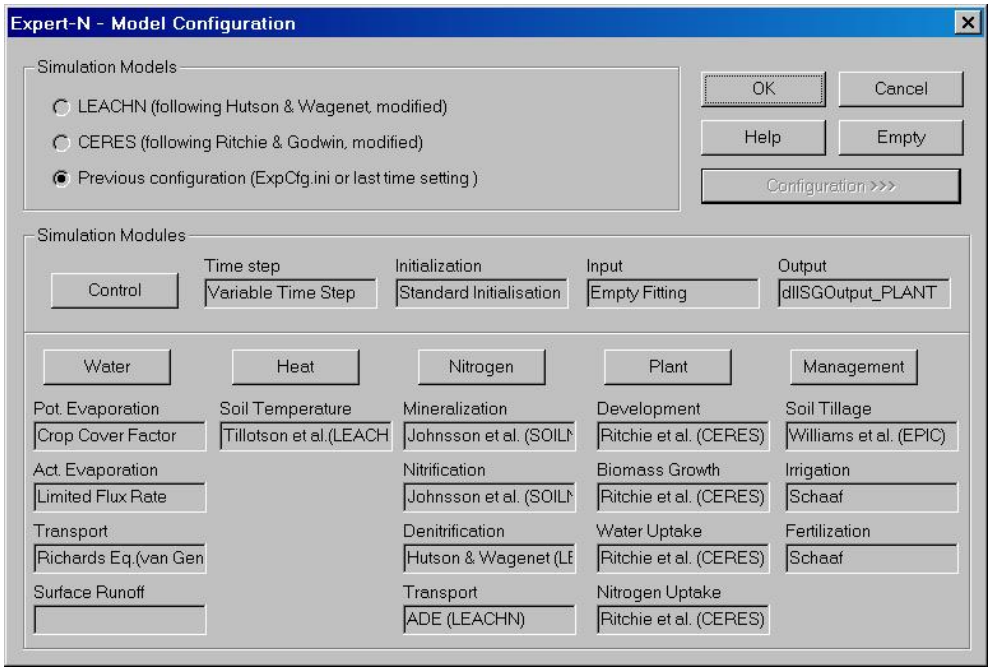

Figure 3.1: The interface of the modular modeling system Expert-N.

3.1.2 Parameterization of hydraulic functions

Water flow in an unsaturated soil zone has traditionally been described by the Richards′ equation, which is obtained by combining the Buckingham -Darcy flux equation with the mass balance law (Jury & Horton, 2004; Priesack, 2006). The macroscopic method for the vertical water flow in a soil -root system is commonly described by the one-dimensional Richards′ equation, in which a sink term representing water extraction by the roots is introduced:

$$\frac{\partial \theta}{\partial t} = C(h)\frac{\partial h}{\partial t} = \frac{\partial}{\partial z}[K(h)(\frac{\partial h}{\partial z}) - 1] - S_w(t, z, h) \tag{3.1}$$

where θ is the volumetric water content $[cm^3/cm^3]$, h is the soil pressure head $[cm]$, C is the differential moisture capacity $\partial\theta/\partial h$ $[1/cm]$, K is the hydraulic conductivity $[cm/s]$, t is time $[s]$, z is the vertical distance taken with positive being upwards $[cm]$, and S_w is the sink term for root water extraction $[cm^3/cm^3/s]$.

Richards′ equation is a nonlinear partial differential equation that does not have a closed-form analytical solution. In the present study, a numerical solver according to the model HYDRUS 6.0 (Simunek *et al.*, 1998b) was used. To solve the equation, one needs to specify the hydraulic functions – the **Soil Water Retention Function** $\theta(h)$ and the **Unsaturated Hydraulic Conductivity Function** $K(h)$ **or** $K(\theta)$. The relationship between the soil water content θ and pressure head h, also referred to the Water Retention Curve (WRC), is fundamental to the characterization of the water-holding properties of a soil (Dane & Topp, 2002; Scheffer & Schachtschabel, 1998). The curve depends to a great extent on the particle-size distribution, which in turn determines the soil texture and soil structure. The saturated hydraulic conductivity K_{sat} quantifies the ability of the porous medium (e.g., soil) to transmit water when this porous medium is saturated or almost saturated (Dane & Topp, 2002; Scheffer & Schachtschabel, 1998). It depends primarily on the status of the pores in the porous medium, such as the pore-size distribution, the roughness, the tortuosity, shape and degree of interconnection of the water conducting pores. The pore spaces in a soil are a result of the arrangement of the soil particles, the relationships between K and θ or h therefore also depend significantly on the soil texture and soil structure.

For use in models, the hydraulic relationships are fitted using a suitable mathematical equation or function. The parameterization problem is then to determine or estimate the independent parameters of a set of water retention and hydraulic conductivity functions. One of the best ways to determine these parameters will be to fit the equations to the data measured for the hydraulic properties. To obtain the shape parameter of $\theta(h)$, traditional techniques involve stepwise equilibrium desorption or sorption experiments in the laboratory (Dane & Topp, 2002). $K(h)$ is often determined by steady-state methods. Such methods are believed to be reproducible and thus more reliable. However, they are often tedious and time consuming if sufficient data to represent the function adequately are to be obtained. On the other hand, the actual soil structure and boundaries for the water flow are disturbed by taking soil samples.

Hence, indirect methods based on **infiltration experiments** have been developed that are fast, conveniently controlled, and relatively inexpensive. One such

technique is parameter estimation by inverse modeling from infiltration data. Infiltration experiments can be performed using a tension disc infiltrometer in situ. With the inverse approach suggested by Simunek & van Genuchten (1997), one can obtain not only $K(h)$ but also $\theta(h)$ from the multiple cumulative tension infiltration data supplemented with the initial and final water contents. These qualities of the tension infiltrometer make it particularly suitable for spatial variability studies that require a number of experiments. However, its disadvantage is that the initial and boundary conditions may not be determined as satisfactorily as by laboratory methods. Furthermore, as shown by Simunek *et al.* (1998a), WRCs obtained by this means did not agree particularly well with those obtained by direct laboratory measurements.

Alternatively, the hydraulic properties may be estimated conveniently through indirect methods by pedo transfer functions (PTFs). PTFs attempt to estimate the desired hydraulic properties from already existing data, such as soil textual data, porosity, soil organic matter content and soil bulk density (Dane & Topp, 2002). The relationship between input and output parameters of such empirical PTFs is determined using mathematical techniques, such as regression or neural networks analysis using empirical coefficients that are determined by minimizing the difference between predicted and observed results. Compared with other methods that involve tedious measurements in the laboratory or in the field, the estimating of hydraulic parameters by PTFs is much simpler and faster. The use of PTFs for solving the Richards′ equation in a computer model is sometimes the only choice if there is no information on the hydraulic properties available. However, the reliability or uncertainty of the PTFs is an important issue as most PTFs are based on data sets that contain sparse data, noise, and sometimes ambiguous data that may yield parameter estimates covering a large confidence interval (Dane & Topp, 2002).

As the relationships between θ, h and K are strongly dependent on the soil texture and the soil structure, this makes the estimation of the hydraulic properties of soils with high heterogeneity even more difficult. The individual measurement of every soil horizon that has a different texture and structure would entail great expense and require work in the field and in the laboratory, which is sometimes not practicable.

Thus, the objective of this chapter is to test a compromise method for estimating the hydraulic parameters of highly heterogeneous soils. In the four soil profiles studied, 26 soil horizons were examined according to their differences in

soil texture, soil bulk density and soil organic matter content. In the first step, one representative top soil horizon and one sub-soil horizon were selected from each of the four soil profiles, giving eight soil horizons. Infiltration experiments were carried out for these eight soil horizons using a tension disc infiltrometer in the field. The hydraulic parameters of these soil horizons were estimated by inverse modeling based on the infiltration data. In the second step, the hydraulic parameters of these 8 soil horizons were estimated using the various pedo transfer functions (PTFs) that are available in Expert-N. Next, the estimated hydraulic properties from PTFs were compared with the results from infiltration experiment. In addition, using these various hydraulic parameter-sets, the soil water balances in two years as well as the crop growth in five years were simulated for the four soil plots, and the predicted soil water content and crop yield were compared with the observed values. Finally, according to the best agreements between the comparisons, the approach, which was most appropriate to estimate the hydraulic parameters for the soil plots studied, was determined. This approach was used to estimate the hydraulic parameters for the 26 soil horizons in the subsequent crop growth simulation.

3.2 Materials and methods

3.2.1 Estimation of hydraulic parameters through a tension infiltrometer experiment

Theory

The inverse method suggested by Simunek & van Genuchten (1997) was used in our study. In this approach, the governing flow equation for radial symmetrical isothermal Darcian flow in a variably -saturated isotropic rigid porous medium is given by following modified form of the Richards′ equation (Warrick, 1992):

$$\frac{\partial\theta}{\partial t} = \frac{1}{r}\frac{\partial}{\partial r}[r \cdot K(h)\frac{\partial h}{\partial r}] + \frac{\partial}{\partial z}[K(h)\frac{\partial h}{\partial z}] + \frac{\partial K(h)}{\partial z} \tag{3.2}$$

where r is a radial coordinate [cm]. Initial and boundary equations applicable to a disc-tension infiltrometer experiment are as follows (Warrick, 1992):

$$\begin{cases} \theta(r,z,t) = \theta_i(z) & \text{for } t = 0 \\ h(r,0,t) = h_0 & \text{for } 0 < r < r_0 \\ -\frac{\partial h(r,0,t)}{\partial z} - 1 = 0 & \text{for } r > r_0 \\ \theta(r,z,t) = \theta_i(z) & \text{for } r^2 + z^2 \longrightarrow \infty \end{cases} \tag{3.3}$$

where θ_i is the initial water content $[cm^3/cm^3]$, h_0 is the supply pressure head imposed by the tension-disc infiltrometer $[cm]$, and r_0 is the disc radius $[cm]$. The van Genuchten - Mualem (vGM) Model by van Genuchten (1980) and Mualem (1976) is chosen to describe the hydraulic properties of the system:

$$\theta(h) = \theta_{res} + \frac{(\theta_{sat} - \theta_{res})}{[1 + (\alpha|h|)^n]^m} \tag{3.4}$$

$$K(h) = K_{sat} S_e^{0.5} [1 - (1 - S_e^{\frac{1}{m}})^m]^2, S_e = \frac{\theta(h) - \theta_{res}}{\theta_{sat} - \theta_{res}} \tag{3.5}$$

where θ is the volumetric water content $[cm^3/cm^3]$, h is the pressure head $[cm]$, θ_{sat} is the saturated volumetric water content $[cm^3/cm^3]$, θ_{res} is the residual volumetric water content $[cm^3/cm^3]$, K is the hydraulic conductivity $[cm/s]$, K_{sat} is the saturated hydraulic conductivity $[cm/s]$, S_e is the effective water content ratio $[-]$, α $[1/cm]$, n $[-]$, m $[-]$ are van Genuchten parameters, $n > 0$, $m > 0$, where it is usually assumed that m=1-1/n.

The system response is represented by a numerical solution of the flow equation argued with the parameterized hydraulic functions and the initial and boundary conditions (Simunek & van Genuchten, 1996, 1997). The hydraulic parameters α, n, θ_s and K_s are estimated by minimization of a suitable objective function, which quantifies the discrepancy between the observed values and the predicted system response. as given by Simunek & van Genuchten (1996), the objective function Φ may be defined as follows:

$$\Phi(\beta, q_m) = \sum_{j=1}^{m} (\nu_j \sum_{i=1}^{n_j} \omega_{ij} [q_j^*(t_i) - q_j(t_i, \beta)]^2) \tag{3.6}$$

where m represents various sets of measurements (e.g. infiltration data, the final water content), n_j is the number of measurements in a particular set, $q_j^*(t_i)$ is the specific measurement at time t_i for the j_{th} measurement set, β is the vector of optimized parameters (e.g. θ_r, θ_s, α, n, K_s), $q(t, \beta)$ represents the corresponding model predictions for parameter vector β, and ν_j are weights associated with a particular measurement set j, and ω_{ij} are weights associated with a measurement i within set j. Initial estimates of the parameters are usually iteratively improved during the minimization process until a desired degree of precision is obtained.

Experiments in the field

For the infiltration experiments in the field, a tension infiltrometer (Soil Measurement Systems, Tuscon, AZ) with a 0.2 m diameter disc was chosen. It consists of

three major components, namely a bubble tower, water reservoir, and a circular disc (Fig. 3.2). The bubble tower contains a moveable air-entry tube. This air-

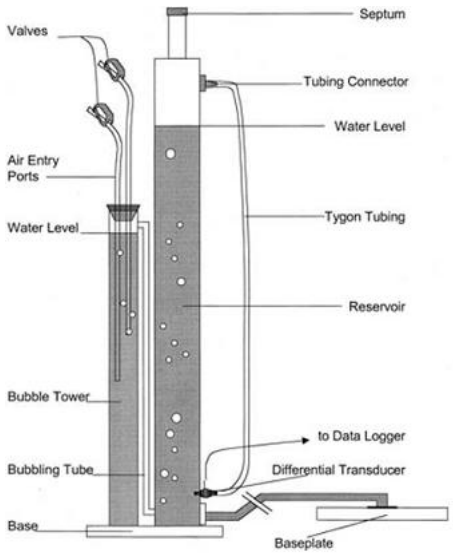

Figure 3.2: Schematic of the construction of the tension infiltrometer

entry tube is used to impose the desired negative water pressure at the base of the disc by varying the distance between the air-entry point and the water level. The other large tube at the side of the bubble tower is a water reservoir, which contains a scale for measuring the drop in the water level. For each imposed negative water pressure, the volume of water infiltrating into the soil is measured by recording the height change for water in the reservoir manually. The disc (base plate), which is to establish hydraulic continuity with the soil, is a Plexiglas plate that has grooves and has been drilled with circular holes, approximately 1.5 mm in diameter, allowing water to pass through freely. The base of the disc is covered with a nylon membrane (400 meshes). In practice, the disc is usually placed on a layer of sand to ensure hydraulic contact between the infiltrometer and the soil (Fig. 3.3).

For multiple tension infiltration experiments, the cumulative outflow is measured over a range of pressure heads of from 0 to 30 cm H_2O. The amount of water infiltrating into the soil can be measured manually by recording the decrease in the water level in the reservoir tower as a function of time. To improve the accuracy of the estimation, disturbed soil samples before and after the experiment are taken for estimation of the initial and final gravimetric water content.

Figure 3.3: Use of tension infiltrometer in the field.

To convert the gravimetric results into volumetric water content, undisturbed soil cores were taken to estimate the soil bulk density.

For our study, field tension infiltrometer experiments were performed in the top soils (A horizon) and in the sub-soils (B horizon) of the four study plots. The soil depth, soil type, initial soil water content and final soil water content are shown in Tab. 3.1.

Table 3.1: Conditions for the infiltration experiments.

Plot	Soil depth [cm]	Soil type	θ_{ini} $[cm^3/cm^3]$	θ_{end} $[cm^3/cm^3]$
S1 top	10	sandy loam	0.265	0.395
S1 sub	40	sandy loam	0.348	0.413
S2 top	3	loamy sand	0.302	0.366
S2 sub	20	clayey sand	0.242	0.310
S3 top	5	sandy loam	0.295	0.394
S3 sub	58	clayey loam	0.365	0.418
S4 top	5	sandy loam	0.320	0.410
S4 sub	41	sandy loam	0.280	0.375

Unsaturated infiltration measurements were completed at h_0= -3 [cm], h_0= -6 [cm], and h_0= -12 [cm] water head one after the other. By optimizing the difference between the observed cumulative infiltration curve and the predicted curve, which was calculated using the vGM hydraulic functions (Eq. 3.4 and Eq. 3.5), vGM parameters of residual soil water content θ_{res}, saturated soil water content θ_{sat}, shape parameters α and n as well as saturated hydraulic conductivity K_{sat} were then estimated using the computer software DISC (Simunek & van Genuchten, 2000), which was developed especially for the analysis of Tension Disc Infiltrometer data through parameter estimation (Dane & Topp, 2002).

3.2.2 Parameterization of hydraulic functions by pedo transfer functions

The hydraulic functions (HFs) and pedo transfer functions (PTFs) used in this study are available in Expert-N. Four combinations of HF and PTF were tested. The abbreviations and the respective HFs and PTFs used in each approach are listed in Tab. 3.2.

Table 3.2: Overview of the hydraulic functions (HFs) and pedo transfer functions (PTFs) used in each approach.

Approach	θ_{sat}	K_{sat}	Shape parameters	Hydraulic function
	estimated by PTF of			
RBBCB	Rawls & Brakensiek			Brooks & Corey-Burdine
VBG	Vereecken			Brutsaert-Gardner
CHCB	Campbell			Hutson & Cass-Burdine
V+CHCB	Vereecken		Campbell	Hutson & Cass-Burdine

1. Approach RBBCB

One of the most commonly used parametric models for water retention function is that suggested by Brooks & Corey (1966). Combined with this model, the model of Burdine (1953) can be applied to predict the unsaturated soil hydraulic conductivity. The whole approach can be written as follows:

$$\theta(h) = \begin{cases} \theta_{res} + (\theta_{sat} - \theta_{res})(h/a)^{-\lambda} & \text{for } h < a \\ \theta_{sat} & \text{for } h \geq a \end{cases} \tag{3.7}$$

$$K(h) = \begin{cases} K_{sat}(h/a)^{-2-3\lambda} & \text{for } h < a \\ K_{sat} & \text{for } h \geq a \end{cases} \tag{3.8}$$

where θ is the volumetric water content $[cm^3/cm^3]$, h is the pressure head $[cm]$, θ_{sat} is the saturated volumetric water content $[cm^3/cm^3]$, θ_{res} is the residual volumetric water content $[cm^3/cm^3]$, K is the hydraulic conductivity $[cm/s]$, K_{sat} is the saturated hydraulic conductivity $[cm/s]$, λ is the Brooks & Corey exponent $[-]$ and a is an empirical parameter that represents the pressure head at the air entry value $[cm]$.

PTFs suggested by Rawls & Brakensiek (1985) were used to parameterize these hydraulic functions, where the porosity $\phi[cm^3/cm^3]$ and the soil textual data (sand content f_{sand} [-], silt content f_{silt} [-] and clay content f_{clay} [-]) are needed. The expressions were re-written by Priesack (2006) as follows:

$$\begin{aligned}\theta_{sat} &= 0.01 - 0.15f_{sand} - 0.22f_{clay} + 0.98\phi \\ &\quad +0.99f_{clay}^2 + 0.36\phi f_{sand} - 1.09\phi f_{clay} \\ &\quad -0.96\phi f_{clay}^2 - 0.24\phi^2 f_{sand} + 1.15\phi^2 f_{clay}\end{aligned} \tag{3.9}$$

$$\begin{aligned}\theta_{res} &= 0.02 + 0.09f_{sand} + 0.51f_{clay} + 0.03\phi \\ &\quad -1.54f_{clay}^2 - 0.11f_{sand}\phi - 1.8\phi^2 f_{clay}^2 \\ &\quad +3.1\phi f_{clay}^2 - 0.24\phi^2 f_{clay}\end{aligned} \tag{3.10}$$

$$\begin{aligned}\log(\lambda) &= -0.78 + 1.78f_{sand} - 1.06\phi - 0.53f_{sand}^2 \\ &\quad -27.3f_{clay}^2 + 1.1\phi^2 - 3.1\phi f_{sand} \\ &\quad +79.9\phi f_{clay}^2 + 2.66\phi^2 f_{sand}^2 - 61.1\phi^2 f_{clay}^2 \\ &\quad -2.4f_{sand}^2 f_{clay} - 0.67\phi^2 f_{clay}\end{aligned} \tag{3.11}$$

$$\begin{aligned}\log(a) &= 5.34 + 18.5f_{clay} - 2.48\phi - 21.4f_{clay}^2 \\ &\quad -4.36\phi f_{sand} - 61.7\phi f_{clay} + 14.4\phi^2 f_{sand}^2 \\ &\quad -85.5\phi^2 f_{clay}^2 - 12.8f_{sand}^2 f_{clay} + 89.5\phi f_{clay}^2 \\ &\quad -7.25\phi f_{sand}^2 + 5.4f_{sand} f_{clay}^2 + 50.0\phi^2 f_{clay}\end{aligned} \tag{3.12}$$

2. Approach VBG

The second approach includes the water retention model suggested by Brutsaert (1966) and the unsaturated hydraulic conductivity model by Gardner (1958), which is independent of any water retention function as follows:

$$\theta(h) = \theta_{res} + \frac{(\theta_{sat} - \theta_{res})}{1 + (\alpha|h|)^n} \tag{3.13}$$

$$K(h) = K_{sat}\frac{1}{1 + (A|h|)^B} \tag{3.14}$$

where θ, h, θ_{sat}, θ_{res} are the same as in Eq. 3.7, α $[1/cm]$ and n $[-]$ are empirical parameters that characterize the shape of the curve, K and K_{sat} are the same as in Eq. 3.8, A and B are parameter Gardner A $[1/cm]$ and Gardner B $[-]$, respectively.

Based on the input data for soil bulk density (ρ_s $[g/cm^3]$), textural data (f_{sand}, f_{silt} and f_{clay}) and organic matter content ($f_{C_{org}}$ [-]), Vereecken *et al.* (1989) suggested the following regression functions to parameterize the model of Brutsaert, as given by Priesack (2006):

$$\theta_{sat} = 0.81 - 0.28\rho_s + 0.13 f_{clay} \tag{3.15}$$

$$\theta_{res} = 0.015 + 0.5 f_{clay} + 1.39 f_{C_{org}} \tag{3.16}$$

$$\log(\alpha) = -2.49 + 2.5 f_{sand} - 35.1 f_{C_{org}} - 2.62\rho_s - 2.3 f_{clay} \tag{3.17}$$

$$\log(n) = 0.05 - 0.9 f_{sand} - 1.3 f_{clay} + 1.5 f_{sand}^2 \tag{3.18}$$

In addition, the model of Gardner can be parameterized by the regression functions of Vereecken *et al.* (1990), as given by Priesack (2006):

$$\log(K_{sat}) = 11.04 - 0.96\log(f_{clay}) - 0.66\log(f_{sand}) - 0.46\log(f_{C_{org}}) - 8.43\rho_s \tag{3.19}$$

$$\log(A) = -0.7 - 1.9 f_{sand} - 5.8 f_{clay} \tag{3.20}$$

$$\log(B) = 0.07 - 0.19\log(f_{clay}) - 0.05\log(f_{silt}) \tag{3.21}$$

3. Approach CHCB

Following the approach used in the simulation program LEACHM (Hutson & Wagenet, 1992), the hydraulic relationships can be described by the combination of the parametric model of Hutson & Cass (1987) and the unsaturated hydraulic conductivity model of Burdine (1953) as follows:

$$\theta(h) = \begin{cases} \theta_{sat}(h/a)^{-1/b} & \text{for } h > h_i \\ \theta_{sat}[1 - (h/a)^2(2b)^{-1}(h_i/a)^{-2-1/b}] & \text{for } 0 \geq h \geq h_i \end{cases} \tag{3.22}$$

$$K = \begin{cases} K(h) = K_{sat}(h/a)^{-2-3/b} & \text{for } h < h_i \\ K(\theta) = K_{sat}(\theta/\theta_{sat})^{2b+3} & \text{for } \theta \geq \theta_i \end{cases} \tag{3.23}$$

where θ, h, θ_{sat}, θ_{res} are the same as in Eq. 3.7, K and K_{sat} are the same as in Eq. 3.8, $\theta_i/\theta_{sat} = 2b/(1+2b)$, $[-]$, $h_i = a[2b/(1+2b)]^{-b}$ which represents the pressure head at the inflexion point $[cm]$, a and b are empirical parameters (also known as Campbell A and Campbell B) with a representing the pressure head at

the air entry value $[cm]$ and b is the inverse of the Brooks and Corey exponent λ, i.e. $b = \lambda^{-1}$.

Using the information on the soil bulk density (ρ_s $[g/cm^3]$) and textural data (f_{sand}, f_{silt} and f_{clay}), the parameters a, b and K_{sat} can be estimated by the PTFs suggested by Campbell (1985). (Priesack, 2006) rewrote the expressions like follows:

$$a = -0.5 d_g^{-1/2} (\rho_s / 1.3)^{0.67b} \tag{3.24}$$

$$b = d_g^{-1/2} + 0.2\sigma_g \tag{3.25}$$

$$K_{sat} = 3.9 \cdot 10^{-5} (1.3/\rho_s)^{1.3b} \exp(-6.9 f_{clay} - 3.7 f_{silt}) \tag{3.26}$$

$$d_g = \exp(e_g) \tag{3.27}$$

$$e_g = f_{clay} \log(d_{clay}) + f_{silt} \log(d_{silt}) + f_{sand} \log(d_{sand}) \tag{3.28}$$

$$\sigma_g = \exp(f_g) \tag{3.29}$$

$$f_g = [f_{clay} \log(d_{clay})^2 + f_{silt} \log(d_{silt})^2 + f_{sand} \log(d_{sand})^2] \tag{3.30}$$

In addition, the saturated water content is set to be equal to the porosity ϕ. If there is no measured value of ϕ, it can be calculated from $\phi = 1 - \rho_s/2.65$, where 2.65 $[g/cm^3]$ is the density of the sand mineral. The residual water content θ_{res} is set at zero.

4. Approach V+CHCB

In addition to the above three approaches, a combined approach was also tested. In this approach, the θ_{sat} and K_{sat} were initially estimated by the PTF of Vereecken. By using these as input parameters for the PTFs of Campbell, the shape parameters a and b (Eq. 3.22 and Eq. 3.23) of the hydraulic functions of Hutson & Cass-Burdine are then estimated using the PTFs of Campbell.

3.2.3 Simulation experiments

In order to compare the effect of different approaches for the hydraulic parameterization on the water balance simulation, crop growth as well as water balance and nitrogen balance in the four study plots were simulated for the growing seasons 2005 and 2006 using the crop models CERES-Wheat and CERES-Maize proposed by Ritchie & Godwin (1989) and Jones & Kiniry (1986).

Dataset

The soil data (textual data, soil bulk density and organic matter content) in addition to the crop yield data for 2005 and 2006 in the four study plots were adopted from the field measurements presented in Chapter 2. The weather data were obtained from the weather station Voglried (section 2.2.4).

High-resolution crop yield maps for 1994, 1997 and 2000 were unpublished data provided by Markus Demmel from Lehrstuhl für Landtechnik, TUM. By combining with GPS, yield and position information were simultaneously registered as data pairs. For estimation of the yield in the four plots studied, the mean values were calculated for the measured points, which were at a radius of 5 m around the locations studied. The recorded data were wet yield data. For estimation of dry yield, a 14% water content of the grain was assumed both for wheat grain and maize corn. The measured water retention data of the other soil plots in the neighboring fields (maximum 1 km away from A15) were also available in the database of the FAM project.

Model configuration

Soil water flow simulations were based on Richards′ equation using a numerical solution according to the model HYDRUS 6.0 proposed by Simunek *et al.* (1998b). Run-off and snow processes were not considered. Free drainage was assumed at the lower boundary. The estimation of evaporation was according to the approach of Penmann-Monteith (FAO). Heat transfer, N-transport and N-turnover were simulated following the approaches of the model LEACHM proposed by Hutson & Wagenet (1992). For the simulation of crop development and crop growth, the generic plant models CERES-Wheat (Ritchie & Godwin, 1989) and CERES-Maize (Jones & Kiniry, 1986) were applied. The phenological parameters required by the crop growth models were adapted to the field data collected at the FAM research station near Munich, southern Germany (Osinski *et al.*, 2005).

Simulation strategy

The objective was to establish the influence of various hydraulic parameterization methods on the simulation of soil water content and crop yield. The soil hydraulic parameters were estimated by the RBBCB, VBG, CHCB and V+CHCB approaches (see Tab. 3.2), respectively. The simulated soil water contents using different hydraulic parameter-sets were then compared with the measured soil

water contents at three soil levels (0 -30 cm, 30 -60 cm and 60 -90 cm) of the four soil plots studied in 2005 and 2006. In addition, the maize yield in 1994, 2000 and 2006 as well as the maize yield in 1997 and 2005 were simulated using the various hydraulic parameterizations. Then the respective simulated crop yields for the four plots were compared with the measured values.

Statistics analysis

The statistical parameter the coefficient of determination R^2 for the regression analysis was used to assess the degree of agreement between the simulated and measured values for soil water content and crop yield.

3.3 Results and discussion

3.3.1 Soil hydraulic parameters estimated by infiltration experiments

The measured and calculated cumulative infiltration curves for the eight experiments are shown in Fig. 3.4. The regression coefficients of calculated versus measured data are at least 0.997 for all optimization processes.

The hydraulic parameters estimated by DISC are listed in Tab. 3.3. In general, the saturated hydraulic conductivities K_{sat} are higher in sandy plots (S1 and S2) than in clayey plots (S3 and S4). An exception is the top soil of S4. An unusually high K_{sat} is found from the infiltration experiment in this soil. This result can be probably due to the preferential flow, because numerous macro pores were observed in the top soils of plot S4 (see section 2.4.2).

Table 3.3: Hydraulic parameters of the top and sub-soils of the four study plots estimated by infiltration experiment. θ_{res}, residual volumetric soil water content $[cm^3/cm^3]$; θ_{sat}, saturated volumetric soil water content $[cm^3/cm^3]$; α, parameter of van Genuchten model; n, parameter of van Genuchten model; K_{sat}, saturated hydraulic conductivity $[cm/s]$, R^2, statistical parameter coefficient of determination.

Plot	θ_{res} $[cm^3/cm^3]$	θ_{sat} $[cm^3/cm^3]$	α [1/cm]	n [-]	K_{sat} [cm/s]	R^2
S1 top	0.078	0.415	0.120	1.374	492	0.999
S1 sub	0.000	0.417	0.027	1.382	181	0.998
S2 top	0.000	0.372	0.044	1.322	156	0.997
S2 sub	0.000	0.314	0.125	1.294	726	0.999
S3 top	0.095	0.398	0.035	1.389	78	0.998
S3 sub	0.068	0.419	0.013	1.181	69	0.998
S4 top	0.065	0.448	0.224	1.284	6800	0.998
S4 sub	0.095	0.426	0.053	1.662	78	0.999

Using the estimated α and n parameters, water retention curves (WRC) were calculated (Fig. 3.5). Compared with the WRC of sub-soils (Fig. 3.5, right), the WRC of the top soils are fairly similar (Fig. 3.5, left). The θ_{sat} of the four top soils are around 0.4 $[cm^3/cm^3]$. The θ_{res} of S1, S3 and S4 are about 0.1 $[cm^3/cm^3]$

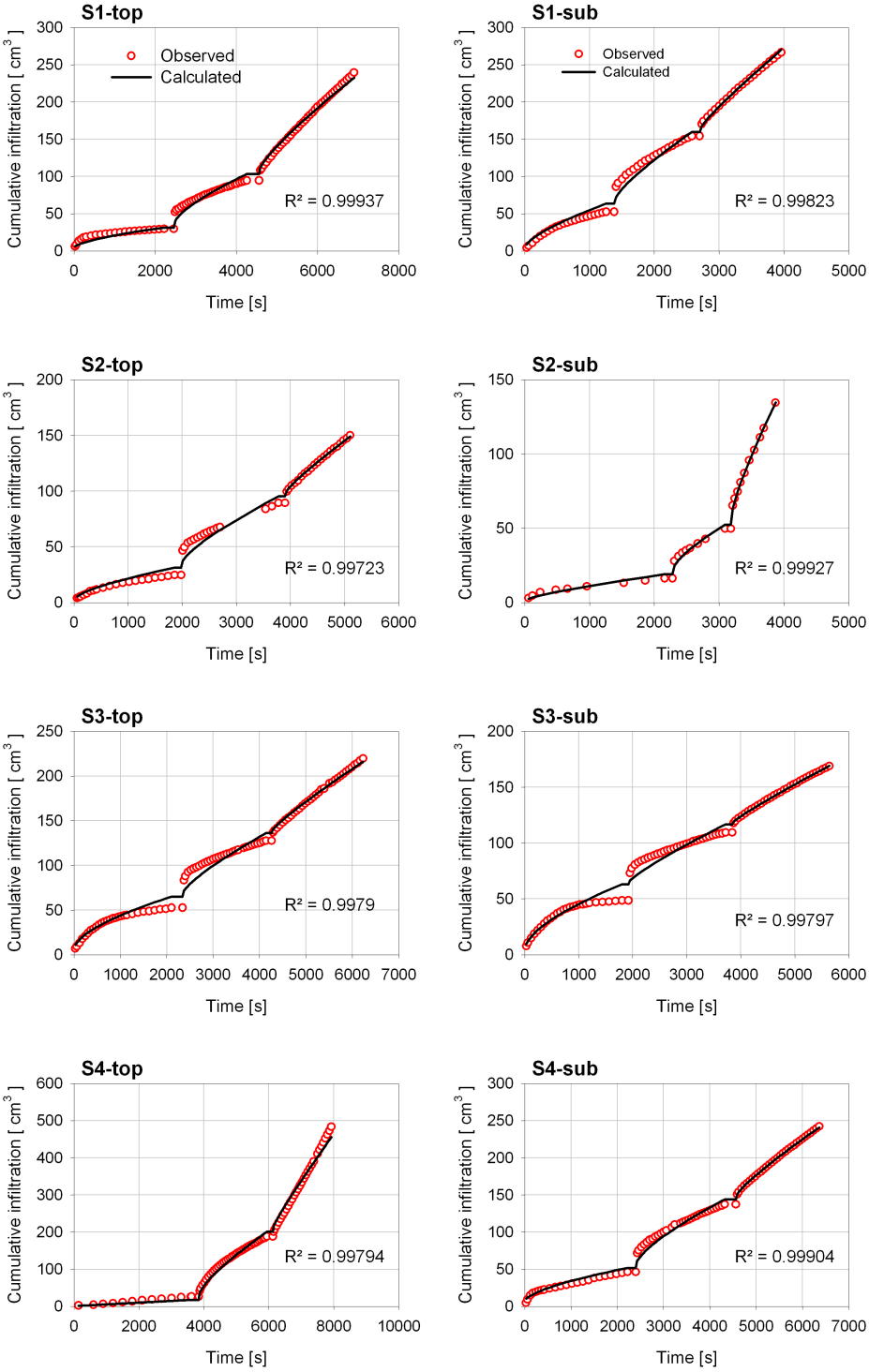

Figure 3.4: Infiltration curves for top soils.

(soil type sandy loam). The θ_{res} of S2 is estimated to be 0.0, the soil type of which is loamy sand. For the sub-soils of S1, S3 and S4, similar θ_{sat} of 0.42 $[cm^3/cm^3]$ are found, while the θ_{sat} of S2 is only 0.31 $[cm^3/cm^3]$. Considering the course and shape of the curves, the curve of S3 lies above the other curves, whereas the curve of S2 is the lowest. This indicates that under the same water head, soil in S3 can hold the most water and that in S2 the least water.

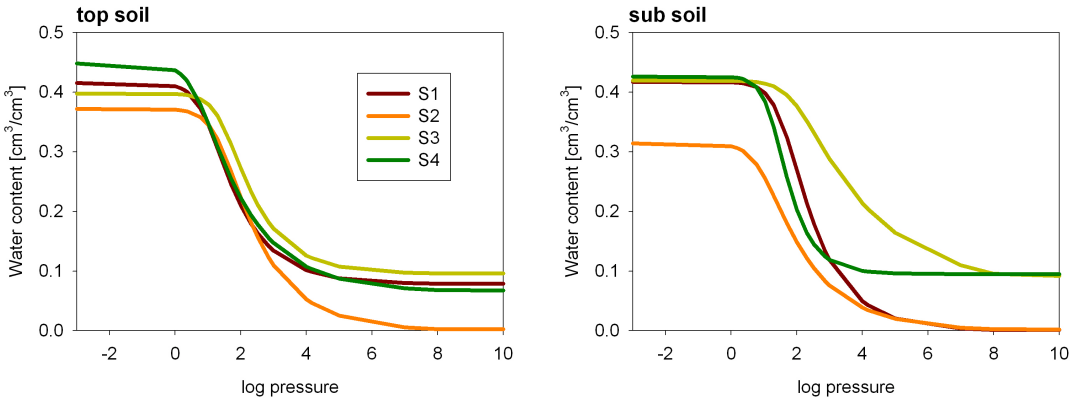

Figure 3.5: Water retention curves estimated by infiltration experiment (left: for top soils; right: for sub soils).

In addition, a comparison between the estimated WRC of the four soil plots and the measured water retention data of the other plots in the neighboring fields (maximum 1 km away from A15) was carried out to establish the plausibility of our estimation. The measured water retention data used for the comparisons were available in the database of the Agriculture-Ecology-System research project (1990 -2003) of the Forschungsverbund Agrarökosysteme München (FAM) (Osinski *et al.*, 2005). All WRCs are shown in Fig. 3.6. These soils show similar water retention behaviors.

3.3.2 Comparison of θ_{sat} and K_{sat} estimated by infiltration experiment and PTFs

According to the soil property measurements, the soil profile 0 -90 cm of the four study plots can be divided into 6 -7 soil horizons all having differences in soil texture, soil bulk density and organic matter content. Based on these basic soil properties, the hydraulic parameters of each soil horizon were estimated using three pedo transfer functions (PTFs) that were introduced by Vereecken

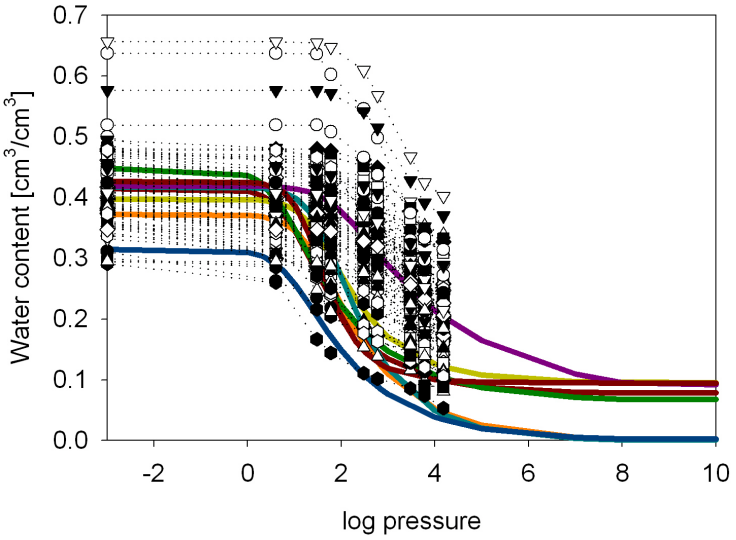

Figure 3.6: Comparison of the estimated water retention curves from infiltration experiment for the four study plots (solid line) and in laboratory measured water retention data for other plots in neighboring fields (dotted line with symbols).

et al. (1989) and Vereecken *et al.* (1990), by Campbell (1985) and by Rawls & Brakensiek (1985), respectively. In Tab. 3.4, the θ_{sat} of the eight soil horizons estimated by infiltration experiment are compared with those estimated by the three PTFs. In general, the θ_{sat} values estimated by PTFs of Vereecken and

Table 3.4: Comparison of θ_{sat} $[cm^3/cm^3]$ estimated by infiltration experiment with values estimated by pedo transferfunctions (PTFs) of Vereecken, Campbell and Rawls & Brakensiek.

Soil horizon	Tension	PTFs of		
	Infiltrometer	Vereecken	Campbell	Rawls & Brakensiek
S1-top	0.42	0.46	0.49	0.40
S1-sub	0.42	0.40	0.43	0.32
S2-top	0.37	0.42	0.45	0.38
S2-sub	0.32	0.35	0.36	0.28
S3-top	0.40	0.50	0.44	0.36
S3-sub	0.42	0.42	0.34	0.25
S4-top	0.45	0.50	0.46	0.38
S4-sub	0.43	0.48	0.38	0.30

PTFs of Campbell are more similar to that estimated by infiltration experiment, while the θ_{sat} values estimated by PTFs of Rawls & Brakensiek are generally lower than the others. The PTFs of Vereecken and Campbell produce similar estimations for sandy soils (plot S1 and S2), which are slightly higher than those from infiltration experiments. For the clayey sub-soils of plots S3 and S4, the θ_{sat} of S3-sub and S4-sub estimated using the PTFs of Campbell are much lower than that estimated by infiltration experiment, whereas the values estimated by PTFs of Vereecken are closer to that estimated by infiltration experiment.

Similarly, comparison between estimations of K_{sat} by infiltration experiment, PTFs of Vereecken and PTFs of Campbell is shown in Tab. 3.5. In general, the

Table 3.5: Comparison of values of K_{sat} $[cm/s]$ estimated by infiltration experiment with those estimated by pedo transfer functions (PTFs) of Vereecken and PTFs of Campbell.

Soil horizon	Tension	PTFs	
	Infiltrometer	Vereecken	Campbell
S1-top	492	394	145
S1-sub	181	80	34
S2-top	156	220	311
S2-sub	726	413	1240
S3-top	78	166	43
S3-sub	69	24	3
S4-top	6800	239	78
S4-sub	78	60	16

three approaches estimated K_{sat} of a particular soil horizon to be of the same order. Compared with the PTFs of Campbell, the K_{sat} estimated by the PTFs of Vereecken are closer to those estimated by the infiltration experiment.

The comparisons showed us that with respect of the hydraulic parameter θ_{sat} and K_{sat}, the results from PTFs of Vereecken agree with the results from the infiltration experiment better than those from PTFs of Rawls & Brakensiek and Campbell.

3.3.3 Impact of hydraulic parameters on simulation of soil water content variability

Using the above three PTFs and their coordinated hydraulic functions (termed RBBCB, VBG and CHCB in Tab. 3.2), the soil water contents in the four soil profiles studied were simulated for the growing seasons 2005 and 2006. In addition, a combined approach V+CHCB was tested.

Comparisons of the measured and simulated water contents using the four approaches are shown in Fig. 3.7. There are 116 soil water data results in total that range from 0.10 to 0.43 $[cm^3/cm^3]$. The high water content data are mostly from the clayey plots (plots S3, S4) and the low water contents are from the sandy plots (plots S1, S2). To distinguish the effect of the various approaches on sandy and clayey soils, the data from sandy plots are indicated by yellow color and the data from clayey plots by grey color in Fig. 3.7. The V+CHCB approach shows the best agreement between the observed and predicted results with an R^2 of 0.89, while the RBBCB approach has the least agreement with an R^2 of 0.70. The RBBCB approach both overestimates the high water content range, which is mostly from the clayey plots, and underestimates the low water content ranges from the sandy plots. Approaches VBG and CHCB show similar regressions with values for R^2 of 0.80 and 0.83, respectively. However, the VBG approach overestimates almost all the data, especially the low water content range from sandy plots. In contrast, approach CHCB overestimates the high water content range from clayey plots. However, compared with the other two approaches, the approach CHCB provides better agreement between the measured and simulated values.

Although the above comparison of the θ_{sat} and K_{sat} estimation indicated that the PTFs of Vereccken produced results in better agreement with those from the infiltration experiment than the PTFs of Campbell, there was little difference shown in the regression analysis between the measured and simulated data using the two PTFs(R^2 =0.80 and 0.83, respectively). However, higher R^2 (=0.89) was obtained using their combination in the V+CHCB approach. It is hard to identify the uncertainty in the simulation introduced by PTFs, because the accuracy of a PTF outside of its development dataset is generally unknown. Thus it can not be easily explained why this set of PTFs works better than the other one if neither was developed and tested in the region for the simulation. Recently, the multimodal ensemble prediction method has been established to

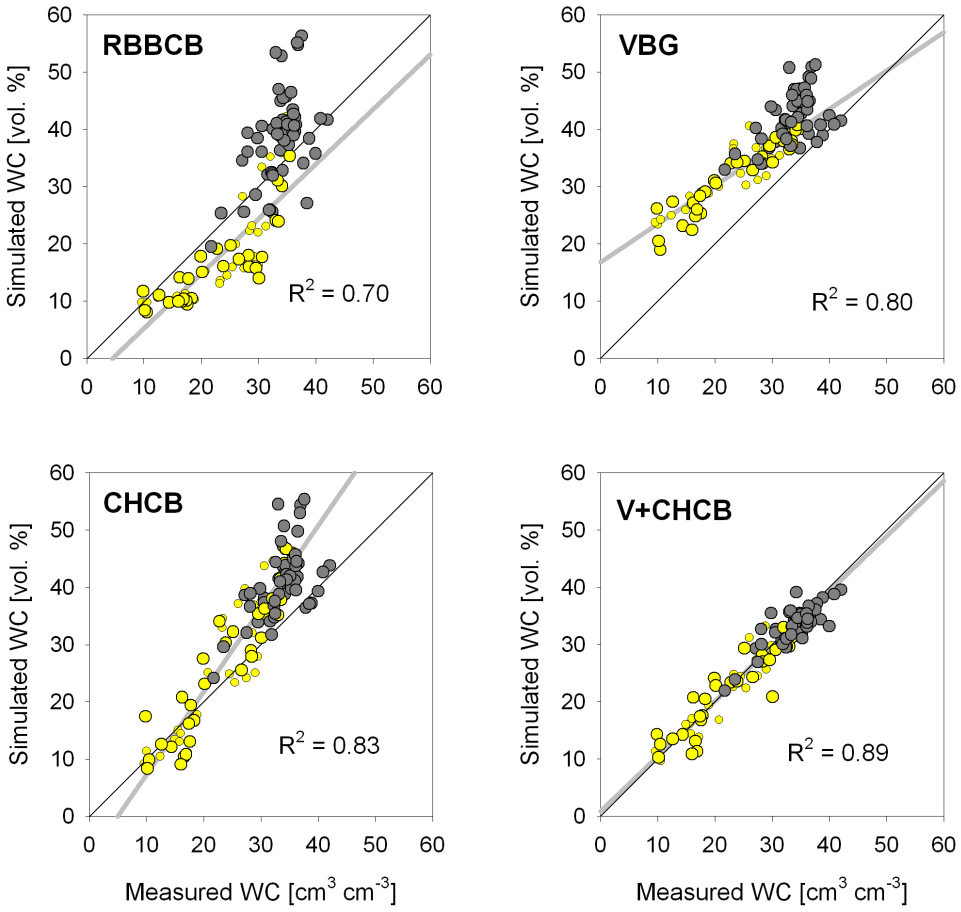

Figure 3.7: Comparison of the measured soil water content in the four soil profiles studied at three soil depths (0 -30 cm, 30 -60 cm and 60 -90 cm) in 2005 and 2006 with the predicted soil water content using four approaches (RBBCB, VBG, CHCB and V+CHCB) for the estimation of hydraulic parameters. Yellow circles indicate the data from sandy plots S1 and S2; grey circles indicate the data from clayey plots S3 and S4. The black line is the 1:1 line. The thick grey line is the regression (number of samples n=116).

address the dilemma in the use of multiple models in regions other than where they were developed and tested. Guber *et al.* (2006) presented their work to estimate the applicability of an ensemble of PTFs for water regime simulations. The basic idea of the method is straightforward since it involves the use of several models and simply averaging prediction from those models. The argument is that at present no underlying theoretical formalism exists from which a probability distribution of model uncertainty can be estimated, and hence that a pragmatic approach is needed. The V+CHCB approach in our study agrees with their idea of pragmatism.

3.3.4 Impact of hydraulic parameters on simulation of crop yield variability

In order to analyze the influence of hydraulic parameterization on the simulation of crop yield variability, the crop yields for the four study plots in 1994, 1997, 2000, 2005 and 2006 were simulated based on the hydraulic parameters estimated by the above four approaches. Fig. 3.8 shows the comparison of the observed data with the data predicted by the approaches RBBCB, VBG, CHCB and V+CHCB, respectively. Wheat was grown in years 1994, 2000 and 2006, with yields of the four plots ranging from 3.3 to 6.6 $[t/ha]$. Maize was grown in 1997 and 2005, with yields ranging from 7.9 to 9.5 $[t/ha]$. There are 20 data results in total. Similar to the soil water content, the V+CHCB approach shows the best prediction of crop yield with an R^2 of 0.78 and the approach RBBCB the worst with the R^2 of 0.46. The results of approaches VBG and CHCB show little difference, with values for R^2 of 0.66 and 0.64, respectively. However, for each approach, the regressions of crop yields are all lower than those for the regressions of the soil water contents.

The simulation results showed that the quality of simulated crop yield is also dependent on the hydraulic parameterization. The goodness of crop yield simulation is related to the goodness of the soil water simulation.

3.4 Conclusion

A comparison of θ_{sat} and K_{sat} estimated by different approaches using PTFs shows that the results from the PTFs of Vereecken are more similar to those from the infiltration experiment than those using the PTFs of Rawls & Brakensiek and Campbell.

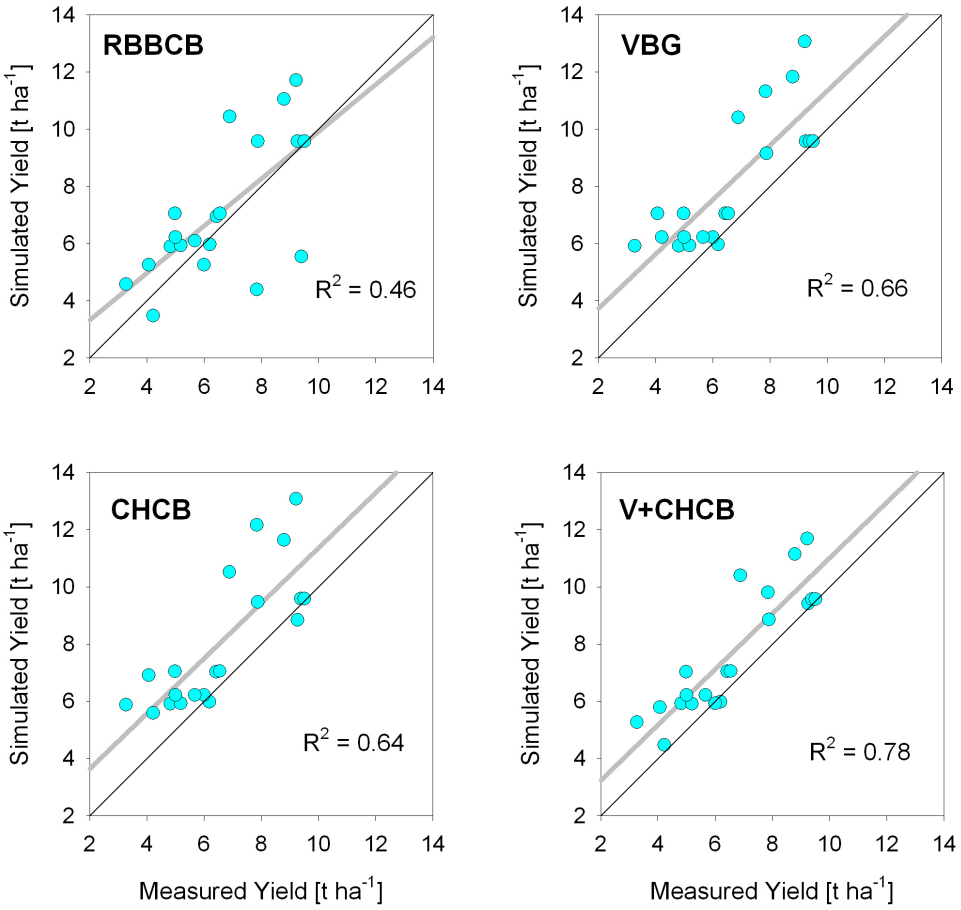

Figure 3.8: Comparison of the measured crop yields in the four soil profiles in 1994, 1997, 2000, 2005 and 2006 with the predicted crop yields using four approaches (RBBCB, VBG, CHCB and V+CHCB) for the estimation of hydraulic parameters. The black line is the 1:1 line. The thick grey line is the regression (number of samples n=20).

The simulation shows that the quality of simulated soil water content and crop yield is dependent on the hydraulic parameterization. The results simulated using the PTFs of Vereecken and Campbell did not show much difference, but were better than those for the PTFs of Rawls & Brakensiek. Compared with the PTFs of Campbell, the PTFs of Vereecken estimated similar values for θ_{sat} but different values for K_{sat}. The difference in the hydraulic parameters of the two approaches leads to some kind of differences in the simulation of the soil water content. However, it does not show a large effect on the simulation of crop yield.

Finally, the combination of the PTFs of Vereecken and Campbell proved to be the best choice for our simulation. The results indicated that the PTFs of Vereecken were suited to the estimation of θ_{sat} and K_{sat}, while the PTFs of Campbell had correctly estimated the parameter for the shape of the curves. The combined use of two sets of PTFs agrees with the idea of Guber *et al.* (2006) to utilize the generic information of multiple PTFs that were developed and tested in various regions in a pragmatic way.

After all, a comparison of the estimations of hydraulic parameters from infiltration experiment with the results from PTFs, in addition to a comparison of simulated soil water contents with the actual measurements is a practical way of choosing suitable PTFs for the soils studied.

Chapter 4

Impact of root growth model on simulation of soil water balance, root growth and crop growth

4.1 Introduction of the current root models

Root growth models are usually oversimplified mainly due to the difficulties involved in investigating roots (Skaggs & Shouse, 2008) and the lack of adequacy of the simplified assumptions of root behavior for heterogeneous and limited conditions for growth (Gregory, 2006; Wang & Smith, 2004). The importance of understanding the roots and their functioning in the vadose zone has received more and more attention in the last decade (Pages *et al.*, 2000; Skaggs & Shouse, 2008; van Noordwijk & van de Geijn, 1996; Wang & Smith, 2004). In particular, when the spatial heterogeneity in agriculture fields needs to be taken into account in crop growth modeling, a better understanding and a more adequate description of the root system and its interactions with different soil conditions are urgently required to quantify the differences in resource acquisition due to the site specific heterogeneity (Darrah *et al.*, 2006; Hopmans & Bristow, 2002).

The current root models have been separated into "Root Depth and Root Length Density Models (RLD)" and "Root System Architecture Models (RA)" by Pages *et al.* (2000). RA models consider the root system as a set of connected axes and they allow both geometrical and structural descriptions of the root system. The initial motivation for constructing such architectural models was to understand the structure and development of a root system. In contrast to the RLD models, the root uptake of water and nutrients was however not the primary

interest of the RA models. In addition, this type of model needs an extensive input of parameters related to the root morphology and branching characteristics and therefore the field application is limited (Wang & Smith, 2004). The present study was focused on the RLD models.

In most crop models such as CERES (Ritchie & Godwin, 1989) and (Jones & Kiniry, 1986), SUCROS (van Laar *et al.*, 1997) and SPASS (Wang & Engel, 2000), the subroutines for root growth simulation belong to the RLD models. Here root system growth has been designated as either vertical penetration of the roots or as a vertical distribution of the root length in separate simulation layers of the whole soil profile. The simulated properties of rooting depth and root length density are then used, together with plant water demand, uptake ability, and soil water/nutrient content to estimate water and nutrient extraction from the soil. The basis of this simplification is a series of assumptions of homogeneity, invariability and non-limitation with respect to root activity, soil impacts on root distribution, and shoot:root carbon partitioning. The complexity of individual models can therefore vary according to the details of the assumptions made. Comprehensive reviews about the root models in the recent years have been presented by Pages *et al.* (2000); van Noordwijk & van de Geijn (1996); Wang & Smith (2004) among others.

The RLD models have reached an advanced stage of development. They are compatible for the quantification of crop growth effects via the root system for soil factors and shoot-root interactions in an empirical way (Pages *et al.*, 2000). All of these models differ mainly in (**1**) the consideration of environmental impacts on root growth in terms of root penetration, root distribution, root senescence and the transformation of root biomass to root length and (**2**) the consideration of shoot -root interaction in terms of carbon partitioning (Pages *et al.*, 2000). The limiting factors of temperature, soil water and nitrogen conditions are considered by some models. However, the effect of soil resistance and soil structure is mostly neglected (Priesack *et al.*, 2008; Wang & Smith, 2004). Wang & Smith (2004) pointed out that the oversimplification of root response to soil drying and hardness probably lead to oversimplification of root growth and water uptake in dense soils.

The root model incorporated in the CERES models by Jones & Kiniry (1986) and Ritchie & Godwin (1989) (termed the CERES-Root Model in the following discussion) is one of the most commonly employed and widely tested root models. However, it is also frequently criticized because of its oversimplification due to the

neglect of soil constraints (Pages *et al.*, 2000). The root model of the SPASS model by Wang & Engel (2000) (termed SPASS-Root Model in the following discussion) has adopted the CERES-Root model and added an additional stress factor of soil temperature beside the water and nitrogen deficit factors that were originally included in the CERES-Root Model. The neglection of the soil constraints effect however may lead to an inaccuracy of root and crop growth simulation when dealing with fields of compact soil or highly structured soil. The stand-alone root growth model by Jones *et al.* (1991) (termed Jones-Root Model from here on) is well known as one of the most comprehensive RLD model in terms of considering soil constraints (Manschadi *et al.*, 1998; Pages *et al.*, 2000; Wang & Smith, 2004). However, this model does not include the effect of soil mineral nitrogen on root distribution and considers only the indirect effect of soil water via its effect on soil constraints. In addition, it differs from the first two root models in the calculation of the daily root length increase in each layer. Above all, Jones-Root Model as a stand-alone model needs to be linked via shoot : root interaction routines as introduced in other models for the application.

4.2 Materials and methods

4.2.1 Description of the new root model

In the present work, the SPASS-Root Model and Jones-Root Model are combined and to some extent modified to create a new model that can be adapted to the conditions of the current study. The new root model is incorporated into the soil -plant -atmosphere modeling package Expert-N (Priesack, 2006; Priesack *et al.*, 2008) and can be linked to the CERES-Maize and CERES-Wheat models proposed by Jones & Kiniry (1986) and Ritchie & Godwin (1989). The constitutive modifications are based on the selection of the particular factors and processes relating soil -root and root -shoot interactions which are most important for our case. The calculations of processes involved, such as the definition of soil stress factors, the daily increase in rooting depth, the root proliferation in soil profile and the root death are described in the following sections.

A. Soil factors affecting rooting

As in the models currently used, the growth impacts were expressed as stress factors ranging from 0.0 (no growth) to 1.0 (no stress). Inferring from our field

measurement of soil properties and vertical root distribution, the stress due to soil temperature, coarse fragment, and soil bulk density, sand content, soil water content and aeration, as well as soil mineral nitrogen content, could be the major effects on the root growth in the field studied. Therefore, stress factors for these soil properties expressed as $\alpha_{strength}$ and α_{coarse}, state variables of the O_2 deficit factor α_{O_2}, water deficit factor α_θ, nitrogen deficit factor α_N, and temperature factor α_{Temp} should be given for the simulation of the root growth. As there was little evidence of the effects due to aluminum toxicity and calcium deficiency, these two parameters were not considered in our model. For the following calculation, the soil profile is divided into simulation layers of 5 cm. The soil factors are calculated for each layer.

Soil hardness stress factor $\alpha_{strength}$ In the Jones-Root Model, the effects of soil bulk density, sand content and water content are combined in the stress factor due to soil hardness. Jones *et al.* (1991) proposed a simple approach using a maximum and optimum bulk density as well as a soil water availability factor to model the effect of soil hardness on root growth. In our model, the quantification of the soil hardness stress is modified. Based on the fact that there is little growth inhibition in the early stages of drying, while the effect becomes more prominent as soil water decreases, a sine function is proposed to approximate the relationship between the soil hardness factor $\alpha_{strength}$ and the relative water saturation $\alpha_{\theta_{PAW}}$ (Eq. 4.1). Based on another fact that sandy soil is even harder if there is no water, the second sine function in Eq. 4.1 is introduced to emphasize the effect of drying on sandy soil:

$$\alpha_{strength} = \alpha_{BD} * \sin(\frac{\pi}{2} * \alpha_{\theta_{PAW}}) * \sin(\frac{\pi}{2} * \alpha_{\theta_{PAW}})^{\frac{f_{Sand}}{2}} \quad (4.1)$$

$$\alpha_{\theta_{PAW}} = \frac{\theta - \theta_{pwp}}{\theta_{fc} - \theta_{pwp}} \quad (4.2)$$

$$\alpha_{BD} = \max[0.0, \min(1.0, \frac{BD_X - BD}{BD_X - BD_O})] \quad (4.3)$$

$$BD_X = 1.3 + 0.004 * f_{sand} \quad (4.4)$$

$$BD_O = 1.7 + 0.005 * f_{sand} \quad (4.5)$$

where $\alpha_{strength}$ [-] is the stress factor due to soil hardness; $\alpha_{\theta_{PAW}}$ [-] is the fractional plant available water content calculated from the actual water content

θ $[cm^3/cm^3]$, field capacity θ_{fc} $[cm^3/cm^3]$ and permanent wilting point θ_{pwp} $[cm^3/cm^3]$ as in Eq. 4.2 proposed by Jones *et al.* (1991); f_{sand} [-] is the sand content of the soil measured as percent by weight; α_{BD} [-] is the stress factor due to the soil bulk density, which is dependent on the BD_X $[g/cm^3]$ and BD_O $[g/cm^3]$ – the moist bulk density at which no growth and maximal root growth occurs, respectively.

O_2 deficit stress factor α_{O_2} The calculation of the stress factor due to poor aeration α_{O_2} is according to the approach in the Jones-Root Model, with a slight modification in the relationship between critical porosity and clay content. In contrast to the Jones-Root Model, we assumed that for a given water content, crop roots in soils of high clayey content are more sensitive to an aeration deficit than in a sandy soil:

$$\alpha_{O_2} = min(1.0, \frac{1 - S_e}{1 - \theta_{cri,poro}}) \tag{4.6}$$

$$\theta_{cri,poro} = 0.4 - 0.008 * f_{clay} \tag{4.7}$$

$$S_e = \frac{\theta}{\theta_{sat}} \tag{4.8}$$

where α_{O_2} [-] is the stress factor due to an O_2 deficit; $\theta_{cri,poro}$ [-] is the critical water-filled porosity, which is related to the clay content f_{clay} [-] as defined in Eq. 4.7; S_e is the effective water content ratio [-]. The stress factor for excessive coarse fragments $>$ 2 mm α_{coarse} [-] were referred to Jones-Root Model (Jones *et al.*, 1991). The calculation of the stress effect due to soil temperature (α_{Temp}) [-], water stress α_θ [-] and nitrogen deficit α_N [-] were from the reference to the SPASS-Root Model (Wang, 1997).

B. Depth increase of rooting front

Initially Jones *et al.* (1991) used the term growth stage (GS) to assess the phenological development of the plant. The GS value ranges from 0.0 to 1.0 from seeding to harvest. In the Jones-Root Model, the downwards progress of the rooting depth is a function of the species-specific maximum rooting depth and the growth stage at which the root system ceases to increase in depth in deep soils without any rooting constraints (GSR). The actual daily increase in root depth can be affected by the stress factors present. In contrast to this, the rooting depth

in the new model is simulated using a genotype-specific maximum root extension rate, reduced by stress due to soil temperature, soil hardness, coarse fragment and aeration in the deepest rooting soil depth. The penetration continues until the crop reaches the development phase of grain filling or when the actual rooting depth exceeds the given genotype-specific maximum rooting depth. This approach was adapted from the SPASS-Root Model (Wang, 1997).

C. Root proliferation in soil profiles

C.1 Definition of the weighted stress index

The most significant modification in the new root model is the introduction of a weighted stress index $\overline{\alpha(i)}$ [-] to assess the relative adequate properties of the simulation layers for root growth. The $\overline{\alpha(i)}$ of the i -simulation layer is estimated by the root distribution factor $\omega(i)$ [-] and the most limiting stress factor present in this layer as follows:

$$\overline{\alpha(i)} = \alpha(i) * \omega(i) \tag{4.9}$$

$$\alpha(i) = \min(\alpha_{Temp}, \alpha_{strength}, \alpha_{coarse}, \alpha_{O_2}, \alpha_{\theta}, \alpha_N) \tag{4.10}$$

$$\omega(i) = \exp(-\xi * \frac{Z_{mid}(i)}{RD_{max}}) \tag{4.11}$$

where the exponential equation for the estimation of root distribution factor $\omega(i)$ [-] is imposed from the CERES-Root Model; $Z_{mid}(i)$ [cm] and RD_{max} [cm] are the depth to the middle of each simulation layer and the maximum rooting depth, respectively, and ξ is a crop-specific parameter.

C.2 Reduction of potential total root growth in a stress environment

In the Jones-Root Model as a stand-alone root model, the daily dry matter allocation to the root system is introduced through an input file. Then the daily potential for root biomass increase in a simulation layer is calculated as a function of the present root length density and a maximum rate (assumed to be 5.0 [km root/ m^3]), modified by the layer-weighting factor (similar to the root distribution factor $\omega(i)$) and the stress factors. The root weight increase is then converted to the root length by the actual length/weight ratio, which is dependent on the species, growth stage and stress factors in each simulation layer. The root increase in each simulation layer is subsequently summed over the rooting profile and compared with the dry matter allocation to the root system, which

is available from the input data. If the calculated total root increase exceeds the dry matter allocation, the actual root increase is re-calculated by partitioning the dry matter allocation according to the former distribution of potential root increase over the rooting depth. Jones *et al.* (1991) ascribed this loss of dry matter underground to the extra energy costs of growing and maintaining roots in a stress environment. In our model, by incorporating the CERES crop model, the daily dry matter allocation to the root system is calculated as a function of the daily total biomass increase and a crop-specific shoot:root ratio. To assess the total stress effects on the loss of allocation for new roots, $\overline{\alpha(i)}$ is summed over the rooting depth giving a factor α_{sum} [-] (Eq. 4.12), which ranges from 0.0 to 1.0 corresponding to "no growth" and "no stress", respectively. This factor is then used to multiply the daily total potential root growth $RBGROW_{pot}$ [kg] to estimate the daily actual total root growth $RBGROW_{act}$ [kg] in Eq. 4.13.

$$\alpha_{sum} = \sum_{i=1}^{n} \overline{\alpha(i)} \tag{4.12}$$

$$RBGROW_{act} = \alpha_{sum} * RBGROW_{pot} \tag{4.13}$$

Under inadequate soil conditions, a possible survival strategy of the plants is to reduce the resource demand by limiting the aboveground size. This process is stimulated by an inhibitory hormone signaled by the roots (Passioura, 2002). In our model, the feasibility of this strategy was initially tested by introducing an interaction between the root and shoot. We assumed that this process occurs only when the soil conditions in sub-soils are much less favourable for root growth than in top soils. The stress index $\overline{\alpha(i)}$ is used here again to assess the relative adequacy of the simulation layers for root growth. On the assumption that a plant prefers to grow roots down to the k -simulation layer, the $\overline{\alpha(i)}$ are only summed together from the $k+1$ -simulation layer to the end of the rooting depth to calculate the $\alpha_{sub,sum}$ [-] as in Eq. 4.14. In this study, we assume that the root growth will be limited within 30 cm soil depth, which is 5 cm below the plough layer of 25 cm. In this case, $k = 6$. The $\alpha_{sub,sum}$ are then compared with the α_{sum} of all soil horizons (Eq. 4.15). If the ratio γ [-] is lower than a critical value γ_{cri} [-], then no root growth occurs (Eq. 4.16). In our model, the γ_{cri} was adjusted to be 0.001 for maize and 0.1 for spring wheat. The radical reduction in root growth results directly in a reduction in the water and nitrogen uptake. If the water and nitrogen supply cannot meet the current demand, then the shoot growth is also

decreased. In this way, a balance between resource supply and crop growth can be reached.

$$\alpha_{sub,sum} = \sum_{i=k+1}^{n} \overline{\alpha(i)} \tag{4.14}$$

$$\gamma = \frac{\alpha_{sub,sum}}{\alpha_{sum}} \tag{4.15}$$

$$if(\gamma \leq \gamma_{cri}), \quad RBGROW_{act} = 0 \tag{4.16}$$

C.3 Partitioning of root biomass growth in simulation layers of soil

Other than the Jones-Root Model, the actual root biomass growth up to this step has already taken into account the loss of dry matter due to a stress environment. Now the total root growth will be partitioned in the simulation layers till rooting depth. For a calculation of the layer-weighting root growth partitioning index $\lambda(i)$, the actual root length/weight ratio $LWA(i)$ is considered in addition to the $\overline{\alpha(i)}$ (Eq. 4.17). Jones *et al.* (1991) proposed an approach to calculate the $LWA(i)$ [km/kg] for each simulation layer as a function of the genotype-specific length/weight ratio of seeding roots $LWS(i)$ [km/kg], the length/weight ratio of a mature root system $LWM(i)$ [km/kg], growth stage GS, the distance between the depth of this layer $Z_{mid}(i)$ [cm] and the actual rooting depth RD [cm], as well as the soil constraints in this layer (Eq. 4.18 and Eq. 4.19). The function results from the fact that there are more fine roots at the beginning of the growth stage or at the rooting front. Roots become thicker when exposed to high soil resistance and a high coarse fragment content. Therefore, Eq. 4.17 reflects the fact that the larger the product, the more appropriate this layer is for root proliferation in comparison with other layers.

$$\lambda(i) = \frac{\overline{\alpha(i)} * LWA(i)}{\sum_{i=1}^{n} \overline{\alpha(i)} * LWA(i)} \tag{4.17}$$

$$LWA(i) = \frac{LWN(i)}{1.0 + 3.0(1.0 - min(\alpha_{strength}, \alpha_{coarse}))} \tag{4.18}$$

$$LWN(i) = LWS - GS(LWS - LWM)(1.0 - \frac{Z_{mid}(i)}{RD}) \tag{4.19}$$

where $LWN(i)$ [km/kg] is the normal root length/weight ratio without any stress effect. This layer-weighting index is then used to calculate the partition of the

total root growth in simulation layers within the rooting depth:

$$RBGROW(i) = \lambda(i) * RBGROW_{act} \tag{4.20}$$

where $RBGROW(i)$ [kg] is the daily actual root biomass increase in each simulation layer.

D. Root death

Death of some roots during the growing phase is calculated based on the approach suggested by Jones *et al.* (1991), with some modification to the assessment of the stress effect. As a first approximation, 1.0% of the dry weight in a layer is assumed to be lost per day. As in the Jones-Root Model, the death rate of maize roots can be increased by a factor up to 2.0 under low soil moisture and poor aeration conditions (Eq. 4.21). With the assumption that wheat is more sensitive to water and aeration conditions, the death rate of wheat roots can even be enhanced by a factor up to 4.0 (Eq. 4.22). The combined effects of the layer water stress factor (α_θ), the layer aeration factor (α_{O_2}) and root weight in a particular layer $RB(i)$ on root death $RBDEATH(i)$ are calculated as:

$$RBDEATH(i) = 0.01 * RB(i) * (1.0 + max(1 - \alpha_\theta, 1 - \alpha_{O_2})) \tag{4.21}$$

$$RBDEATH(i) = 0.01 * RB(i) * (1.0 + max(1 - \alpha_\theta, 1 - \alpha_{O_2}))^2 \tag{4.22}$$

where max(arguments) is the maximum value in the argument list. Jones *et al.* (1991) provided an option to specify the growth stage at which normal root senescence due to whole-plant senescence begins in determinate crops, the GSD [-]. When the growth stage (GS) is greater than the GSD, an additional increment of root death is added to the calculation as:

$$RBDEATH(i) = RBDEATH(i) + RB(i) * (\frac{GS - GSD}{1.0 - GSD})^{3.0} \tag{4.23}$$

where $RB(i)$ [kg] is the actual root biomass in the i -simulation layer. This function causes rapid root system senescence as the crop reaches physiological maturity (Jones *et al.*, 1991).

E. Daily root biomass and root length density

The actual daily root biomass increase in each layer $RBGROW(i)$ is then corrected by excluding the actual root death (Eq. 4.24), and the actual daily root

length increase in each layer $RLGROW(i)$ is then calculated by multiplying the $RBGROW(i)$ by the actual root length/weight ratio $LWA(i)$ (Eq. 4.25)

$$RBGROW(i) = RBGROW(i) - RBDEATH(i) \quad (4.24)$$

$$RLGROW(i) = RBGROW(i) * LWA(i) \quad (4.25)$$

Finally, the actual daily root biomass/length density in each layer is updated according to the actual root growth, the layer depth and the previous root biomass/length density.

4.2.2 Simulation experiments

In order to examine the capabilities of the new root model, crop growth as well as water balance and nitrogen balance were simulated for the growing seasons of 2005 and 2006 by incorporating the new root model into the CERES-Maize of Jones & Kiniry (1986) and CERES-Wheat of Ritchie & Godwin (1989). Simulated soil water content, root length density and crop growth were then compared with the measured values.

Dataset

Data for soil properties, weather and crop yield were the same as those used in the Chapter 3. In addition, the root length density data were from the field observations presented in Chapter 2. The hydraulic parameters K_{sat}, θ_{sat}, Campbell -A and Campbell -B were estimated by the **V+CHCB** approach given in Chapter 3. The soil input data are listed in Tab. 4.1.

Model configuration

The models used for the simulation of soil water flow, heat transfer, N-transport and N-turnover were the same as those described in Section 3.2.3. As opposed to the simulation in Chapter 3, only the hydraulic functions of Hutson & Cass and the pedo transfer functions of Campbell and Vereecken were used here for the parameterization of the water flow model. Both the original CERES Model (termed as CERES in the following discussion) and the modified CERES Model (termed as CERES+ from here on), into which the new root growth model was incorporated, were used for the subsequent simulation. The crop genetic parameters used by the new root model are presented in Tab. 4.2.

Table 4.1: Soil properties of plot S1, S2, S3 and S4 for simulation input. Z, soil depth; ρ, bulk density; K_{sat}, saturated conductivity; θ_{sat}, saturated soil water content; a, Campbell A; b, Campbell B.

Soil horizon	Z	Clay	Silt	Sand	Rock	ρ_s	C_{org}	K_{sat}	θ_{sat}	a	b
	$[cm]$	[%]	[%]	[%]	[%]	$[g/cm^3]$	[%]	$[mm/d]$	$[cm^3/cm^3]$	$[kPa]$	[-]
Plot S1											
1	0-10	23.5	33.5	43.0	1.5	1.34	1.33	394	0.49	-2.4	7.3
2	10-20	23.5	33.5	43.0	1.5	1.68	0.92	80	0.37	-7.3	7.3
3	20-30	23.5	33.5	43.0	1.5	1.56	0.24	80	0.43	-5.0	7.3
4	30-45	19.0	19.2	61.8	1.5	1.52	0.17	185	0.48	-2.5	5.88
5	45-65	12.5	17.7	69.8	1.5	1.38	0.17	970	0.53	-1.3	4.47
6	65-85	7.3	16.2	76.5	1.5	1.38	0.15	970	0.53	-0.98	3.37
7	85-90	4.2	13.7	82.1	1.5	1.24	0.15	1533	0.55	-0.68	2.68
Plot S2											
1	0-10	13.3	21.3	65.4	1.5	1.45	1.14	220	0.45	-1.7	4.81
2	10-20	13.3	21.3	65.4	1.5	1.69	0.78	220	0.36	-2.7	4.81
3	20-30	13.0	3.7	83.3	1.5	1.57	0.15	32	0.41	-1.3	3.82
4	30-55	5.6	2.8	91.6	30.0	1.54	0.10	85	0.42	-0.83	2.34
5	55-75	2.1	2.5	95.4	30.0	1.43	0.05	2611	0.48	-0.62	1.74
6	75-90	2.4	3.9	93.7	30.0	1.43	0.05	2611	0.48	-0.65	1.86
Plot S3											
1	0-10	20.4	48.2	31.4	4.6	1.47	0.75	166	0.50	-4.4	7.25
2	10-20	20.4	48.2	31.4	2.0	1.72	0.34	26	0.50	-9.5	7.25
3	20-45	36.7	38.6	24.7	2.4	1.64	0.32	39	0.38	-17	10.1
4	45-60	40.3	31.7	28.0	8.0	1.74	0.29	24	0.42	-28	10.5
5	60-75	31.9	34.8	33.3	8.0	1.87	0.17	11	0.46	-25	8.95
6	75-90	27.7	15.7	56.6	53.0	1.88	0.17	9	0.46	-11	7.59
Plot S4											
1	0-10	18.9	43.9	37.2	3.3	1.43	1.06	239	0.50	-3.3	6.8
2	10-20	18.9	43.9	37.2	3.3	1.73	0.81	24	0.50	-7.9	7.3
3	20-40	21.2	45.8	33.0	3.3	1.63	1.08	60	0.48	-7.2	8.54
4	40-45	28.1	43.8	28.1	9.0	1.59	0.87	110	0.48	-9.3	7.94
5	45-50	23.9	48.8	27.3	3.1	1.59	0.53	105	0.48	-8.1	7.06
6	50-70	18.7	51.2	30.1	3.9	1.67	0.41	113	0.48	-7.9	7.42
7	70-90	19.8	54.5	25.7	4.6	1.67	0.31	182	0.48	-9.3	7.7

Table 4.2: Genetic parameters for the root model of maize (MZ) and wheat (WH). GSD, growth stage when normal root senescence begins; GSR, growth stage when root depth reaches maximum; LWM, normal ratio of root length to weight in plough layer at maturity; LWS, normal ratio of root length to weight in seeding; ξ, crop-specific parameter for the estimation of root distribution factor; RD_{max}, maximal rooting depth.

Crop	GSD [-]	GSR [-]	LWM [m/g]	LWS [m/g]	ξ	RD_{max} [cm]
MZ	0.8	0.6	200	100	6.0	100
WH	0.8	0.7	500	250	8.0	200

Simulation strategy

The objective was to establish the influence of the two root subroutines on the simulation of soil water content, root length density distribution and crop growth.

After running the simulation using the two root models, the respective simulated root length density distributions, soil water contents and crop growths were compared with the measured values from the four study plots in 2005 and 2006. The sensitivity of the two root models to water supply were compared by running the simulation for 2005 and 2006 using modified daily precipitation rate data. Data-sets of minus 25%, minus 50%, plus 25% and plus 50% of the original rainfall data were used for maize growth simulation and additional data-set of plus 75% was used for spring wheat. Finally, the performance of the new root model was verified by simulating the crop yield for an additional three years (wheat in 1994 and 2000 and maize in 1997). For comparison, simulations for the five years were also run by the CERES Model using the same soil, weather data as well as the model configuration for the simulation of soil water and nitrogen balance.

Statistical analysis

In order to access the degree of agreement between simulated and measured values for dry yield, the statistical parameter coefficient of determination R^2 for the regression analysis and modeling efficiency (EF) were used. As suggested by

(Yang *et al.*, 2004), EF is calculated as follows:

$$EF = 1 - \frac{\sum_{i=1}^{n}(P_i - M_i)^2}{\sum_{i=1}^{n}(M_i - \overline{M_i})^2} \tag{4.26}$$

where P_i denotes the predicted values, M_i the measured values, $\overline{M_i}$ the mean of M_i, and n the number of the measurements. EF = 1 indicates perfect agreement of the model predictions with the direct measurements of the parameter. An EF = 0 indicates that the model predictions are as accurate as the mean of the observed data, whereas an efficiency less than zero (EF $<$ 0) occurs when the observed mean $\overline{M_i}$ is a better predictor than the model. Essentially, the closer the EF is to 1, the more accurate the model is.

4.3 Results and discussion

4.3.1 Comparison of measured and simulated RLD distribution in 2005 and 2006

A comparison of measured and simulated root length density at maturity of the crops in 2005 and 2006 using models CERES and CERES+ is illustrated in Fig. 4.1. Fig. 4.2 presents the regression lines of the measured and simulated RLDs for both years using the two models. Equations for the regression lines, coefficient of determination R^2 and modeling efficiency (EF) are also given in the Fig. 4.2. The observation of maize root length densities shows that plot S2 has the highest RLD at the depth of 0 -15 cm among the other plots. Moreover, the relative distribution of the RLDs at these three depths for plot S1 is different from that of plots S2, S3 and S4. The RLDs predicted by the new root model are in close agreement with the measured data (Fig. 4.1). The difference in vertical distribution where the roots in plot S1 prefer sub-soil and the roots in plot S2 prefer top soil is well reproduced by model CERES+, whereas the RLDs predicted by CERES have little difference in the vertical distribution in all four plots. In comparison with the maize RLD, the measured RLD for spring wheat shows that more wheat roots are found in the sub-soils. Compared with plots S1 and S4, plots S2 and S3 have much lower RLD. No more roots could be found below depths of 60 and 90 cm at these two plots, respectively. At plot S2, the RLD already decreases dramatically below a depth of 40 cm. The predicted RLDs by CERES+ are also in reasonable agreement with observed values (Fig. 4.1, right), except that the RLDs in the sub-soils of plots S1 and S2 are slightly overestimated and the RLDs in plot S3 below a soil depth of 15 cm and in plot S4 below 40 cm are slightly underestimated. Compared to CERES+, CERES generally overestimates the wheat RLDs in all soil depths (Fig. 4.1). For both maize and wheat, the RLDs predicted by CERES+ are much closer to the measured values than that by CERES. The improvement of CERES+ is supported by the R^2 of regression and modeling efficiency (EF) for the data of both years (Fig. 4.2). Model CERES+ has increased the R^2 of regression from 0.42, obtained by model CERES, to 0.78. The modeling efficiency (EF) of CERES+ is 0.73, which indicates a good agreement of the model predictions with the measurements. Whereas the EF of CERES is -4.31, which indicates that the observed mean is a better predictor than the model.

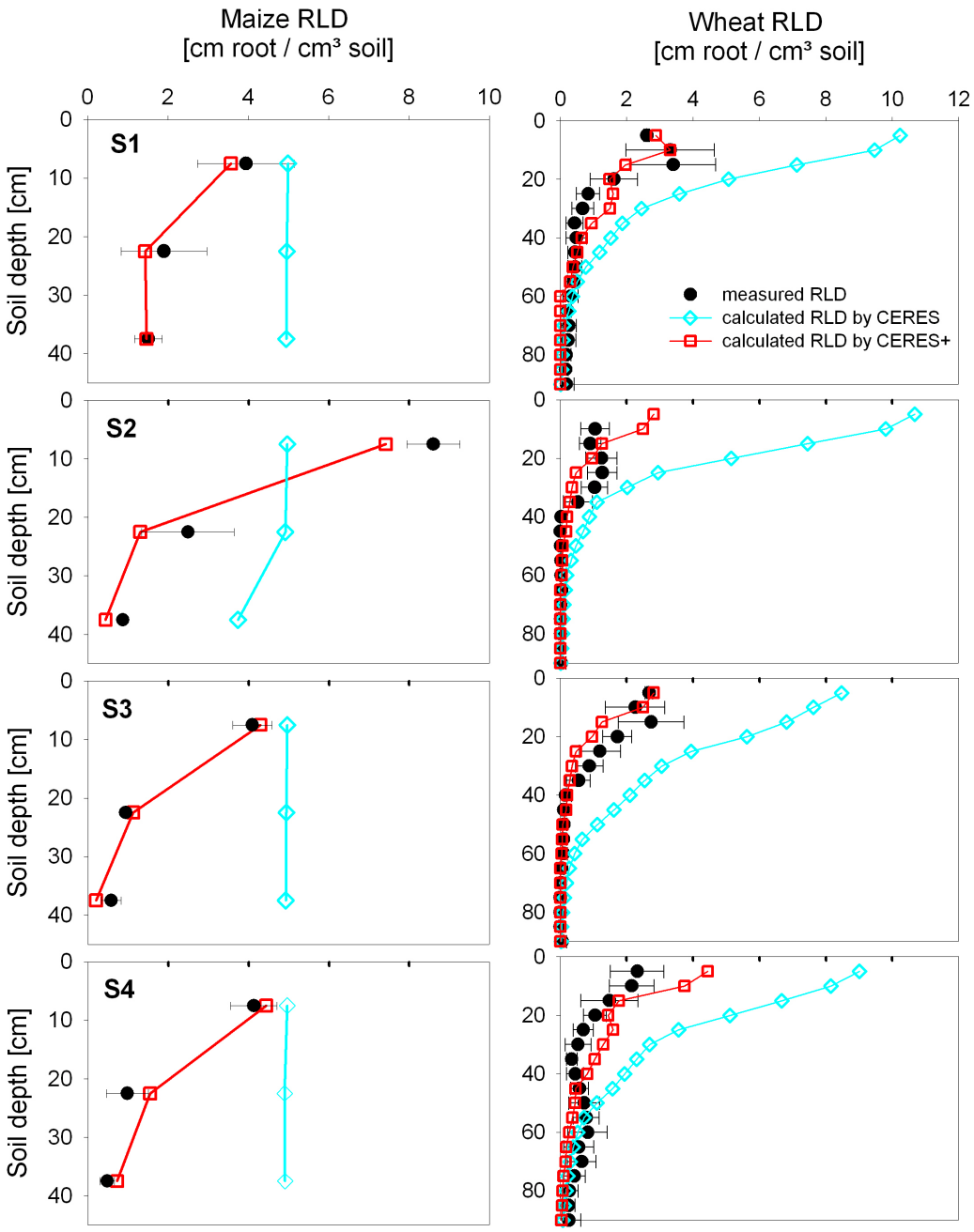

Figure 4.1: Comparison of observed and simulated root length density (RLD) of maize on 12^{th} Oct.2005 (left) and RLD of spring wheat on 12^{th} July 2006 (right) at plots S1, S2, S3 and S4. For each figure, black close circles and error bars represent mean and standard errors of measured RLD, cyan lines with open cyan diamonds represent simulated RLD using CERES, red lines with open red squares represent simulated RLD using CERES+

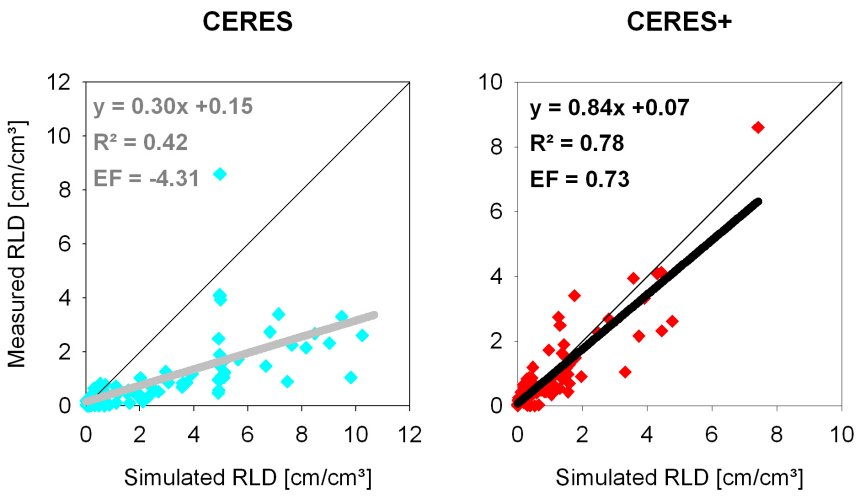

Figure 4.2: Regression lines of the measured RLD for four plots in 2005 and 2006 with those predicted by the original CERES model (left, cyan diamonds) and by the CERES+ Model (right, red diamonds). Thin black line is the 1:1 curve, thick grey line and black lines are regressions for the simulation by CERES and by CERES+, respectively (number of samples n = 84). R^2, coefficient of determination; EF, modeling efficiency.

The present root growth model in CERES+ differs significantly from the subroutine for root growth simulation in original CERES in following considerations:

1. including the stress effect due to soil hardness, which is related to the soil bulk density, soil texture and soil water content, and the stress effect due to a deficiency of O_2;

2. including the reduction of potential total root growth in a stress environment, which is assessed by the stress index $\overline{\alpha(i)}$;

3. including the adaptive partitioning of root growth in soil depth in response to heterogeneous soil conditions.

The modeling approaches for stress effect due to soil hardness and O_2 deficiency were adapted from the Jones-Root Model with slight modifications. The success of the CERES+ in representing the observed RLDs in this study revealed that the root growth model framework developed by Jones *et al.* (1991) can be adapted and successfully applied for the prediction of maize and wheat root growth and distribution under limited soil conditions. Similar conclusion

was drawn for example by Benjamin *et al.* (1996) for maize rooting patterns and Manschadi *et al.* (1998) for faba bean root growth.

The significant improvement of the simulation for both total RLD and root distribution in the soil depth using CERES+ indicated that the assumptions considering the adaptive response of the root growth and root distribution to the limited soil conditions could meet the reality. A general discussion with respect to the root distribution affected by soil constraints and resource availability is given in Section 6.2.

4.3.2 Comparison of measured and simulated soil water contents in 2005 and 2006

Because there is little difference between the soil water contents (SWCs) in 2005 and 2006 predicted by models CERES and CERES+, only the simulated SWCs using model CERES+ are compared with the measured soil water content in Fig. 4.3. The regression lines of the measured SWCs and the simulation values using the two models, the equations for the regression lines, coefficient of determination R^2 and modeling efficiency (EF) are presented in Fig. 4.4.

Fig. 4.3 shows us that there is generally higher water content observed in the soil profile of the clayey plots S3 and S4 than in the sandy plots S1 and S2. Plot S2 is obviously the driest one and plot S3 the wettest one. In addition, the WC in sandy plots shows greater differentiation over three soil depths than in clayey plots. The SWCs in plots S1 and S2 decrease with the soil depth, while the SWCs in plots S3 and S4 are slightly higher in the sub-soil than in top soil. These differences between the four plots, shown by the observation, are well represented by the simulation. The predicted soil water contents in 2006 are generally lower than those in 2005, which corresponds well with the differences in rainfall and temperature for the two years. In accordance with the measurements, the simulation clearly shows the drop in SWC in the dry period in July 2006, especially in the two sandy plots. In general, the simulated SWCs are in close agreement with the observed values (Fig. 4.4). Having a R^2 of 0.91, the simulation using model CERES+ is slightly better than that using model CERES ($R^2 = 0.89$). The modeling efficiencies (EFs) of both models are 0.90, which indicates a very good agreement of the model predictions with the measurements.

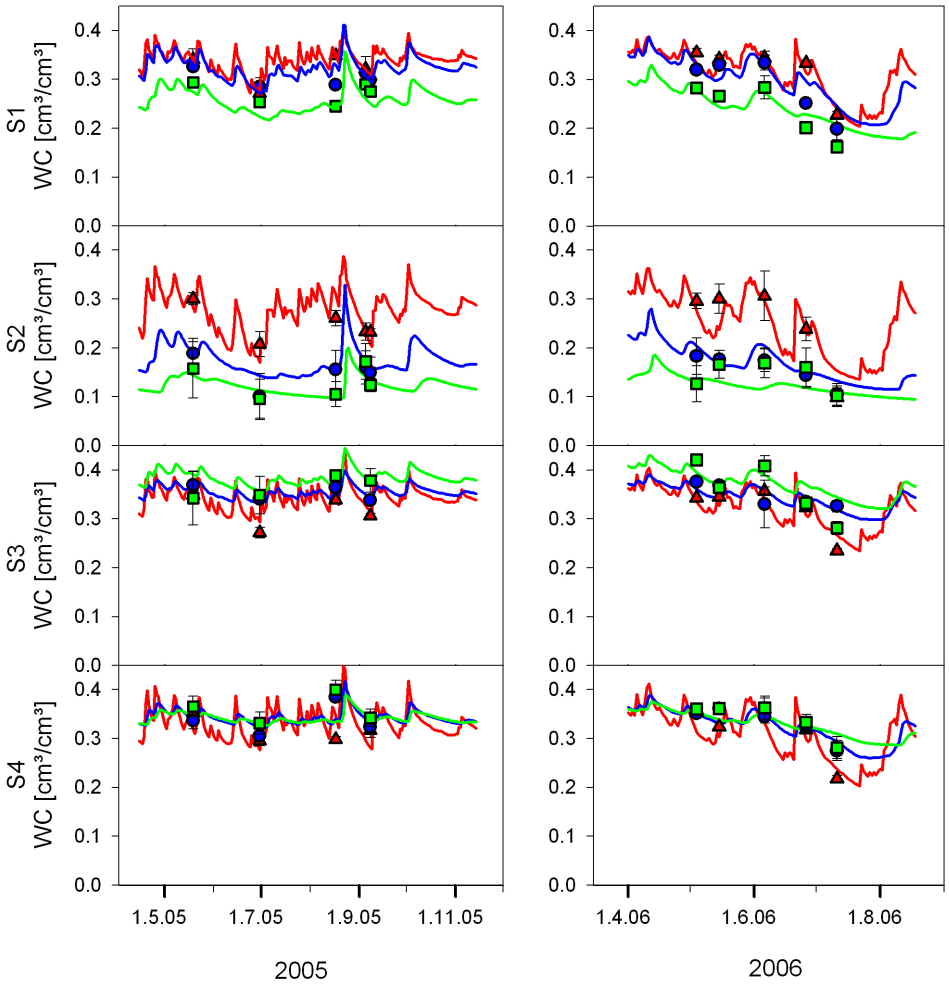

Figure 4.3: Comparison of observed (symbols and error bars = mean and SD) and simulated (lines) volumetric soil water contents for growing season 2005 (left) and 2006 (right) at plot S1, S2, S3 and S4 using CERES+. In each soil water content figure, red lines and red triangles = WC in the 0 -30 cm soil depth; blue lines and blue circles = WC in the 30 -60 cm soil depth; green lines and green squares = WC in the 60 -90 cm soil depth.

4.3.3 Comparison of measured and simulated crop growth in 2005 and 2006

The observed and simulated crop growths with respect to the total aboveground biomass (2005), LAI (2006) and yield in both years are compared in Fig. 4.5 and Fig. 4.6, respectively.

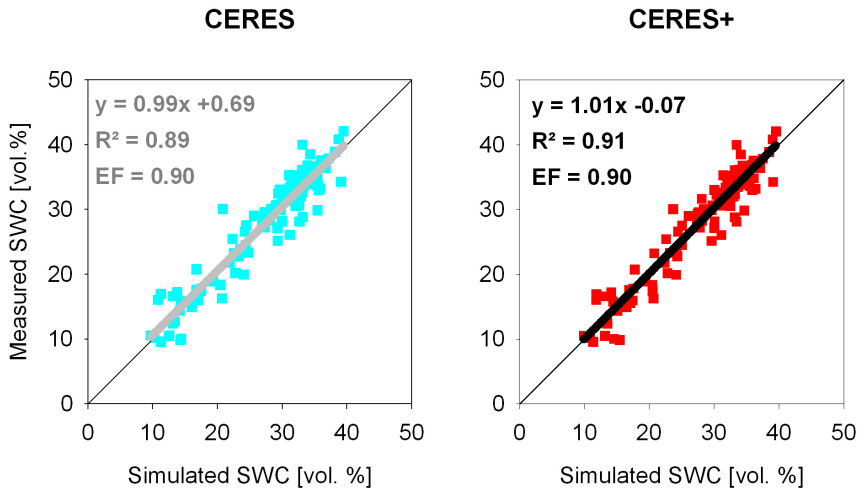

Figure 4.4: Regression lines of the measured soil water content for four plots in 2005 and 2006 with those predicted by the original CERES model (left, cyan squares) and by the CERES+ Model (right, red squares). Thin black line is the 1:1 curve, thick grey line and black lines are regressions for the simulation by CERES and by CERES+, respectively (number of samples n = 116). R^2, coefficient of determination; EF, modeling efficiency.

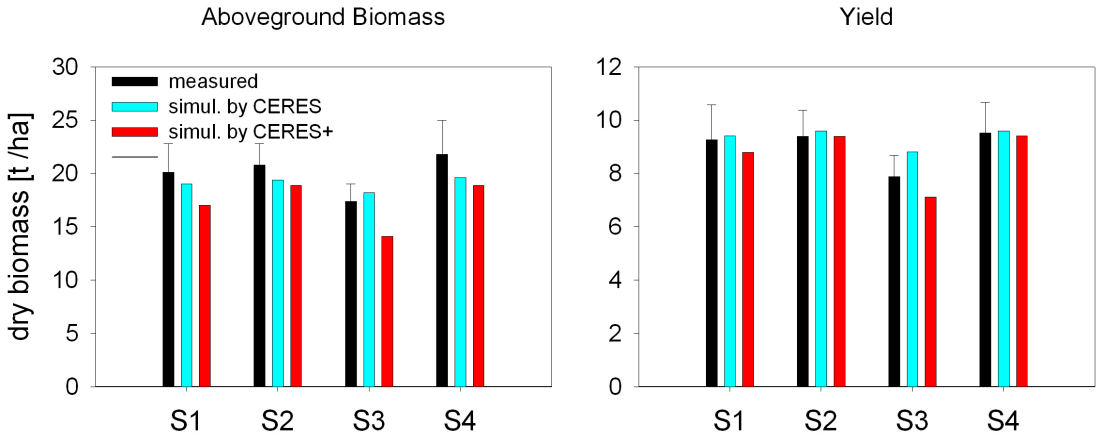

Figure 4.5: Comparison of observed and simulated above-ground biomass and yield for maize at harvest in 2005. Black bars, measured value; cyan bars, simulation by original CERES-Maize; red bars, simulation by modified CERES-Maize (CERES+).

In 2005, the lowest biomass and grain yield are found in plot S3, while they are similar in other three plots (Fig. 4.5). The predicted aboveground biomass and grain yield correspond well to the measured data. In 2006, an obvious degradation of LAI and yield are found in plots S2 and S3 in comparison with plot S4 (Fig. 4.6). The simulation reproduces the sequence corresponding to the degree of degradation very well. However, the predicted LAI overestimates the first measurement at all plots and the second measurement at plot S1.

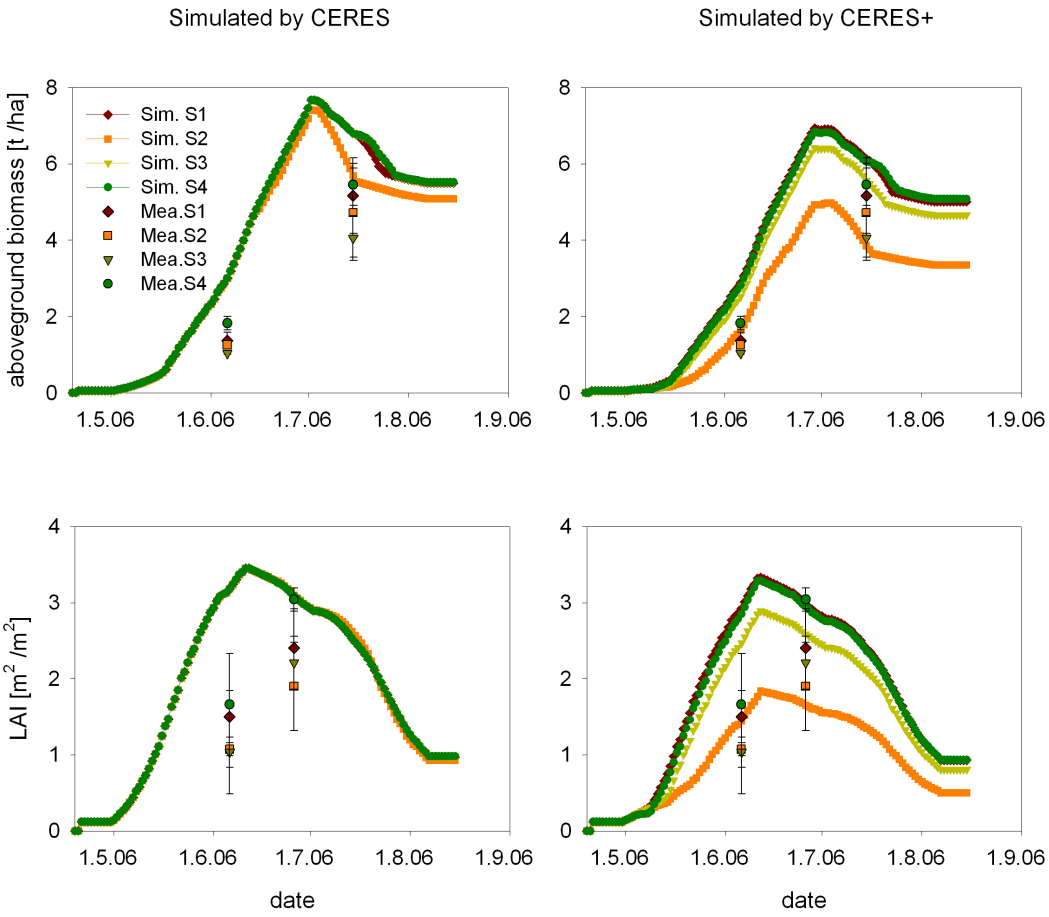

Figure 4.6: Comparison of observed (symbols and error bars = mean and SD) and simulated (lines plotted with symbols) total aboveground biomass and LAI for spring wheat in the growing season of 2006, respectively. Left figures, calculation by CERES: right figures: calculation by CERES+. In each figure, dark red diamonds indicate plot S1, orange squares indicate plot S2, dark yellow triangles indicate plot S3 and green circles indicate plot S4.

4.3.4 Response of crop yield simulation to precipitation

Fig. 4.7 shows the response for the simulated yields of maize and spring wheat using CERES+ by changing the daily precipitation. For 2005, simulations are run using the daily precipitation multiplied by the scenario factors 0.5, 0.75, 1.25 and 1.5, respectively, in addition to the original precipitation data. The same calculations are done for spring wheat in 2006. In all four plots, the change in water supply impacts clearly on the grain yield of both crops. Each curve shows an optimum under the given water supply scenarios, which suggests that both lack of water and excess of water, can lead to yield degradation. However, the highest yields among the given cases for the four plots are found with different water supply scenarios. The best growth of maize at plot S2 is for the case of original rainfall (total = 531 mm); for plot S1 and S4, it is for the case of reducing the rainfall by 25% (total = 398 mm); and for plot S3, it is in case of reducing rainfall by 50% (total = 265 mm). For spring wheat, the highest yields at plots S2 and S1 are reached by increasing the original rainfall by 50% (total = 482 mm), for plot S4 by increasing rainfall by 25% (total = 402 mm) and for plot S3, it is under the original weather conditions (total = 321 mm). It is clearly that the crop at plot S2 requires a higher water supply to reach the highest growth rate among the given cases than the crops at other plots, while a lower water supply is better for the crop at plot S3.

The response curves differ also in their fluctuations. Of these, plot S4 always has the highest yield of both crops under all scenarios. Moreover, both crops at plot S4 show the smallest change in yield under the given conditions, which is for maize a maximum 14% reduction and for spring wheat a 26% reduction of the optimum. However, the maximum reduction of maize and spring wheat yields at plot S2 are up to 96% and 80%, at plot S1 58% and 44%, at plot S3 40% and 47% of the optimum, respectively. The highest mean maize yield for the four plots is for the scenario of 398 mm total precipitation and the second highest is for the scenario of 531 mm. For spring wheat, the two highest mean yields are for the scenario of 402 mm and 482 mm precipitation. The range from 400 to 500 mm total precipitation in a growing season might be the optimal amount of water supply for this field.

Besides crop yield, the change in water supply can also influence other parameters related to crop growth. Tab. 4.3 presents the simulated yield, total aboveground biomass (abv.BM), shoot:root ratio (τ), cumulative water uptake (Wupt) and cumulative nitrogen uptake (Nupt) at maturity for crops in 2005

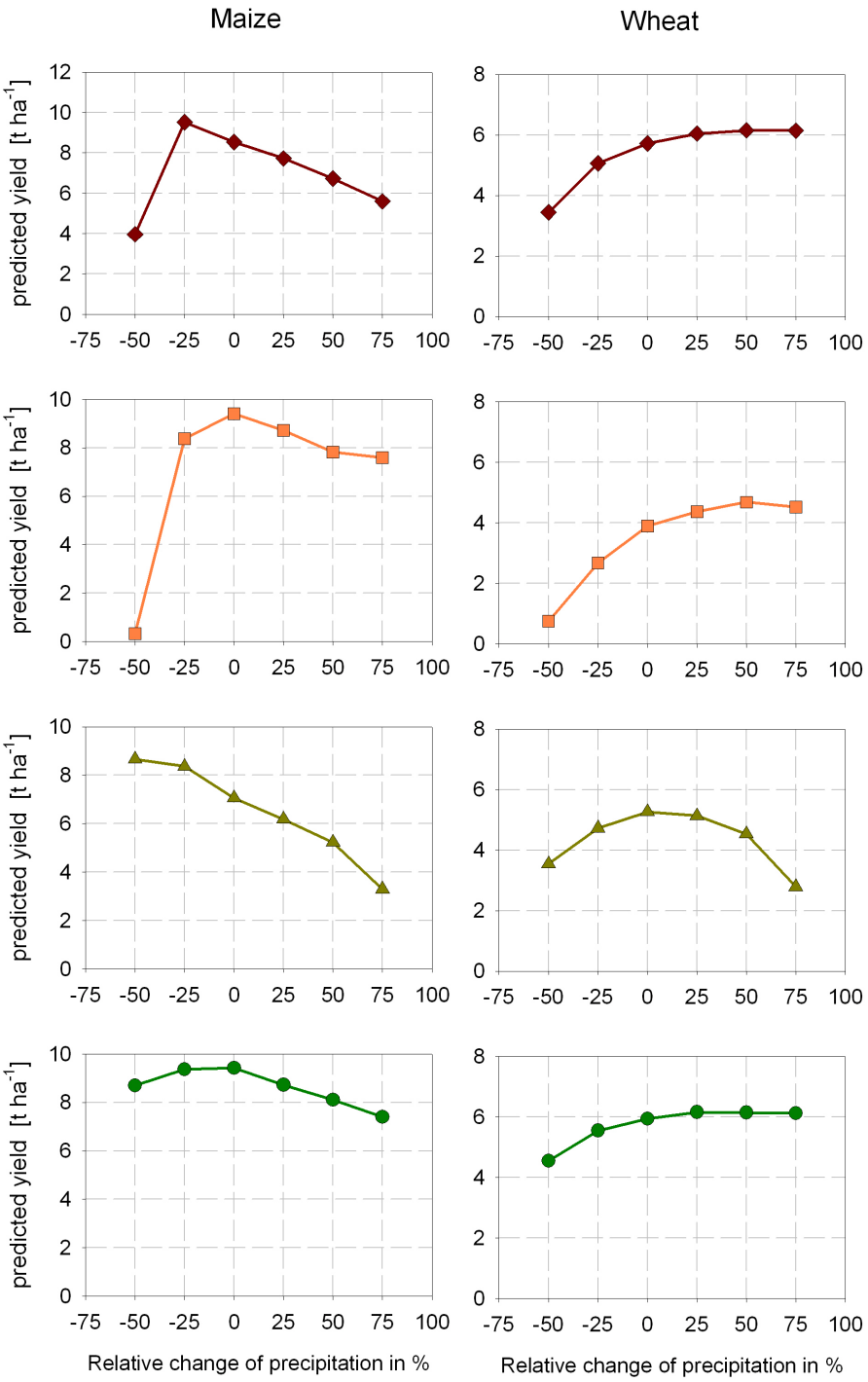

Figure 4.7: Response of simulated grain yield for maize (left) and spring wheat (right) using CERES+ to changes in the daily precipitation. In each figure, dark red diamonds in line indicate plot S1, orange squares in line indicate plot S2, dark yellow triangles in line indicate plot S3 and green circles in line indicate plot S4.

and 2006 under the different rainfall scenarios mentioned above. At all four plots, the change in water supply has clear impacts on the total aboveground biomass, such as on the yield. The change in water supply also affects the root growth. The condition for highest shoot:root ratio τ corresponds to the conditions for the highest yield, if the unreasonable high values of τ in the case of half the rainfall (total = 265 mm) for maize at plots S1 and S2 are not accounted for (Tab. 4.3, τ = 54.8 and 144.3, respectively). The high values of τ at plots S2 and S1 are results of a very low root growth under the extreme drought conditions of this scenario.

Table 4.3: Scenario calculation of yield, total aboveground biomass (abv.BM), shoots:root ratio (τ), cumulative water uptake (Wupt) and cumulative nitrogen uptake (Nupt) at maturity of maize in 2005 and spring wheat in 2006 for different daily precipitation rates.

		Maize					Spring Wheat				
Scenario % of prec.	Plot	Yield [t/ha]	abv.BM [t/ha]	τ	Wupt [mm]	Nupt [kg N/ha]	Yield [t/ha]	abv.BM [t/ha]	τ	Wupt [mm]	Nupt [kg N/ha]
100				(531 mm)					(321 mm)		
	S1	8.5	17.0	6.6	185	245	5.7	11.1	7.7	221	265
	S2	9.4	18.9	8.0	233	241	3.9	7.5	7.4	167	139
	S3	7.1	14.1	6.2	122	218	5.3	10.2	7.8	207	229
	S4	9.4	18.9	7.4	268	244	5.9	11.2	8.3	219	270
75				(398 mm)					(241 mm)		
	S1	9.5	19.1	8.0	250	243	5.1	10.3	7.1	220	240
	S2	8.4	15.2	14.1	217	159	2.7	5.4	6.9	130	92
	S3	8.4	16.7	7.9	174	226	4.7	9.7	7.6	212	218
	S4	9.4	18.7	8.7	269	229	5.5	10.8	7.9	219	252
50				(265 mm)					(161 mm)		
	S1	4.0	6.4	54.8	88	51	3.4	8.3	6.2	192	192
	S2	0.3	0.5	144.3	6	7	0.7	2.2	4.7	53	39
	S3	8.7	16.4	10.6	232	192	3.5	8.0	6.9	180	176
	S4	8.7	16.0	12.4	229	175	4.5	9.6	7.7	211	214
125				(664 mm)					(402 mm)		
	S1	7.7	14.5	6.0	144	230	6.0	11.4	7.9	221	277
	S2	8.7	18.0	7.1	185	249	4.4	8.4	7.7	181	164
	S3	6.2	11.6	5.8	98	189	5.1	9.5	6.8	173	215
	S4	8.7	17.2	6.5	198	244	6.2	11.4	8.4	219	276
150				(796 mm)					(482 mm)		
	S1	6.7	12.4	6.7	112	175	6.2	11.5	7.9	217	280
	S2	7.8	16.5	6.3	156	251	4.7	8.6	7.7	178	170
	S3	5.2	9.0	7.0	73	146	4.5	8.0	6.1	138	182
	S4	8.1	15.4	5.7	159	241	6.1	11.4	8.2	219	276

The difference in biomass can also be related to the difference in water or nitrogen uptake. For both maize and wheat, the highest yield corresponds to the highest water uptake and nitrogen uptake by each plot among the given cases.

4.3.5 Extrapolation to other years

The new root model has not only shown its sensitivity to different rainfall conditions in the scenario calculations, but also its capability for dealing with real weather conditions. In Tab. 4.4 and Fig. 4.8, the measured mean yields for four plots over five years are compared with the mean yields predicted by using the CERES Model as well as the CERES+ Model, into which the new root model was incorporated. In general, the predicted mean yields with the new root

Table 4.4: The predicted mean yield, the coefficient of determination R^2 and modeling efficiency (EF), which are obtained using various model configurations. **CERES** indicates the original CERES Model, **CERES+** indicates the CERES models modified by linking with the new root model. Prec., cumulative precipitation in the vegetation period; Mean: mean of the crop yield; MZ, maize; WW, winter wheat; and SW, spring wheat.

Year	Crop	Prec.	Measured	Predicted by **CERES**			Predicted by **CERES+**		
			Mean (SD)	Mean	R^2	EF	Mean	R^2	EF
		[mm]	[t/ha]	[t/ha]			[t/ha]		
1994	WW	463	4.87 (1.21)	5.77	0.81	-0.31	5.27	0.80	0.64
2000	WW	624	5.51 (1.20)	6.73	0.65	-0.81	6.26	0.88	0.32
2006	SW	321	5.22 (0.79)	5.71	0.59	-0.01	5.20	0.88	0.82
1997	MZ	466	8.19 (1.03)	10.76	0.60	-7.63	9.84	0.94	-2.92
2005	MZ	531	9.01 (0.76)	9.35	0.99	0.43	8.61	0.93	0.31
all years					0.78	-1.85		0.85	-0.20

model (CERES+) are closer to the measured values than without it (CERES). CERES overestimates the mean yield in all cases. Using the new root model, R^2

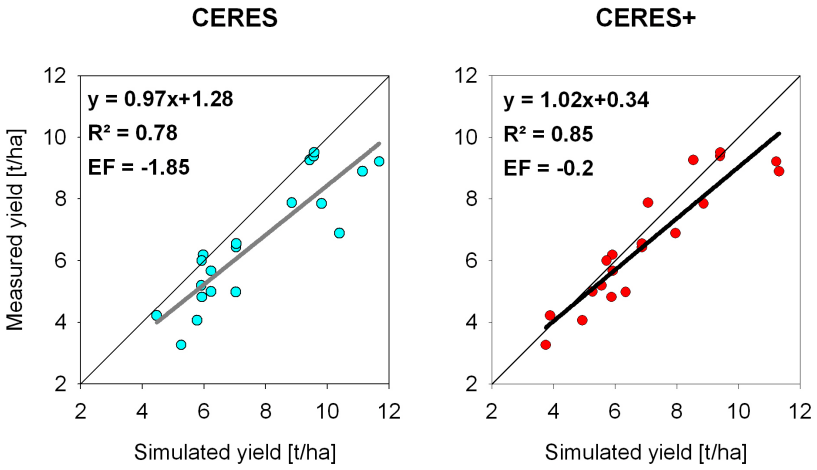

Figure 4.8: Regression lines of the measured yield at four plots over five years with that predicted by the original CERES Model (left, cyan circles) and by the CERES+ Model (right, red circles). Thin black line is the 1:1 curve, thick grey line and black lines are regressions for the simulation by CERES and by CERES+, respectively (number of samples n = 20). R^2, coefficient of determination; EF, modeling efficiency.

values for regression range from 0.80 to 0.94 for the five years. With the original CERES, three R^2 values are around 0.6, one case for maize is of 0.99 and one case for wheat of 0.81. For all the measurement-prediction pairs over the five years, the new root model has increased the R^2 of regression from 0.78, obtained by the original CERES models, to 0.85. This improvement in the agreement between model predictions and measurements is also supported by the modeling efficiency (EF). The EFs when using the new root model range from 0.32 to 0.82 for wheat, which indicates a good match of simulated data to the observed values. In contrast, the EFs predicted using CERES for wheat are all negative, which suggests that the observed mean is a better predictor than the model. For maize in 2005, an EF of 0.31 is obtained by using CERES+. This is the only exception where the EF of the new root model is lower than that of original CERES (EF =0.43). However, the EFs for maize in 1997 are negative by using both CERES (EF =-7.63) and CERES+ (EF =-2.92). The low EFs in this year might be due to the overestimation of maize yield in plots S1 and S4 (Fig. 4.9). In both simulations, the maize growth seem to have no restriction in the two plots. Hence the overestimation could be due to the adaption of the phenological parameters required by the crop growth models. Nevertheless, CERES+ has predicted the

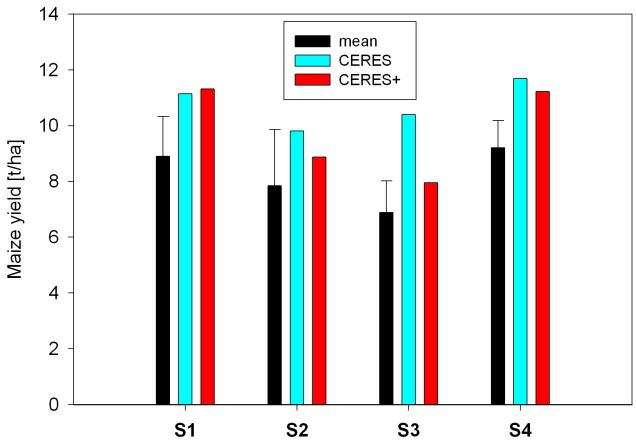

Figure 4.9: Comparison of the measured yield (black bars) at four plots in 1997 with those predicted by original CERES Model (cyan bars) and by the CERES+ Model (red bars).

yield degradation in the plot S3 more accurately than CERES, that is also the reason why the EF of CERES+ is higher than that of CERES in this year.

As a conclusion, with respect to the simulation of crop yield variability, the general higher R^2s for the five years obtained by using CERES+ than using CERES indicated that the new root growth model has increased the sensibility of the crop models for the simulation of crop yield in response to varied environmental conditions. The EFs close to 1.0 obtained for wheat simulation by using CERES+ indicates the good agreement of the model predictions with the measurements. In contrast, the negative EFs obtained by the CERES indicate that the mean of the measurements is a better predictor than the simulation model. For maize simulation, both models showed their capability as a better predictor than the mean of the measurements except for data of one year. For the other year, both models overestimated the yields for plots S1 and S4. This inaccuracy leaded to the negative EFs for this year.

Chapter 5

Simulation of crop yield maps on a field scale

5.1 Materials and methods

Dataset

Soil data Basic soil properties (textual data, soil bulk density and organic matter content) at the nodes of a rectangular grid of 50 x 50 m, which covers field A15, were available in the database of the Agriculture-Ecology-System research project (1990 -2003) of the Forschungsverbund Agrarökosysteme München (FAM) (Osinski *et al.*, 2005). The soil input data are listed in Tab. 5.1. The hydraulic parameters K_{sat}, θ_{sat}, Campbell-A and Campbell-B were estimated by the **V+CHCB** approach described in Chapter 3.

Table 5.1: Soil properties of 13 grid points for simulation input. Z, soil depth; ρ, bulk density; K_{sat}, saturated conductivity; θ_{sat}, saturated soil water content; a, Campbell A; b, Campbell B; GP, grid point.

Soil horizon	Z	Clay	Silt	Sand	Rock	ρ_s	C_{org}	K_{sat}	θ_{sat}	a	b
	$[cm]$	[%]	[%]	[%]	[%]	$[g/cm^3]$	[%]	$[mm/d]$	$[cm^3/cm^3]$	$[kPa]$	[-]
GP 150130											
1	0-20	20.5	40.8	38.7	4.6	1.41	1.37	292	0.44	-3.1	6.98
2	20-30	19.3	45.6	35.1	3.6	1.58	0.85	96	0.39	-5.5	6.94
3	30-50	30.9	42.3	26.8	2.6	1.46	0.28	327	0.44	-6.3	9.04
4	50-75	35.8	30.5	33.7	3.5	1.57	0.18	121	0.41	-10.0	9.58
5	75-90	34.5	31.8	33.7	0.9	1.60	0.12	111	0.40	-11.0	9.36

continued on next page

– continued from previous page

Soil horizon	Z	Clay	Silt	Sand	Rock	ρ_s	C_{org}	K_{sat}	θ_{sat}	a	b
	$[cm]$	[%]	[%]	[%]	[%]	$[g/cm^3]$	[%]	$[mm/d]$	$[cm^3/cm^3]$	$[-kpa]$	[-]
GP 160120											
1	0-30	22.4	42.4	35.2	3.1	1.45	1.28	203	0.43	-4.0	7.40
2	30-40	35.6	33.3	31.1	0.0	1.65	0.41	41	0.39	-15.0	9.63
3	40-45	39.2	32.2	28.6	3.0	1.65	0.29	50	0.40	-18.0	10.30
4	45-65	34.0	39.8	27.1	1.9	1.65	0.17	74	0.39	-15.0	9.52
5	65-90	43.9	32.1	24.0	0.2	1.65	0.14	66	0.40	-25.0	11.3
GP 170130											
1	0-30	17.6	53.6	28.8	2.8	1.38	1.23	534	0.45	-3.2	6.96
2	30-40	35.6	38.7	25.7	2.0	1.57	0.97	65	0.42	-12.0	9.84
3	40-60	29.0	45.4	25.6	0.8	1.57	1.28	68	0.41	-9.5	8.79
4	60-85	30.9	36.9	32.2	3.9	1.57	0.16	152	0.41	-8.7	8.83
5	85-90	32.7	37.6	29.7	17.1	1.57	0.13	228	0.40	-9.8	9.20
GP 180120											
1	0-15	24.0	53.2	22.8	2.4	1.52	1.08	150	0.41	-7.2	8.17
2	15-25	27.9	54.4	17.7	0.7	1.53	0.52	190	0.42	-9.6	9.05
3	25-55	29.6	55.0	15.4	0.0	1.43	0.18	734	0.45	-6.9	9.47
4	55-75	34.6	60.4	5.0	0.0	1.42	0.19	1409	0.46	-9.7	11.20
5	75-85	26.4	55.8	17.8	0.0	1.41	0.13	1023	0.45	-5.6	8.82
6	85-90	32.6	62.9	4.5	0.0	1.28	0.20	5083	0.49	-4.3	10.90
GP 180130											
1	0-15	24.0	52.4	23.6	1.4	1.43	1.37	274	0.44	-5.0	8.13
2	15-25	37.0	42.2	20.8	1.4	1.52	0.65	130	0.43	-11.0	10.30
3	25-40	44.0	37.5	18.5	1.7	1.52	0.24	189	0.44	-15.0	11.70
4	40-55	43.0	44.9	12.1	0.3	1.52	0.20	270	0.44	-18.0	12.00
5	55-90	43.3	52.2	4.5	0.0	1.52	0.19	524	0.44	-22.0	12.90
GP 190120											
1	0-30	18.2	54.4	27.4	1.9	1.53	1.38	140	0.40	-5.5	7.11
2	30-40	25.1	51.1	23.8	1.0	1.53	0.84	140	0.41	-7.5	8.29
3	40-50	27.3	48.0	24.7	0.0	1.53	0.24	219	0.42	-7.9	8.57
4	50-70	25.3	41.8	32.9	0.0	1.53	0.20	212	0.41	-6.1	7.92
5	70-90	17.9	37.8	44.3	0.0	1.53	0.20	243	0.40	-3.7	6.39
GP 190130											
1	0-20	28.6	49.9	21.5	0.5	1.42	1.05	297	0.45	-5.7	8.94
2	20-30	25.0	57.7	17.3	0.0	1.49	0.32	370	0.43	-7.5	8.64
3	30-50	25.0	55.2	19.8	0.0	1.39	0.23	915	0.45	-4.8	8.49
4	50-90	21.1	48.9	30.0	0.0	1.37	0.17	1113	0.45	-3.3	7.41
GP 190140											
1	0-25	21.9	51.8	26.3	1.3	1.47	1.02	227	0.43	-5.2	7.69
2	25-35	25.4	53.9	20.7	0.7	1.51	0.38	256	0.42	-7.7	8.49
3	35-40	24.8	50.6	24.6	0.3	1.51	0.22	298	0.42	-6.9	8.20
4	40-65	23.6	52.7	23.7	0.3	1.47	0.22	449	0.43	-5.7	8.07
5	65-90	23.3	52.9	23.8	0.5	1.54	0.18	277	0.41	-7.3	8.02

continued on next page

– continued from previous page

Soil horizon	Z	Clay	Silt	Sand	Rock	ρ_s	C_{org}	K_{sat}	θ_{sat}	a	b
	$[cm]$	[%]	[%]	[%]	[%]	$[g/cm^3]$	[%]	$[mm/d]$	$[cm^3/cm^3]$	$[-kpa]$	[-]
GP 200130											
1	0-25	21.5	36.2	42.3	0.9	1.49	1.19	132	0.42	-3.9	7.01
2	25-35	18.0	32.5	49.5	0.8	1.60	0.44	88	0.38	-4.0	6.21
3	35-65	10.8	32.1	57.1	0.0	1.46	0.17	649	0.42	-1.9	4.82
4	65-90	9.3	27.8	62.9	0.0	1.35	0.15	1880	0.44	-1.3	4.34
GP 200140											
1	0-25	19.7	43.3	37.0	0.8	1.51	1.26	129	0.41	-4.3	6.93
2	25-35	21.7	49.4	28.9	0.0	1.50	0.49	228	0.42	-5.4	7.55
3	35-60	25.0	46.9	28.1	0.2	1.50	0.33	244	0.42	-6.0	8.07
4	60-90	19.2	37.5	43.3	0.4	1.49	0.17	351	0.42	-3.5	6.62
GP 210130											
1	0-10	17.2	33.6	49.2	1.5	1.51	1.11	131	0.41	-3.1	6.10
2	10-20	17.3	24.8	57.9	0.5	1.49	0.75	162	0.41	-2.4	5.77
3	20-50	2.5	4.6	92.9	0.1	1.46	0.10	2451	0.40	-0.68	1.91
4	50-90	4.5	2.1	93.4	3.4	1.52	0.05	1236	0.39	-0.75	2.11
GP 220140											
1	0-25	10.8	23.2	66.0	0.0	1.62	1.18	83	0.37	-2.1	4.40
2	25-35	9.1	13.5	77.4	0.0	1.62	0.69	111	0.37	-1.5	3.58
3	35-65	5.8	3.0	91.2	0.0	1.62	0.09	630	0.36	-0.91	2.38
4	65-90	6.5	3.0	90.5	0.0	1.62	0.08	659	0.36	-0.95	2.51
GP 220150											
1	0-20	11.2	35.4	53.4	20.9	1.57	1.38	161	0.38	-2.6	5.04
2	20-30	14.2	35.6	50.2	17.2	1.69	0.63	63	0.35	-4.2	5.61
3	30-35	23.1	36.3	40.6	11.5	1.54	0.37	180	0.40	-4.9	7.32
4	35-75	25.8	42.3	31.9	4.7	1.51	0.30	231	0.42	-5.9	8.04
5	75-90	25.1	53.1	21.8	1.1	1.51	0.20	339	0.42	-7.3	8.39

Measured crop yield map High-resolution crop yield maps for 1994, 1997 and 2000 were unpublished data provided by Markus Demmel from Lehrstuhl für Landtechnik, TUM. By combining with the GPS data, yield and positional information were simultaneously registered as data pairs. For the estimation of the yield at the 13 grid points, the mean value was calculated from the measured points within disks of 5 m radius centered at each of the 13 grid points. Unfortunately, the recorded data were slightly erroneous. For example, where there was more than one yield result registered for one position, or some yield values approximated zero. These errors could have been due to failure of the harvesting machine or to the position estimation. Hence the data were first corrected by removing any excess results and any values less than 1.0 [t/ha]. In addition, the registered data were for wet yields. For the estimation of dry yields, a 14% water

content of the grain was assumed both for the wheat grain and the maize corn.

Weather data The weather data were obtained from the weather station Voglried (see Section 2.2.4).

Model configuration

The model configurations were the same as that described in Section 4.2.2.

Simulation strategy

The objective was to examine the transferability of the approach used for the hydraulic parameterization (introduced in Chapter 3) and the new root growth model (introduced in Chapter 4) to simulate the crop yield variability represented by other soil plots in the same study field. The hydraulic parameters of the 13 soil plots were estimated using the V+CHCB approach introduced in Chapter 3. For these 13 soil profiles, the wheat yields in 1994 and 2000 and maize yield in 1997 were simulated using the original CERES Model and the CERES+ Model by incorporating the new root growth model, respectively.

Statistical analysis

The statistical parameter coefficient of the determination R^2 for the regression analysis and modeling efficiency (EF) were used to assess the extent of the agreement between simulated and measured values.

5.2 Results and discussion

To examine how representative the average yields of the grid points are for the whole field, we first compare the mean yield estimated from different sources. A comparison between the measured and simulated yields is performed firstly at the plot level to demonstrate the capabilities of the models used in response to different soil conditions. In this way, we can obtain a quantitative measure of the agreement between the model predictions and the measured values. In addition, the same results are presented again in relation to the field.

Tab. 5.2 presents the mean yields for wheat in 1994 and 2000 as well as for maize in 1997 that were estimated from:

1. the measured values from the whole yield map in high-resolution;
2. the measured values within disks of 5 m radius centered at each of the 13 grid points;
3. the simulated yields at the 13 grid points with the original CERES Model;
4. the simulated yields at the 13 grid points with the CERES+ Model.

Table 5.2: Comparison of the overall mean of the measured and simulated yields in 1994, 2000 and 1997. Prec., cumulative precipitation in the vegetation period; Mean 1, mean of the measured yields of the whole field; Mean 2, mean of the measured yields of the 13 grid points; 'Mean 3, mean of the simulated yields of the 13 grid points using CERES; Mean 4, mean of the simulated yields of the 13 grid points using CERES+; SD, standard deviation; MZ, maize; and WW, winter wheat.

Year	Crop	Prec. [mm]	Mean 1 (SD) [t/ha]	Mean 2 (SD) [t/ha]	Mean 3 (SD) [t/ha]	Mean 4 (SD) [t/ha]
1994	WW	463	4.87 (0.90)	4.65 (0.62)	5.68 (0.21)	4.90 (0.80)
2000	WW	624	4.65 (1.27)	5.04 (1.12)	6.67 (0.27)	5.75 (0.59)
1997	MZ	466	7.66 (1.80)	8.28 (0.54)	11.22 (0.57)	9.17 (1.22)

For the wheat yield maps, the averages of the measurements around the grid points ("Mean 2" in Tab. 5.2) are good representations of both the average yield

and the standard deviation (SD) of the whole field ("Mean 1" in Tab. 5.2)). For the maize yield map, the average yield of the whole field can be represented by the measurements around the grid points, but the SD is underestimated. This underestimation suggests that using only the information at these grid points would not represent the maize yield variability in 1997. If we compare the mean measured values with those predicted by the models, the CERES+ ("Mean 4" in Tab. 5.2)) can obviously predict the mean yield and SD both of wheat and of maize better than the CERES ("Mean 3" in Tab. 5.2)). In all cases, CERES has overestimated the mean yield but underestimted the SD, especially for the maize growth.

The quantitative differences between observed yields and the predicted yields at specific soil plots can be seen in Fig. 5.1. The observed values show a very clear variability from grid point to grid point. The maximum observed value is 1.6 times that of the minimum value in 1994, 2.4 times that in 2000, and 1.3 times that in 1997. All of the predicted yields from the original CERES model approximate the maximum observed yields in the three years, such that they do not reflect the observed variability. The yields predicted using the model CERES+ show, however, significantly better matching with respect to the variability. To obtain a more quantitative measurement of the improvement in the CERES+, we represent the data in the form of regression curves in Fig. 5.2. It can clearly be seen that overall the CERES+ predictions have significantly higher values of R^2 and EF.

The capability of better matching the yield variability of CERES+ can be visually demonstrated in the form of the yield maps. In Fig. 5.3, Fig. 5.4 and Fig. 5.5 we show the yield maps for the years 1994, 2000 and 1997, respectively. The figures (A) show the fine meshed measurement data. The figures (B) show the corresponding averaged data around the 13 grid points mesh, and the figures (C) show the simulated data of the 13 grid points from CERES+.

As discussed in the Section 2.1, the crop yield maps at high resolution present a clear yield variability pattern (figures (A) in Fig. 5.3, Fig. 5.4 and Fig. 5.5). A comparison of the top and middle maps shows that the yield variability can be adequately reproduced by the averaged data down to the 13 grid points mesh, except for missing information for the high yield pattern at the top-left side of the field. This is a disadvantage of the sampling scheme being defined in a regular grid, in that there is no grid point located in the high yield pattern. By comparing the (B) and (C) figures, we can see that the measured characteristic variability patterns can be well predicted by CERES+.

Models CERES and CERES+ used in this study differ only in their subroutine

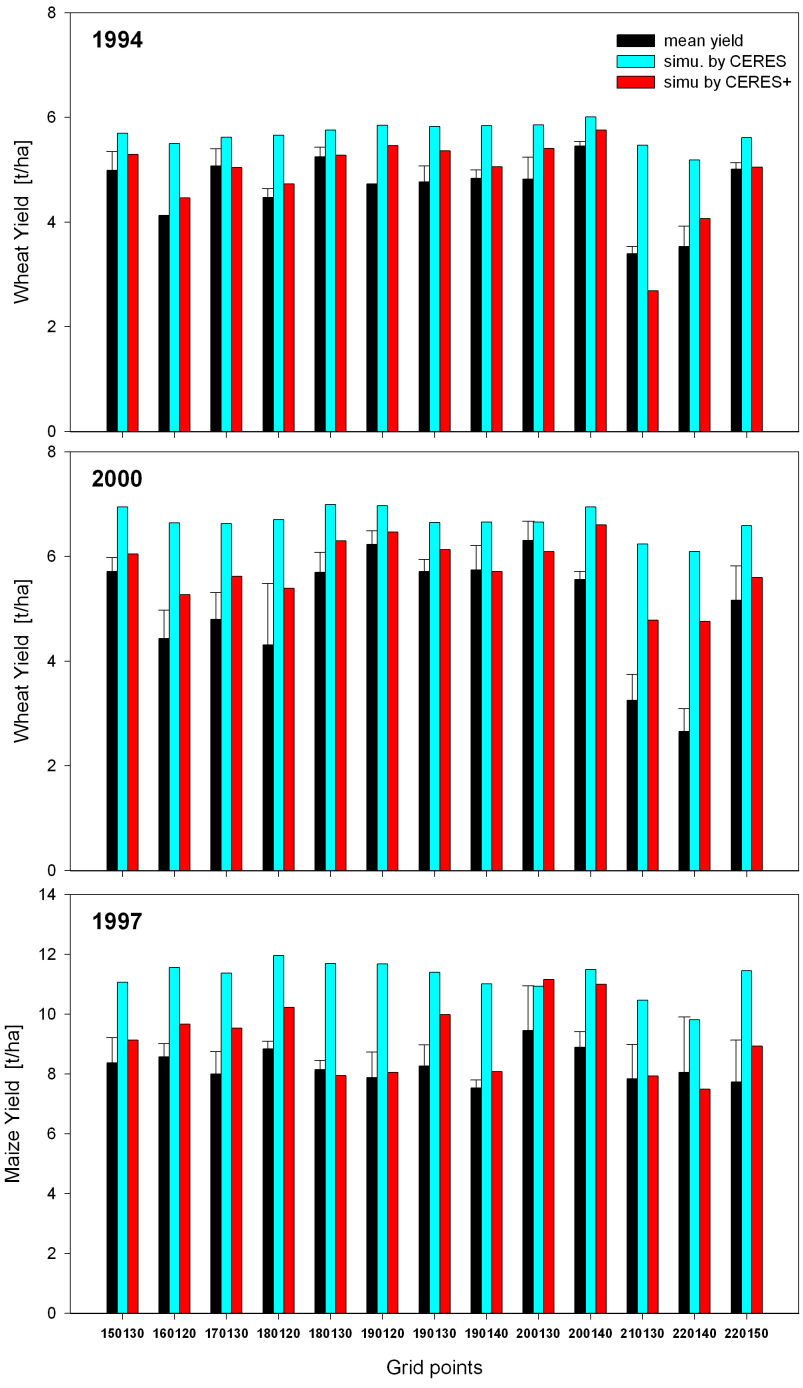

Figure 5.1: Observed and simulated crop yield at 13 grid points in 1994 (top), 2000 (middle) and 1997 (bottom). Black bars, measured value; cyan bars, simulation with the original CERES; red bars, simulation with CERES+.

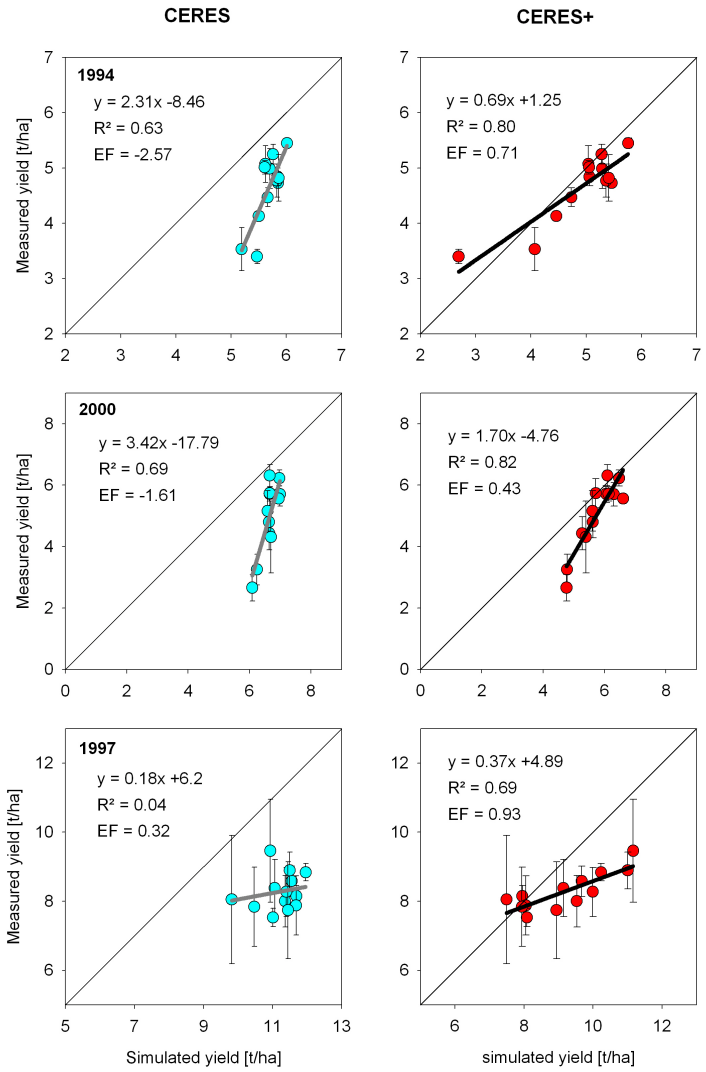

Figure 5.2: Comparison of the regression curves for meaured yields at 13 grid points in 1994 (top), 2000 (middle) and 1997 (bottom) versus simulated results with the original CERES Model (cyan circles) and with the CERES+ Model (red circles). The thin black line is the 1:1 curve, thick grey lines and black lines are regression curves for the simulations by CERES and CERES+, respectively (number of samples n = 13). R^2, coefficient of determination; EF, modeling efficiency.

for root growth simulation. The simulation results show that both models are able to simulate the maximum observed yield of the study field. This suggests that both models can produce similar results if they deal with optimum growth conditions. However, when they deal with yield limitation, which could be due to unfavorable soil and weather conditions, the yield at each grid point predicted by CERES+ was closer to the observed value than that predicted by CERES. The interactions between root and soil incorporated into the new root model were based on the analysis of field observations in 2005 and 2006. By adding this new root model, the yield variability for both wheat and maize in other years could be readily reproduced. This suggests that the assumed interactions do indeed govern the study site. The yield limitation in this field could be mostly caused by the dryness in sandy soils, by the O_2 deficiency in clayey soils, and by the soil hardness. Moreover, the success of the simulation for the 13 additional field plots shows that the V+CHCB approach to parameterize the water flow model introduced in Chapter 3 seems to be appropriate for the study field.

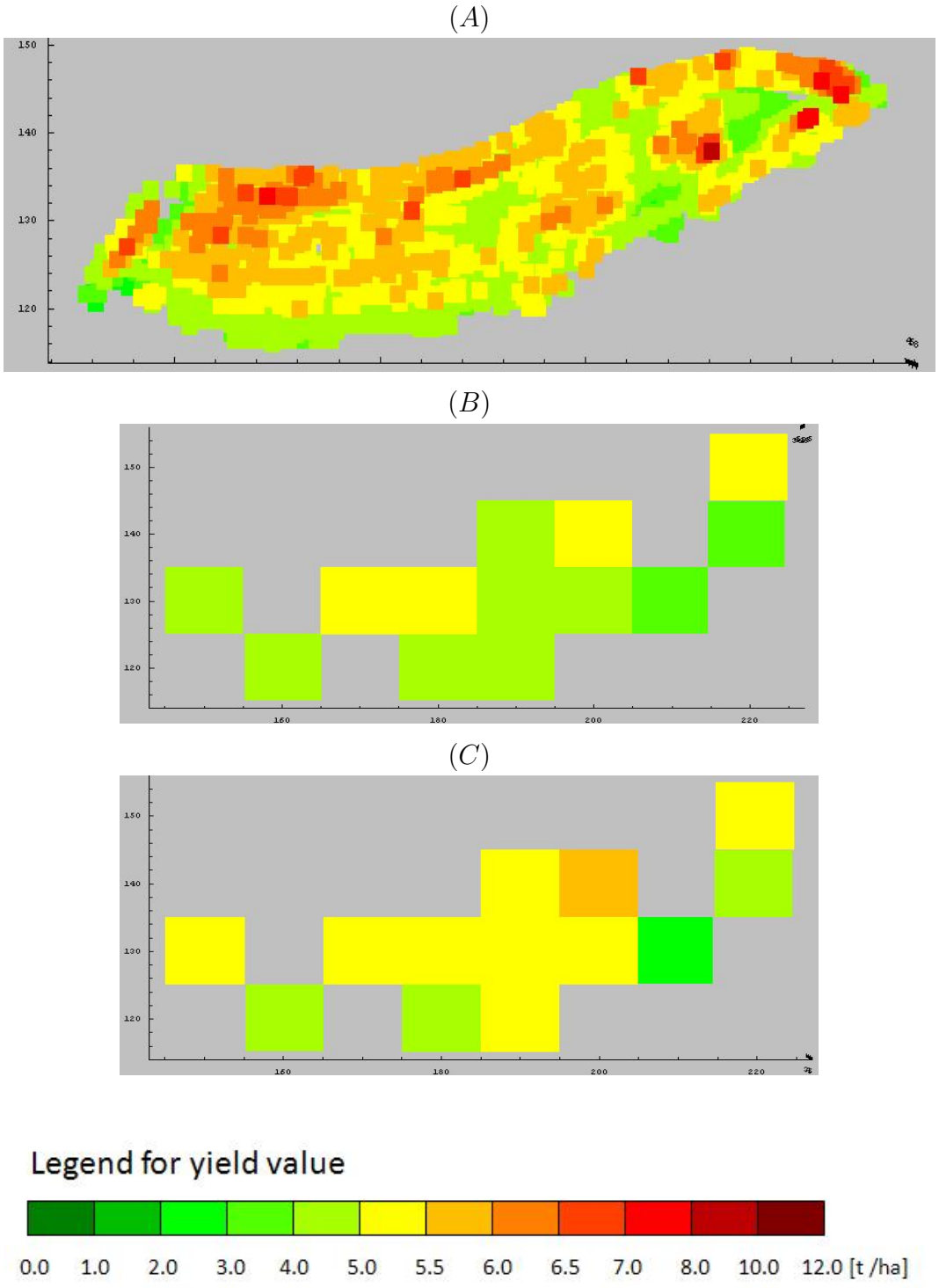

Figure 5.3: Wheat yield maps 1994. (A), crop yield map represented by fine meshed measurement data; (B), crop yield map represented by the averaged data down to the 13 grid points mesh; (C), crop yield map represented by simulation data of the 13 grid points predicted by CERES+.

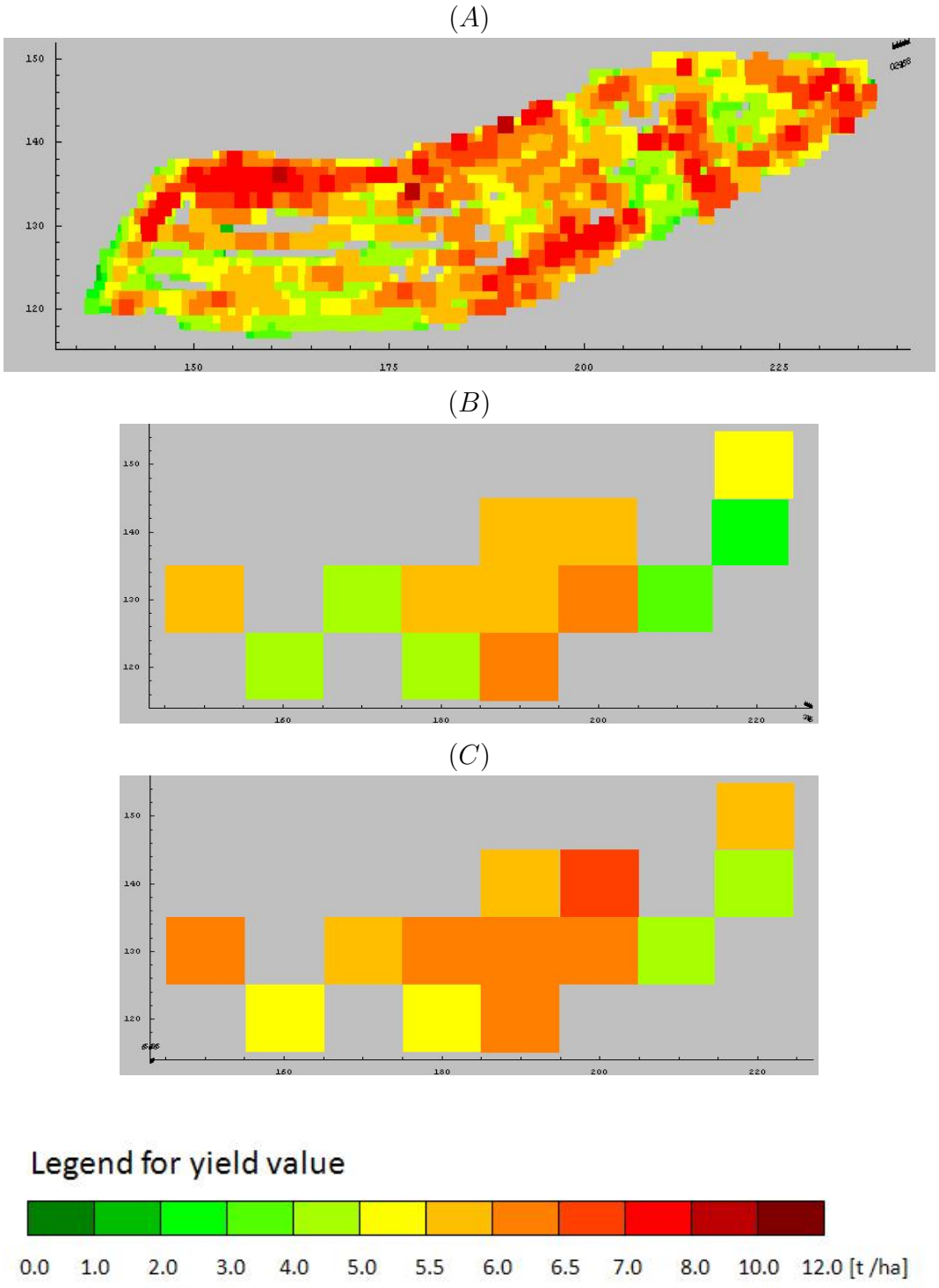

Figure 5.4: Wheat yield maps 2000. (A), crop yield map represented by fine meshed measurement data; (B), crop yield map represented by the averaged data down to the 13 grid points mesh; (C), crop yield map represented by simulation data of the 13 grid points predicted by CERES+.

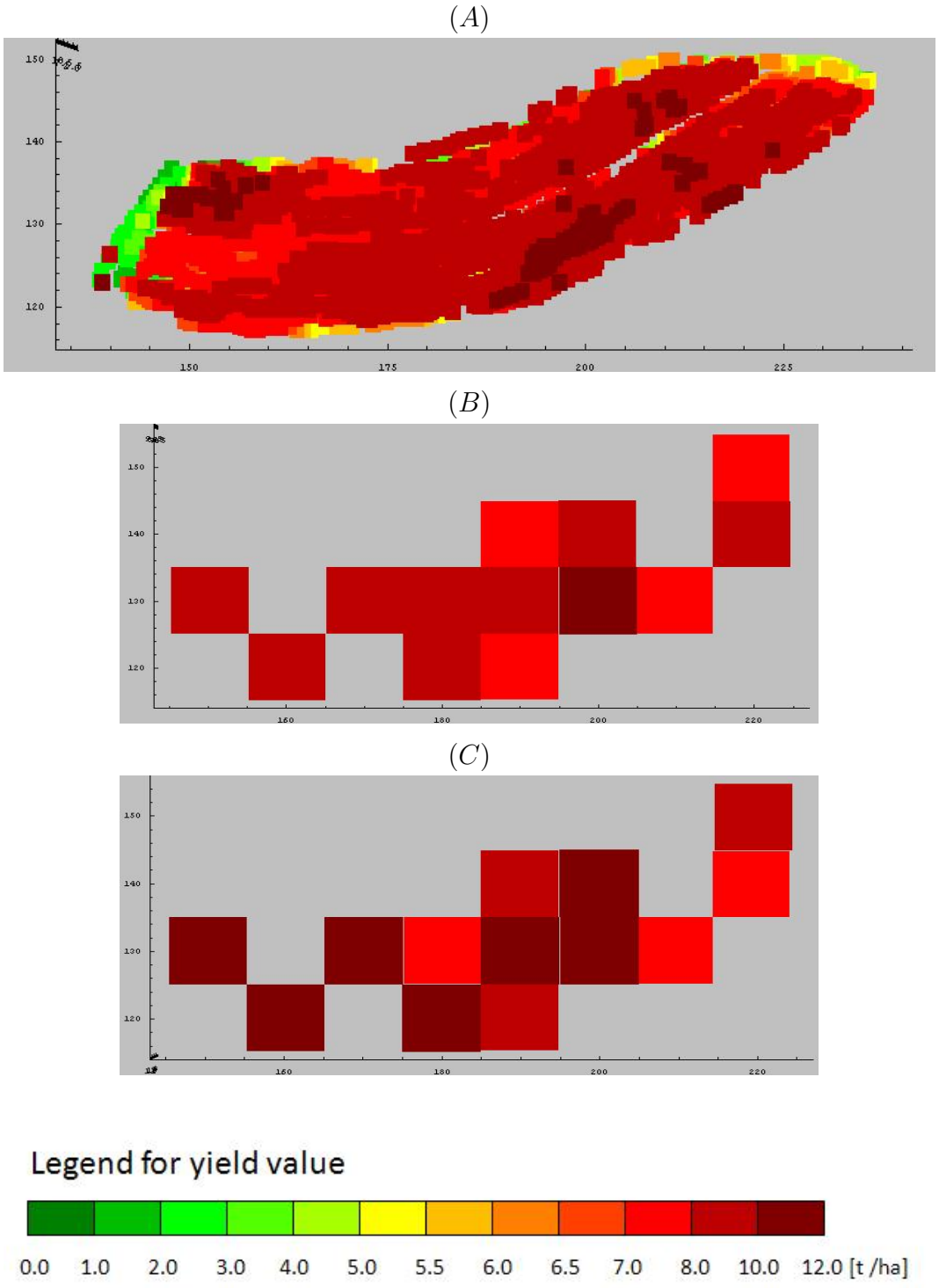

Figure 5.5: Maize yield maps 1997. (A), crop yield map represented by fine meshed measurement data; (B), crop yield map represented by the averaged data down to the 13 grid points mesh; (C), crop yield map represented by simulation data of the 13 grid points predicted by CERES+.

Chapter 6

General discussion and conclusion

6.1 Impact of soil heterogeneity on water balance at field scale

As shown by Fig. 2.10, the study site is characterized by the high heterogeneity of the soil properties including soil texture, rock fraction, bulk density and soil organic content especially at sub-soil level. As suggested by Sinowski & Auerswald (1999) and Sommer *et al.* (2003), this soil heterogeneity could be due to the different soil forming processes. The differences in soil composition and structure lead to different hydraulic behavior of the soils with respect to water holding capacity and hydraulic conductivity. As a result, large differences in soil water balance are observed in the four study sites (Fig.2.12). The low SWC in site S2 corresponds to its high content of gross sand and gravel underground. Hence the water infiltrating from the surface soil would percolate fast through this site. On the contrary, the high SWC in site S3 could be due to its high clay content and high bulk density, which could hinder the water flow and lead to high water storage (Scheffer & Schachtschabel, 1998). A high water content in soil is often related with a low O_2 content. From the soil profile observations of site S3, the grey color of the bulk soil and red -brown color of iron coating are found to be distributed in the sub-soils. This is a typical indicator of temporal water saturation (Scheffer & Schachtschabel, 1998). However, it is difficult to determine the soil O_2 content at a field level. A comparison of measured and simulated SWCs shows that our model CERES+ is able to simulate the differences in soil water balance at the different sites.

6.2 Root distribution affected by soil constraints and resource availability

Corresponding to the different soil and SWC conditions at sites S2 and S3, both maize and spring wheat RLDs in their sub-soils are much lower in comparison with sites S1 and S4 (Fig. 4.1). The most prominent soil environmental factors that limit the root growth in sites S2 and S3 could be the physical soil constraints and the inadequate soil water status, which result in a water deficit in a drought phase and an O_2 deficit at heavy rainfalls as indicated by the simulation results.

Many studies have pointed out that high soil hardness is one of the most common limitations to soil exploration by roots (Doussan *et al.*, 2003; Jones *et al.*, 1991; Wang & Smith, 2004). Soil hardness is usually measured in terms of penetrometer resistance, which is mostly affected by soil bulk density, soil water content, soil texture, soil structure, organic matter content and the amounts of saturating cations present (Wang & Smith, 2004). However, the main difficulty in modeling the effect of soil hardness on root growth is the prediction of soil hardness from the common soil properties. The approach proposed by Jones *et al.* (1991), which estimates the soil hardness using maximum and optimum bulk density defined for a given crop and a soil water availability factor, seems to be simple and effective. In addition to the factors used by Jones *et al.* (1991), the effect of sand content is also considered in our root model. This modification is based on the observations that the hardness of the soil increases rapidly when a soil of high sand content is short of water. By introducing this new factor, the simulated RLDs in the sub-soil of site S2 is much lower (i.e., closer to the measured RLD) than without it, which suggests that the high soil resistance due to drought and high sand content might be the major limitation to the root growth here. The high soil hardness is also responsible for the root growth restriction in site S3. However, unlike site S2, the hardness in this instance is primarily related to the high bulk density of almost 1.9 $[g/cm^3]$ in the sub-soils (Tab.4.1).

The observations of soil water content suggest that anaerobic conditions may occur in site S3. It is difficult to monitor the O_2 status and its effect on root and crop growth at a field site. Thus many crop models developed for agricultural soils under semi-arid conditions do not include the effect of anaerobic conditions (Wang & Smith, 2004). In our model, we adopted the calculation of the aeration index proposed by Jones *et al.* (1991), but with a modification to the estimation of the critical water-filled porosity $\theta_{cri,poro}$. As opposed to the approach used in the Jones Model, the $\theta_{cri,poro}$ is reduced depending on the clay content so that

roots in clayey soils would be more likely to suffer stress from an O_2 deficit. With this modification, the simulated root biomass growth in site S3 is more restricted and closer to the measured root biomass values than without it.

6.3 Root plasticity and crop yield optimization

The proportion of assimilate partitioned to root (expressed as shoot:root ratio τ) is another important parameter in root growth simulation. The ratio τ controls the daily potential root biomass growth. In most crop models, the ratio τ is treated as a function of the development stage. Experimental data show that the shoot:root ratio changes with environmental factors such as temperature, soil water and nutrient supply. However, how a plant regulates its biomass partitioning to adapt to the external conditions is still poorly understood (Wang & Smith, 2004). In some models, such as CERES proposed by Ritchie *et al.* (1986), the ratio τ is increased if the plant is under water or nitrogen stress. The assumption is that the plant survives from a water or nitrogen deficit by enlarging its root system to explore new resources. However, in contrast to this assumption, the observed root system in site S2 is smaller than that of site S1, although a soil water deficit is more likely occur in site S2. Based on this observation, we assume that plants can also survive under unfavorable soil conditions by reducing their aboveground biomass size to minimize resource demand. The underground stress conditions stimulate roots to release hormones, through which the aboveground part of the plant is informed about the stress situation and reduces the shoot growth (Aiken & Smucker, 1996; Passioura, 2002). However, the question is, how can the critical moment be assessed by modeling when a crop is changing its biomass partitioning to adapt to the stress condition? In our root model, we perform a simple test to simulate this situation by using the information on stress distribution. We implemented a feedback: Root growth reduction leads to water/nitrogen uptake reduction, which leads to shoot growth reduction, which leads to appropriate root growth. This process is initialized in cases where the sub-soil below the plough layer are much less adequate for root growth than the top soils. The close agreement between measured and simulated root and crop data indicates that the assumed process might indeed represent the stressed crop growth behavior. The way in which we choose to assess the critical soil conditions to stimulate the crop growth regulation seems feasible. A direct halt to root growth, which only serves as a preliminary assumption here, however appears discrete and radical. To represent a more continuous and reasonable plant

physiological process, not only the allocation to the root but also the shoot:root ratio τ has to be reduced. We did not change the calculation of τ in the CERES model because it required modifying the crop model itself. However, it provides a further alternative to simulate limitation of crop growth.

When adapting to the limited and heterogeneous supply of water or nutrients, crops can not only regulate the root system size, but also the root proliferation in a soil horizon. Soil constraints hinder the root exploration in soil on the one hand, but on the other, roots often prefer proliferating within a water or nutrient-rich zone when they encounter it (Doussan *et al.*, 2003; Hodge, 2004). The root growth partitioning index $\lambda(i)$ in our model is used to rank the condition of soil horizons with respect to soil constraints and the resource availability. Root growth is favored in the soil horizons with less stress. This approach is different from that of the Jones Model, where the potential root growth is calculated directly for each simulation layer and possibly reduced by the minimum of all the stress factors. The latter approach considered the reduction effect of soil constraints and resource deficit on root growth, but does not take the selective root growth in resource-rich zones into account. By using the partitioning index, the simulated RLDs well represent the measured relative root distributions in sites S1 and S2. Owing to the high sand content and soil water deficit in the sub-soil, roots in site S2 preferred to proliferate in the upper 30 cm soil depth. Soil conditions in site S1 are fairly similar to site S2, but with a slightly lower sand content and therewith a less critical water deficit. In the simulation, there are no differences in the other input data except for the soil data. The crucial difference occurs for the comparison of the stress situation. The partitioning index along the soil profile of site S2 has a much steeper gradient between top and the sub-soils than that of site S1. Thus, more roots are favored to grow in the top soils of site S2 than in site S1, which agrees with the observations.

By adjusting its root proliferation in the soil environment, a crop is able to increase the resource acquisition and thus optimize yield under the given conditions. The scenario calculation suggests that water supply is a crucial factor for crop growth in the study sites especially in site S2. Owing to the high sand content and low water holding capacity in site S2, the average available soil water for the 0 -90 cm soil depth in 2005 and 2006 was about 60% of that for sites S3 and S4, and about 67% of that for site S1. Moreover, the observations of the roots for both years showed that only the top 60 cm soil depth in site S2 could be penetrated by roots (Fig. A.2). In spite of this limitation, no decrease in the yield for maize compared with the other sites was observed here in 2005. The plentiful

roots in the top 30 cm found in the same year suggest that maize has guaranteed its yield by enhancing the root growth in water-rich top soils. Nevertheless, the root plasticity differs from crop to crop. Maize can only rely on top soils because it is a species that prefers flat rooting. In contrast, the deep-rooting species wheat is not so fortunate when the sub-soil is inadequate for root growth. Compared with other sites, the lowest yield for spring wheat found in site S2 is related to the lowest RLD and the shallowest rooting depth observed. However, the plasticity of the root and crop to adapt to the environmental conditions has limits. As demonstrated by the scenario calculation, maize in site S2 can still remain at 90% yield through reducing the precipitation by 25%. However, there is hardly any yield if 50% of the precipitation is removed. By such scenario calculations, it might be possible to determine the threshold of root plasticity in response to heterogeneous soil conditions, which is important in case of site-specific management.

6.4 Model application in precision agriculture

A number of studies have reported the co-existence of within-field crop growth variability and field-scale spatial site heterogeneity as well as a temporal change in the crop variability patterns according to the weather conditions, for example, the work of Andales *et al.* (2007); Green & Erskine (2004); Kravchenko *et al.* (2005); Perez-Quezada *et al.* (2003); Sommer *et al.* (2003); Wong & Asseng (2006). The numerous inherent properties combined with temporal variations make it very difficult to identify and manage the variability pattern, which poses an enormous challenge for the precision agriculture. As suggested by Ahuja *et al.* (2002), Priesack *et al.* (2008) and Ascough *et al.* (2008), process-oriented crop models are very useful tools to identify the prominent yield-affecting factors in individual cases. However, the applied crop model needs to be responsive to the changes in soil conditions.

In the present study, the inadequate supply of water, which resulted in water stress in some places and a deficit of O_2 in other places, was assumed to be one of the relevant factor that resulted in the observed crop growth variability. The water uptake by crop roots is determined by the interactions between the soil water flow and root distributions, both of which are strongly influenced by the soil heterogeneity and climate conditions. Hence, to simulate the crop yield variability in the study field, the water flow model is required to be adequately parameterized for the heterogeneous soils and the root growth model is required to be sensitive to various environmental conditions. After improving the accuracy of the

hydraulic parameterization and improving the modeling of root-soil interactions, the sensibility of the applied crop model CERES in response to heterogeneous soil conditions and variable weather condition was actually enhanced. The calibrated crop model can then be used to develop and evaluate alternative methods for sustainable management. For example, by scenario calculation, we can examine the change in crop yield pattern in response to the change in the supply of water or fertilizer. The information provides reference for the decision-making in the precision agriculture.

6.5 Conclusion

To analyze the impact of heterogeneous soil conditions on the crop growth variability for a study field, root density distributions on harvesting of maize and spring wheat were investigated. Based on the observations, a new root model has been implemented and incorporated into the crop model CERES-Maize and CERES-Wheat. The new root model builds on the strengths of the root length model of Jones *et al.* (1991) and includes additional modifications for estimating the adaptive root growth and root distribution in the soil profiles under stress conditions. Simulation results agree well with the measured soil water content, root length density and crop yield of four sites with large difference in soil properties. Compared with the original root growth model in the CERES Model, the use of the new root model has improved the sensitivity of CERES-Maize and CERES-Wheat, proposed by Jones & Kiniry (1986), in response to heterogeneous soil conditions and variable weather condition. The simulations demonstrate how root penetration and proliferation might be affected by the high soil strength, water deficit and O_2 deficit that were present in the study field. By reducing both shoot and root size and favoring the root proliferation in a resource-rich zone, crop yield can be ensured up to a crop specific limited threshold. Thus, the present root model has shown its potential in the study of interactions between roots and soil, and in the root/crop plasticity due to variable environmental conditions. This makes it possible to analyze and represent the within-field yield variability and therewith the model can help for the decision-making in precision agriculture.

Chapter 7

Summary

To simulate crop yield variability caused by soil heterogeneity, the applied crop model needs to be sensitive to the differences in soil conditions. The most difficult problem in the application of a model is how to determine appropriate values for the various model parameters of the different system components and how they change with environmental stresses and management practices.

In the proposed work, the within-field crop yield variability in a study field has been analyzed by both field observation and model simulation. In the growing season 2005 for maize and 2006 for wheat, it was observed that the soil water content, the root length density distribution as well as the dry matter yield at four soil plots in the field were strongly related to the soil properties and the weather condition. In order to evaluate the response of root and crop growth to the variable soil and weather conditions, crop growth at the four soil plots was simulated using the crop model CERES which is implemented as sub-model in the model package Expert-N. The parameterization of the water flow model and the simplified modeling of root growth were the crucial considerations that mainly lead to the insufficient simulation of the crop growth variability under highly heterogeneous soil conditions (Fig. 3.8 and Fig. 4.8).

An approach that combines the use of data from infiltration experiment and of pedo transfer functions (PTF) was developed to conveniently parameterize the water flow model for the different soils. The comparison of the hydraulic parameters estimated by infiltration experiments and by different pedo transfer functions showed that using the PTF Vereecken to estimate saturated water content (θ_{sat}) and saturated hydraulic conductivity (K_{sat}) and using the PTF Campbell to parameterize the hydraulic functions of Hutson & Cass-Burdine were mostly appropriate for the investigated soils. By using this approach, the R^2 of regression of the measured vs predicted soil water content for the four investigated soil plots

in two years was 0.89 and the R^2 of regression of the measured vs predicted crop yields in five years was 0.78. Using the information from the root length density (RLD) observation in the field, a new root model has been developed and linked to the existing crop models CERES Maize and CERES Wheat (Jones & Kiniry, 1986) and (Ritchie & Godwin, 1989). In this new root model, which adopts the strength of the root growth model by Jones *et al.* (1991), root penetration and proliferation can be affected by numerous stresses. These stress factors include stress of the root growth caused by inadequate soil strength, coarse fraction, soil temperature as well as the availability of water, mineral nitrogen and oxygen. In addition, the new root model features the adaptive root response to inadequate soil conditions. By using a layer-weighted stress index, root growth is favored to grow in the simulation layers with a less critical stress situation. In addition, no root growth is considered in soil depth 5 cm below the plough horizon (plough horizon = 25 cm in the investigated field) if the stress index in the upper 30 cm soil depth is much lower than that in the rest soils. The suitability of the new root model was demonstrated by the comparisons of measured soil water content, RLD distribution and the yield for maize and spring wheat with the values predicted by the modified CERES models. By incorporating the new root model, the CERES crop models increased the R^2 of regression of the measured vs predicted five years crop yields for the four investigated soil plots from 0.78 to 0.85. Both the simulation of the scenario calculation and the real conditions demonstrated that the capability of crop models for the simulation of crop yield variability under varying environmental conditions can be enhanced by improving the modeling of root-soil interactions.

Finally, the simulation of wheat and maize yields for other 13 soil plots in the investigated field confirmed the suitability of the approach to estimate soil hydraulic parameter and the integration of the new root model in the CERES model to simulate the observed crop yield variability (R^2 of regression was 0.80 for wheat growth in 1994, 0.82 for wheat growth in 2000 and 0.69 for maize growth in 1997). The calibrated crop model may be used to develop and evaluate alternative methods for sustainable management with respect to precision agriculture.

Appendix A

Data of field experiment

Table A.1: Schedule of field cultivation and sampling actions in 2005 and 2006

Date	Day after sowing	BBCH	Cultivation	Sampling for
2005, Maize				
May 22nd.	2	0	Sowing, Input of 32 kgN/ha	
May 23rd.	2		Input of 222 kgN/ha	
May 29th.	8			WC
Jun. 22th.		24		
Jun. 30th.	50			WC
Aug. 27th.	98			WC
Sep. 5th.	227			WC (S2,S2)
Sep. 8th.	220			WC
Oct. 22th.	254			Crops
Oct. 24th.	259			Roots
Nov. 24th.	287	92	Harvest	
2006, Spring Wheat				
Apr. 20th.			Input of 30 kgN/ha	
Apr. 22th.	2	0	Sowing	
May 03th.	23			WC
May 04th.	24	9	Input of 40 kgN/ha	
May 25th.	25			WC
May 22th.		24		
May 25th.	35		Input of 40 kgN/ha	
Jun. 06th.	47			WC, Crops
Jun. 27th.		37		
Jun. 24th.	65	49	Input of 40 kgN/ha	
Jun. 26th.	67			WC, Crops
Jul. 03rd.	74	52	Input of 40 kgN/ha	
Jul. 22th.	82			WC, Soils, Roots
Jul. 25th.	86			Crops
Aug. 27th.	229	89	Harvest	Crops

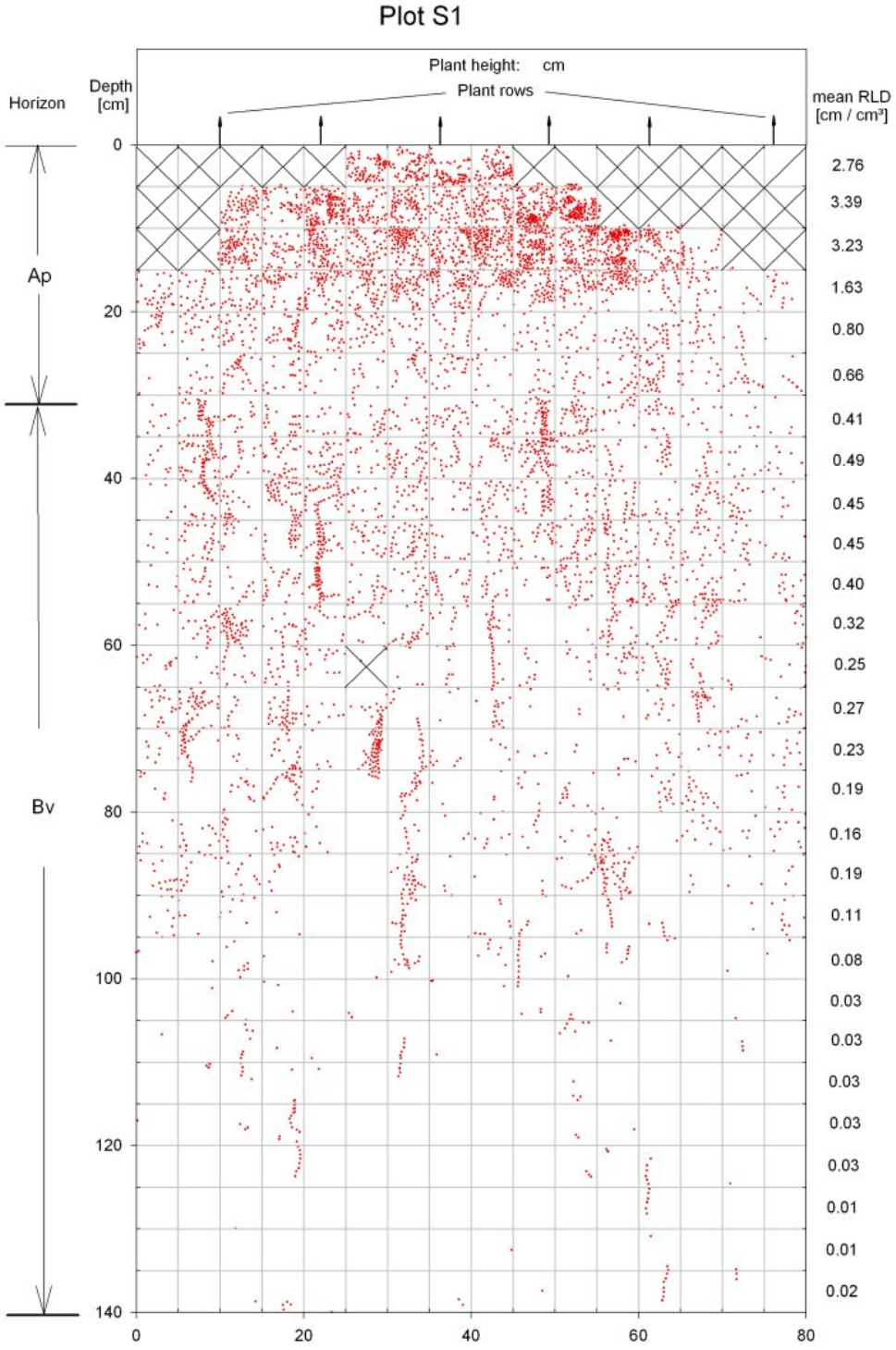

Figure A.1: Soil-root profile map at plot S1.

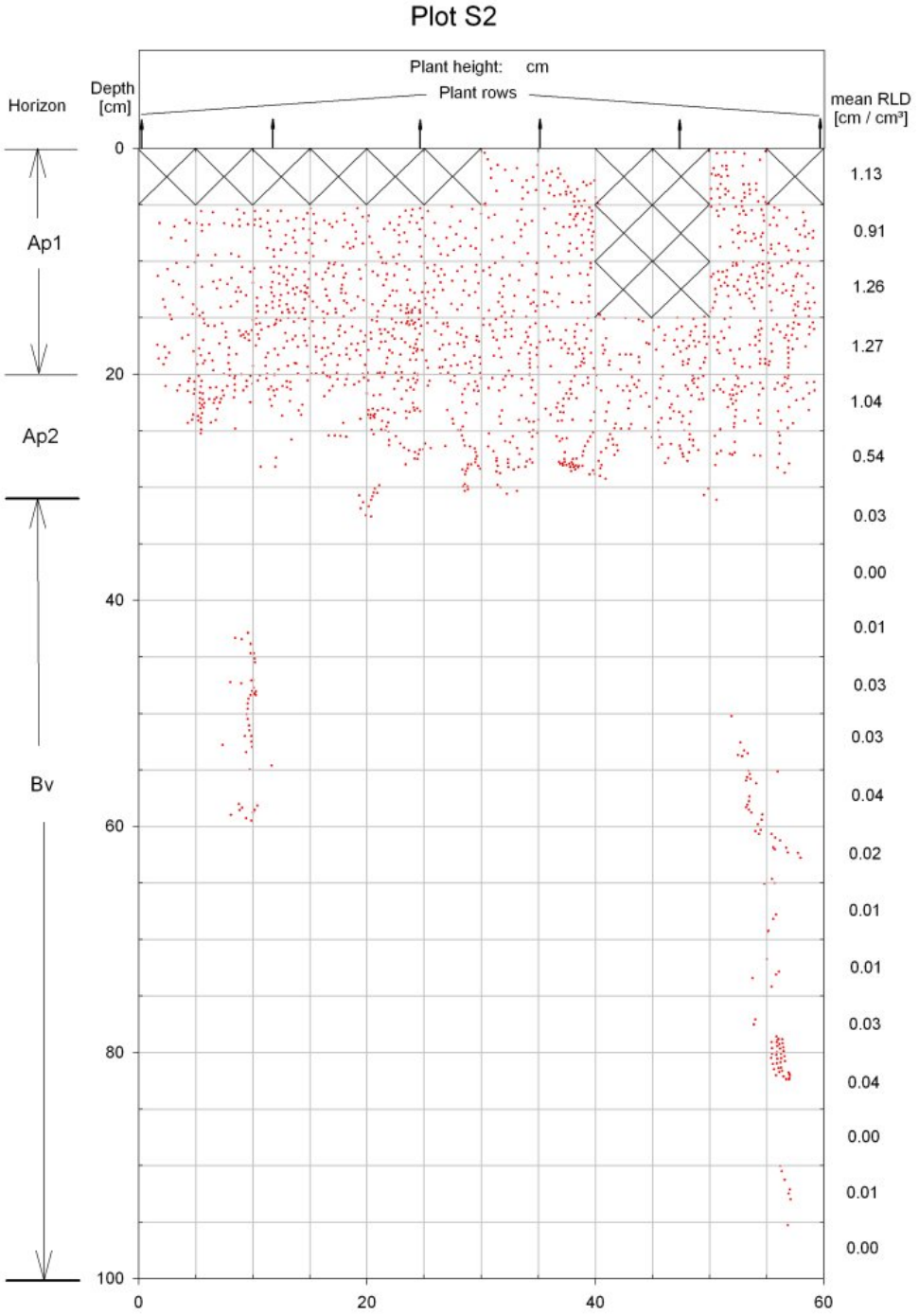

Figure A.2: Soil-root profile map at plot S2.

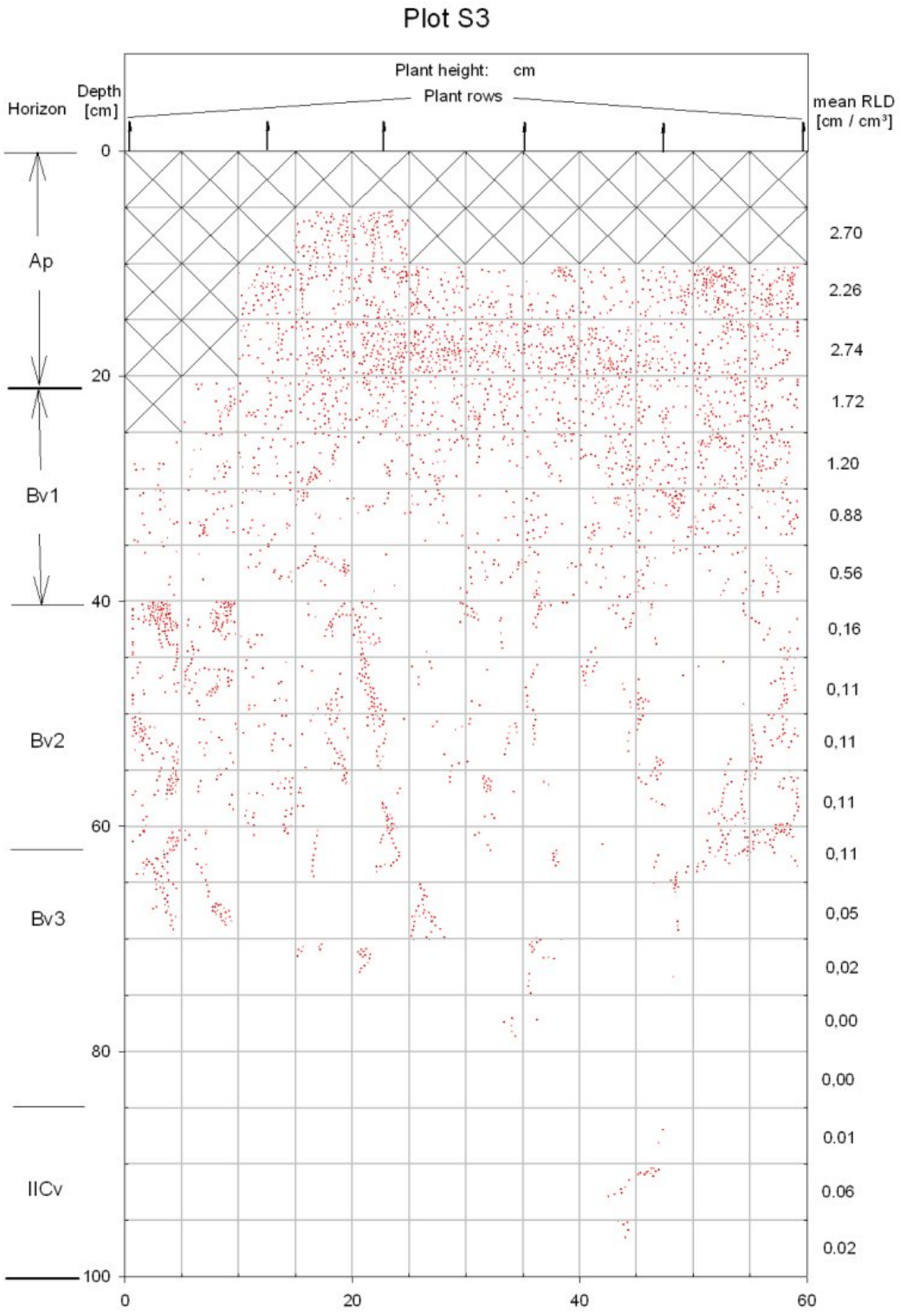

Figure A.3: Soil-root profile map at plot S3.

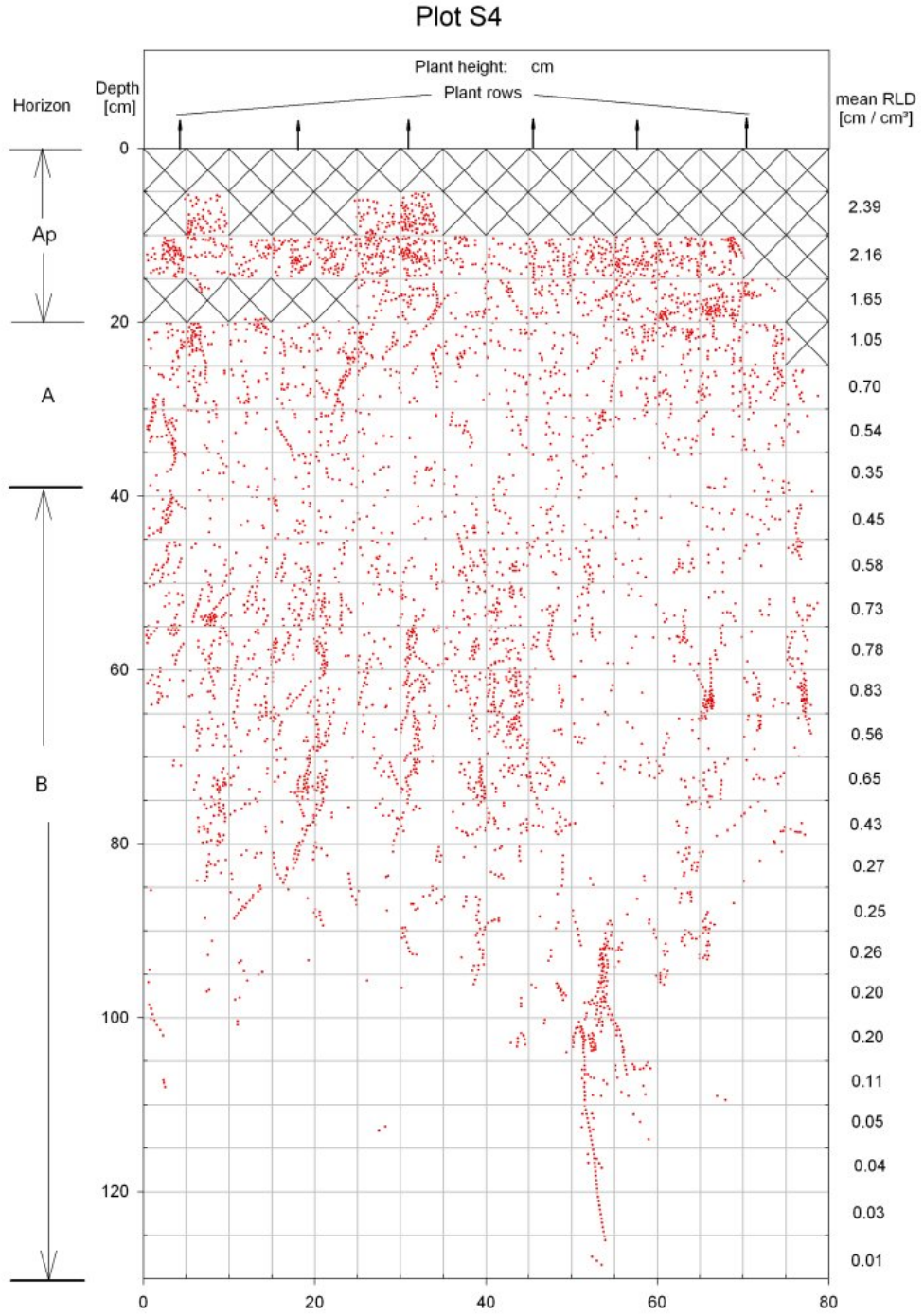

Figure A.4: Soil-root profile map at plot S4.

References

Ahuja, L. & Ma, L. (2002). Parameterization of agricultural system models: current approaches and future needs. In L. Ahuja, L. Ma & T. Howell, eds., *Agricultural System Models in Field Research and Technology Transfer*, chap. 14, 273–316, Lewis publishers, Boca Raton, FL.

Ahuja, L., Rojas, K., Hanson, J., Shaffer, M. & Ma, L., eds. (2000). *Root Zone Water Quality Model*. Water Resources Publication, Englewood.

Ahuja, L., Ma, L. & Howell, T., eds. (2002). *Agricultural System Models in Field Research and Technology Transfer*. Lewis publishers, Boca Raton, FL.

Aiken, R. & Smucker, A. (1996). Root system regulation of whole plant growth. *Annu. Rev. Phytopathol.*, **34**, 325–346.

Andales, A., Green, T., Ahuja, L., Erskine, R. & Peterson, G. (2007). Temporally stable patterns in grain yield and soil water on a dryland catena. *Agr. Syst.*, **94**, 119–127.

Ascough, J., Ahuja, L., McMaster, G., Ma, L. & Andales, A. (2008). Agriculture models. In S. Jorgensen, ed., *Encyclopedia of Ecology*, 85–95, Elsevier, Amsterdam.

Benbi, D. & Nieder, R., eds. (2003). *Handbook of Processes and Modeling in the Soil-Plant-System*. Food Products Press and The Haworth Reference Press, New York.

Benjamin, J., Ahuja, L. & Allmaras, R. (1996). Modelling corn rooting patterns and their effects on water uptake and nitrate leaching. *Plant Soil*, **179**, 223–232.

Böhm, W. (1979). *Methods of Studying Root Systems*. Springer, Berlin.

Brooks, H. & Corey, A. (1966). Properties of porus media affecting fluid flow. *Proc. Am. Soc. Civ. Eng.*, **92**, 61–88.

Brutsaert, W. (1966). Probability laws for pore size distributions. *Soil Sci.*, **101**, 85–92.

Burdine, N. (1953). Relative permeability calculations from pore size distribution data. *Trans. AIME*, **198**, 71–77.

Campbell, G. (1985). *Soil Physics with BASIC, Transport Models for Soil-Plant Systems*. Bd. 14 of Developments in Soil Science, Elsevier, New York.

Dane, J. & Topp, G., eds. (2002). *Methods of Soil Analysis, Part 4–Physical Methods.*. Soil Science Society of America, Madison, Wisconsin.

Darrah, P., Jones, D., Kirk, G. & Roose, T. (2006). Modelling the rhizosphere: a review of methods for 'upscaling' to the whole-plant scale. *Eur. J. Soil Sci.*, **57**, 13–25.

Doussan, C., Pages, L. & Pierretc, A. (2003). Soil exploration and resource acquisition by plant roots: an architectural and modelling point of view. *Agronomie*, **23**, 419–431.

Duffera, M., White, J. & Weisz, R. (2007). Spatial variability of southeastern u.s. coastal plain soil physical properties: Implications for site-specific management. *Geoderma*, **137**, 327–339.

Engel, T. & Priesack, E. (1993). Expert-N, a building block system of nitrogen models as resource for advice, research, water management and policy. In H. Eijsackers & T. Hamers, eds., *Integrated Soil and Sediment Research: A Basis for Proper Protection*, 503–507, Kluwer Academic Publishers, Dordrecht, Netherlands.

Fitter, A. & Stickland, T. (1991). Architectual analysis of plant root systems iii. studies on plants under field conditions. *New Phytol.*, **118**, 375–382.

Fitter, A., Stickland, T., Harvey, M. & Wilson, G. (1991). Architectual analysis of plant root systems I. architectural correlates of exploitation efficiency. *New Phytol.*, **118**, 375–382.

Gardner, W. (1958). Some steady state solutions of the unsaturated moisture flow equation with application to evaporation from a water table. *Soil Sci.*, **85**, 228–232.

Green, T. & Erskine, R. (2004). Measurement, scaling, and topographic analyses of spatial crop yield and soil water content. *Hydrol. Process*, **18**, 1447–1465.

Gregory, P. (2006). Roots, rhizosphere and soil: the route to a better understanding of soil science? *Eur. J. Soil Sci.*, **57**, 2–12.

Guber, A., Pachepsky, Y., van Genuchten, M., Rawls, W., Simunek, J., Jacques, D., Nicholson, T. & R.E., C. (2006). Field-scale water flow simulations using ensembles of pedotransfer functions for soil water retention. *Vadose Zone J.*, **5**, 234–247.

Hansen, S., Jensen, H., Nielsen, N. & Svendsen, H. (1990). *DAISY - Soil Plant Atmosphere System Model*. The Royal Veterinary and Agricultural University, Copenhagen.

Hodge, A. (2004). The plastic plant: root responses to heterogeneous supplies of nutrients. *New Phytol.*, **162**, 9–24.

Hoogenboom, G., Wilkens, P. & Tsuji, G. (1999). *Decision Support System for Agrotechnology Transfer version 3, Vol. 4*. University of Hawaii, Honolulu.

Hopmans, J. & Bristow, K. (2002). Current capabilities and future needs of root water and nutrient uptake modeling. *Adv. Agron.*, **77**, 103–183.

Hupet, F., van Dam, J. & Vanclooster, M. (2004). Impact of within-field variability in soil hydraulic properties on transpiration fluxes and crop yields: A numerical study. *Vadose Zone J.*, **3**, 1367–1379.

Hutchings, M. & John, E. (2004). The effects of environmental heterogeneity on root growth and root/shoot partitioning. *Ann. Bot. London*, **94**, 1–8.

Hutson, J. & Cass, A. (1987). A retentivity function for use in soil-water simulation models. *J. Soil Sci.*, **38**, 105–113.

Hutson, J. & Wagenet, R. (1992). *LEACHM: Leaching Estimation and Chemistry Model. Version 3.0*. Department of Soils, Crops and Atmospheric Sciences, Cornell University, Ithaca, NY.

Jones, C. & Kiniry, J. (1986). *CERES-Maize: A Simulation Model of Maize Growth and Development*. College Station, Texas, Texas a&M University Press.

Jones, C., Bland, W.L., Ritchie, J. & Williams, J. (1991). Simulation of root growth. In J. Hanks & J. Ritchie, eds., *Modeling Plant and Soil Systems*, 91–123, ASA/CSSA/SSSA, Madison, Wisconsin.

Jury, W. & Horton, R. (2004). *Soil Physics*. Wiley, Hoboken, NJ, 6th edn.

Klier, C. (2006). *Environmental fate of the herbicide glyphosate in the soil-plant system: Monitoring and modelling using large-scale weighing lysimeters*. Ph.D. thesis, Technische Universität München.

Kravchenko, A., Robertson, G., Thelen, K. & Harwood, R. (2005). Management, topographical, and weather effects on spatial variability of crop grain yields. *Agron. J.*, **97**, 514–523.

Kribaa, M., Hallaire, V., Curmi, P. & Lahmar, R. (2001). Effect of various cultivation methods on the structure and hydraulic properties of a soil in a semi-arid climate. *Soil Tillage Res.*, **60**, 43–53.

Manschadi, A., Sauerborn, J., Sttzelb, H., Gbelc, W. & Saxenac, M. (1998). Simulation of faba bean (vicia faba l.) root system development under mediterranean conditions. *Eur. J. Agron.*, **9**, 259–272.

McCown, R., Hammer, G., Hargreaves, J., Holzworth, D. & Freebairn, D. (1996). APSIM: a novel software system for model development, model testing, and simulation in agricultural systems research. *Agr. Syst.*, **50**, 255–271.

Mualem, Y. (1976). A new model predicting the hydraulic conductivity of unsaturated porous media. *Water Resour. Res.*, **12**, 513–522.

Osinski, E., Meyer-Aurich, A., Huber, B., Rhling, I., G., G. & Schröder, P., eds. (2005). *Landwirtschaft und Umwelt - ein Spannungsfeld*. oekom verlag, München.

Pages, L., Asseng, S., Pellerin, S. & Diggle, A. (2000). Modelling root system growth and architecture. In A. Smit, A. Bengough, C. Engels, M. van Noordwijk, S. Pellerin & S. van de Geijn, eds., *Root Method: A Hand Book*, 113–146, Springer, Berlin.

Passioura, J. (2002). Soil conditions and plant growth. *Plant Cell Environ.*, **25**, 311–318.

Perez-Quezada, J., Pettygrove, G. & Plant, R. (2003). Spatial-temporal analysis of yield and soil factors in two four-crop-rotation fields in the sacramento valley, california. *Agron. J.*, **95**, 676–687.

Pierret, A., Doussan, C., Capowiez, Y., Bastardie, F. & Pages, L. (2007). Root functional architecture: A framework for modeling the interplay between roots and soil. *Vadose Zone J.*, **6**, 269–281.

Plant, R. (2001). Site-specific management: the application of information technology to crop production. *Comput. Electron. Agr.*, **30**, 9–29.

Priesack, E. (2006). *Expert-N Dokumentation der Modell-Bibliothek. FAM Bericht 60*. Hieronymus, München.

Priesack, E. & Gayler, S. (2009). Agricultural crop models: Concepts of resource acquisition and assimilate partitioning. In *Progress in Botany*, chap. 4, 195–222, Springer, Berlin, Heidelberg.

Priesack, E., Berkenkamp, A., Gayler, S. & Loos, C. (2008). Development and application of agro-ecosystem models. In *Perspectives for Agroecosystem Management*, chap. 4.1, 329–349, Elsevier, Amsterdam.

Rawls, W. & Brakensiek, D. (1985). Prediction of soil water properties for hydrologic modeling. In E. Jones & T. Ward, eds., *Watershed Management in the Eighties, Proc. of the Symposium ASCE, 30.April-2.May 1985*, 293–299, Denver, CO.

Ritchie, J. & Godwin, D. (1989). *CERES Wheat 2.0 Documentation for Version 2 of the CERES Wheat Model. http://nowlin.css.msu.edu/wheat_book/*.

Ritchie, J., Godwin, D. & Otter-Nacke, S. (1986). *CERES-Wheat: A Simulation Model of Wheat Growth and Development, CERES Model Description*. Department of Crop and Soil Science, Michigan State University, East Lansing.

Scheffer, F. & Schachtschabel, P. (1998). *Lehrbuch der Bodenkunde. 14. Auflage*. Enke, Stuttgart.

Shaffer, M., Bartling, P. & Ascough, J. (2000). Object-oriented simulation of integrated whole farms: GPFARM framework, comput and electron. *Agriculture - London*, **28**, 29–49.

Simunek, J. & van Genuchten, M. (1996). Estimating unsaturated soil hydraulic properties from tension disc infiltrometer data by numerical inversion. *Water Resour. Res.*, **32**, 2683–2696.

Simunek, J. & van Genuchten, M. (1997). Estimating unsaturated soil hydraulic properties from multiple tension disc infiltrometer data. *Soil Sci.*, **162**, 383–398.

Simunek, J. & van Genuchten, M. (2000). *The DISC Computer Software for Analyzing Tension Disc Infiltrometer Data by Parameter Estimation. Version 1.0. Research Report*. U.S. Salinity Laboratory, USDA-ARS, Riverside, CA.

Simunek, J., Angulo-Jaramillo, R., Schaap, M., Vandervaere, J. & van Genuchten, M. (1998a). Using an inverse method to estimate the hydraulic properties of crusted soils from tension-disc infiltrometer data. *Geoderma*, **86**, 61–81.

Simunek, J., Huang, K. & van Genuchten, M. (1998b). *The HYDRUS Code for Simulating the One-dimensional Movement of Water, Heat and Multiple Solutes in Variably Saturated Media. Version 6.0*. U.S. Salinity Laboratory, Riverside USA.

Sinowski, W. & Auerswald, K. (1999). Using relief parameters in a discriminant analysis to stratify geological areas with different spatial variability of soil properties. *Geoderma*, **89**, 113–128.

Skaggs, T. & Shouse, P. (2008). Roots and root function: Introduction. *Vadose Zone J.*, **7**, 1008–1009.

Smit, A., Bengough, A., Engels, C., van Noordwijk, M., Pellerin, S. & van de Geijn, S., eds. (2000). *Root Method: A Hand Book*. Springer, Berlin.

Sommer, M., Wehrhan, M., Zippricha, M., Wellera, U., zu Castella, W., Ehrichа, S., Tandlera, B. & Selige, T. (2003). Hierarchical data fusion for mapping soil units at field scale. *Geoderma*, **112**, 179–196.

Stenger, R., Priesack, E., Barkle, G. & Sperr, C. (1999). Expert-N. A tool for simulating nitrogen and carbon dynamics in the soil-plant-atmosphere system. In M. Tomer, R. M. & G. Gielen, eds., *Modelling of Land Treatment Systems.NZ Land Treatment Collective Proceedings Technical Session 20*, 19–28, New Plymouth New Zealand.

Tsuji, G., Uehara, G. & Balas, S. (1994). *DSSAT version 3*. University Hawaii, Honolulu.

van Genuchten, M. (1980). A closed-form equation for predicting the hydraulic conductivity of unsaturated soils. *Water Resour. Res.*, **44**, 892–898.

van Laar, H., Goudriaan, J. & van Keulen, H. (1997). *SUCROS97: Simulation of Crop Growth for Potential and Water-limited Production Situation. (Bd. 14 von Quantitative Approaches in System Analysis)*. C.T. de Wit Graduate School for Production Ecology and Resourde Conservation, Wageningen.

van Noordwijk, M. & van de Geijn, S. (1996). Root, shoot and soil parameters required for process-oriented models of crop growth limited by water or nutrients. *Plant Soil*, **183**, 1–25.

VDLUFA-Methodenbuch, ed. (2004). *VDLUFA -Methodenbuch für die Untersuchung von Böden, Band I*. VDLUFA (Verband Deutscher Landwirtschaftlicher Untersuchungs- und Forschungsanstalten).

Vereecken, H., Maes, J., Feyen, J. & Darius, P. (1989). Estimating the soil moisture retention characteristic from texture, bulk density and carbon content. *Soil Sci.*, **148**, 389–403.

Vereecken, H., Maes, J. & Feyen, J. (1990). Estimating unsaturated hydraulic conductivity from easily measured soil properties. *Soil Sci.*, **149**, 1–12.

Wang, E. (1997). *Simulation of phenological development of wheat crops*. Ph.D. thesis, Technische Universität München.

Wang, E. & Engel, T. (2000). SPASS: A generic process-oriented crop model with versatile windows interfaces. *Environ. Model. Softw.*, **15**, 179–188.

Wang, E. & Smith, C.J. (2004). Modelling the growth and water uptake function of plant root systems: A review. *Aust. J. Agr. Res.*, **55**, 501–523.

Warrick, A. (1992). Models for disc infiltrometers. *Water Resour. Res.*, **28**, 1319–132.

Williams, J. & Renard, K. (1985). Assessment of soil erosion and crop productivity with process models (epic). In R. Follett & B. Stewart, eds., *Soil Erosion and Crop Productivity*, 68–102, American Society of Agronomy, Madison.

Wong, M. & Asseng, S. (2006). Determining the causes of spatial and temporal variability of wheat yields at sub-field scale using a new method of upscaling a crop model. *Plant Soil*, **283**, 203–215.

Yang, H., Dobermann, A., Lindquist, J., Walters, D. & Cassman, K. (2004). Hybrid-maize - a maize simulation model that combines different crop modeling approaches. *Field Crop. Res.*, **87**, 131–154.